

**Causes and impacts of changes in  
the stratospheric meridional circulation  
in a chemistry-climate model**

Dissertation  
der Fakultät für Physik der  
Ludwig-Maximilians-Universität München

vorgelegt von Hella Garny  
aus Starnberg

München, den 30. Juli 2010

1.Gutachter: Prof. Dr. Martin Dameris, LMU München

2.Gutachter: Prof. Dr. George Craig, LMU München

Tag der mündlichen Prüfung: 26. Oktober 2010

## Abstract

The climate of the stratosphere is known to be subject to long-term changes induced by anthropogenic emissions of long-lived greenhouse gases (GHGs) as well as by emissions of ozone depleting substances (primarily chlorofluorocarbons, CFCs). Enhanced concentrations of CFCs have led to strong ozone depletion over the last decades. Thanks to the Montreal Protocol and its amendments and adjustments, the stratospheric halogen loading is expected to retreat again in the future. Emissions of GHGs, on the other hand, are not yet controlled sufficiently, and concentrations of GHGs are projected to increase further in the future. The effects of enhanced GHG concentrations on the stratosphere include decreasing temperatures, as well as changes in the dynamical balances and interactions with the troposphere, and thus changes in the large-scale circulation. In particular, the stratospheric meridional circulation is projected to be subject to changes. These GHG-induced changes will also affect stratospheric ozone chemistry and transport of ozone. Therefore, the expected recovery of ozone due to decreasing CFC concentrations will coincide with alterations of the ozone layer by climate change.

This study aims to diagnose and explain long-term changes in the stratospheric meridional circulation using the chemistry-climate model E39CA. The dynamical causes for these changes are identified, and the impact of changes in the meridional circulation on the future development of ozone is quantified.

In a changing climate, the meridional circulation is found to strengthen in the tropical lower stratosphere. In particular, tropical upwelling in the lowermost stratosphere intensifies at a rate of about 3% per decade over the analysed period of 1960 to 2049. This enhanced upwelling is balanced by downwelling in the subtropics at latitudes around 20-40°N/S. The increase in tropical upwelling can be explained by stronger local forcing by large scale waves. It is shown that enhanced tropical upwelling is driven by processes induced by increases in tropical sea surface temperatures (SSTs). Higher tropical SSTs cause both a) a strengthening of the subtropical jets and b) modifications of deep convection, leading to changes in the strength and location of latent heat release. While the former (a) can modify wave propagation and dissipation, the latter (b) affects tropical wave generation. Evidence is presented that the dominating mechanism leading to enhanced vertical wave propagation into the lower stratosphere is an upward shift of the easterly shear zone due to the strengthening and upward and equatorward shifts of the subtropical jets.

In addition to the increase in tropical upwelling caused by climate change, the changes in CFC concentrations also affect the dynamical forcing of the meridional circulation. The CFC-induced depletion of ozone in the past has led to changes in the background wind field in the southern hemisphere in summer, which cause enhanced wave propagation into the middle stratosphere and thus a strengthening of the meridional circulation. This effect is reversed in the future, when CFC concentrations decline.

The future development of ozone is found to be dominated by changes in local chemistry in most regions of the stratosphere. Both decreasing CFC concentrations and stratospheric cooling due to enhanced GHG concentrations lead to less efficient ozone destruction, and thus increasing ozone concentrations. However, changes in transport of ozone due to the strengthening of the meridional circulation play an important role in the tropical lower stratosphere, where ozone concentrations decrease due to more export of ozone. Furthermore, it is found that the chemically induced positive ozone trend in southern high latitudes in the future is counteracted by decreased ozone transport from middle to high latitudes. This decrease in transport is due to the weakening of the meridional circulation in the southern hemisphere in summer, which, in turn, is induced by ozone changes.

## Zusammenfassung

Das Klima der Stratosphäre wird bekanntermaßen durch anthropogene Emissionen von langlebigen Treibhausgasen (GHGs) sowie von Ozon zerstörenden Substanzen (hauptsächlich Fluor-Chlor-Kohlen-Wasserstoffen, FCKWs) beeinflusst. In den letzten Jahrzehnten führten erhöhte FCKW Konzentrationen zu starkem Ozonabbau. Dank des Montrealer Protokolls wird erwartet, dass die Halogen Beladung der Stratosphäre in der Zukunft wieder abnimmt. Die Emissionen von GHGs sind allerdings noch nicht ausreichend reglementiert, so dass die Konzentrationen von GHGs in der Zukunft weiterhin ansteigen werden. Die Auswirkungen von erhöhten GHG Konzentrationen in der Stratosphäre umfassen zurückgehende Temperaturen, aber auch Änderungen im dynamischen Gleichgewicht und den Wechselwirkungen mit der Troposphäre und somit Änderungen im großskaligen Zirkulationssystem. Insbesondere wird erwartet, dass sich die meridionale Zirkulation der Stratosphäre verändert. Diese durch GHGs induzierten Veränderungen werden auch die Ozonchemie und den Transport von Ozon beeinflussen. Somit wird die durch zurückgehende FCKW Konzentrationen erwartete Erholung der Ozonschicht mit Änderungen in der Ozonverteilung durch den Klimawandel einhergehen.

Diese Studie hat zum Ziel, die langzeitlichen Änderungen in der stratosphärischen meridionalen Zirkulation zu untersuchen. Dazu wird das Klima-Chemie Modell E39CA verwendet. Die Ursachen für diese Änderungen werden identifiziert und der Einfluss der Änderungen in der meridionalen Zirkulation auf die zukünftige Entwicklung von Ozon wird quantifiziert.

Es wurde festgestellt, dass sich die meridionale Zirkulation in einem Klima mit erhöhten GHG-Konzentrationen in der unteren Stratosphäre verstärkt. Insbesondere intensiviert sich das Aufsteigen von tropischen Luftmassen in der untersten Stratosphäre während des untersuchten Zeitraums von 1960 bis 2049 mit einer Rate von 3% pro Dekade. Ausgeglichen wird dieses verstärkte Aufsteigen von Luftmassen durch Absinken in den Subtropen in einem Breitenbereich von 20-40°N/S. Die Verstärkung im tropischen Aufsteigen kann mit einem verstärkten lokalen Antrieb durch großskalige Wellen erklärt werden. Es wird gezeigt, dass die Verstärkung im tropischen Aufsteigen durch Prozesse induziert wird, die auf erhöhte tropische Meeresoberflächentemperaturen (SSTs) zurückzuführen sind. Höhere tropische SSTs führen sowohl a) zu einer Verstärkung der subtropischen Jets als auch b) zu Änderungen in hochreichender Konvektion, was wiederum die Stärke und Lage der Freigabe von latenter Wärme beeinflusst. Ersteres (a) wirkt sich auf die Wellenausbreitung und Dämpfung aus, während Letzteres (b) tropische Wellenanregung beeinflusst. Es wurden Hinweise dafür gefunden, dass der dominierende Mechanismus, der zu verstärkter Wellenpropagation in die untere Stratosphäre führt, auf die Verschiebung und Verstärkung der Subtropenjets zurückzuführen ist.

Es wurde festgestellt, dass sich zusätzlich zu der Verstärkung von tropischem Auf-

steigen, welche durch den Klimawandel verursacht ist, auch Änderungen in FCKW Konzentrationen auf den dynamischen Antrieb der meridionalen Zirkulation auswirken. Der durch FCKWs bedingte Abbau von Ozon in der Vergangenheit führte dazu, dass sich der mittlere zonale Wind in der südlichen Hemisphäre im Sommer veränderte und somit Wellen vermehrt vertikal in die mittlere Stratosphäre propagieren konnten. Dies führt zu einer Verstärkung der meridionalen Zirkulation. Dieser Effekt kehrt sich in der Zukunft um, wenn FCKW Konzentrationen wieder abnehmen.

Die zukünftige Entwicklung von Ozon Konzentrationen wird, laut den Ergebnissen dieser Studie, in den meisten Regionen der Stratosphäre durch lokale Änderungen in der Chemie dominiert. Sowohl zurückgehende FCKW Konzentrationen, als auch die stratosphärische Abkühlung aufgrund erhöhter GHG Konzentrationen, führen zu geringerem Ozonabbau und in folge dessen zu ansteigenden Ozon Konzentrationen. In der tropischen unteren Stratosphäre spielen jedoch Änderungen im Transport von Ozon durch die verstärkte meridionale Zirkulation eine wichtige Rolle. Dort nehmen Ozon Konzentrationen aufgrund von verstärktem Export von Ozon ab. Es wurde außerdem festgestellt, dass in der Zukunft dem chemisch induzierten positiven Trend im Ozongehalt in den südlichen hohen Breiten verminderter Ozon Transport von den mittleren in die hohe Breiten entgegenwirkt. Diese Abnahme im Transport wird durch die Abschwächung der meridionalen Zirkulation in der südlichen Hemisphäre im Sommer, welche wiederum durch Ozon Änderungen induziert wird, bewirkt.

# Contents

<b>1</b>	<b>Introduction</b>	<b>1</b>
1.1	State of the art . . . . .	2
1.1.1	The Brewer-Dobson Circulation . . . . .	2
1.1.2	Stratospheric ozone . . . . .	8
1.2	Thesis Objectives and Outline . . . . .	11
<b>2</b>	<b>Model description and simulation set-ups</b>	<b>15</b>
2.1	Model description of E39CA . . . . .	15
2.2	Simulation set-ups . . . . .	16
2.2.1	Transient simulations . . . . .	16
2.2.2	Sensitivity simulations . . . . .	20
<b>3</b>	<b>Diagnosing changes in the meridional circulation</b>	<b>23</b>
3.1	Background state . . . . .	23
3.2	Mean tropical upwelling . . . . .	26
3.3	Residual circulation . . . . .	29
3.4	Age of Air . . . . .	31
3.5	Width of the upwelling region . . . . .	33
3.6	Summary . . . . .	35
<b>4</b>	<b>Drivers of circulation changes</b>	<b>37</b>
4.1	Impact of changes in GHGs, SSTs and CFCs . . . . .	37
4.1.1	Utilisation of the simulations to assign changes to the boundary conditions . . . . .	37
4.1.2	Background state . . . . .	40
4.1.3	Residual Circulation . . . . .	44
4.2	Impact of tropical versus extratropical SSTs . . . . .	45
4.3	Summary . . . . .	50
<b>5</b>	<b>Wave forcing of the meridional circulation and tropical upwelling</b>	<b>51</b>
5.1	Wave forcing of tropical upwelling . . . . .	52
5.1.1	Downward control . . . . .	52
5.1.2	EP fluxes . . . . .	58

5.2	Discussion . . . . .	65
5.2.1	Climatological forcing of tropical upwelling . . . . .	66
5.2.2	Changes in wave generation . . . . .	67
5.2.3	Changes in wave propagation . . . . .	71
5.3	Summary . . . . .	73
<b>6</b>	<b>Impact of changes in the stratospheric circulation on transport and ozone</b>	<b>75</b>
6.1	Evolution of atmospheric ozone . . . . .	76
6.1.1	Trends in ozone . . . . .	76
6.1.2	Drivers of ozone changes . . . . .	77
6.2	Attribution of ozone changes to chemistry and transport . . . . .	80
6.2.1	Ozone origin diagnostic . . . . .	81
6.2.2	Transport of ozone and air masses . . . . .	88
6.2.3	Attribution of long-term changes in ozone . . . . .	96
6.3	Discussion and summary . . . . .	101
<b>7</b>	<b>Conclusions and Outlook</b>	<b>105</b>
7.1	Conclusions . . . . .	105
7.2	Outlook . . . . .	113
<b>A</b>	<b>Glossary and Abbreviations</b>	<b>117</b>
<b>B</b>	<b>The TEM equations and downward control</b>	<b>121</b>
<b>C</b>	<b>Linear least square regression modelling</b>	<b>125</b>

# Chapter 1

## Introduction

The climate on Earth is a complex system with interactions between Earth's surface, the deep oceans and the atmosphere. Various different processes act together to determine the climate state of Earth, such as radiative transfer, chemical reactions or dynamically induced circulations. Living on Earth's surface, humans experience the local weather and climate conditions in the atmospheric boundary layer. The boundary layer is the lowest part of the troposphere and spans about one kilometre in mid-latitudes. The weather and climate at the surface are strongly influenced by the atmospheric layers above. The stratosphere, which is situated above the troposphere at altitudes around 10 km to 50 km, is largely separated from the troposphere through its positive temperature gradient that inhibits vertical motion. Nonetheless, the stratosphere plays an important role in the climate system and various dynamical and radiative interactions exist between troposphere and stratosphere. The stratospheric ozone layer is important to the climate on Earth's surface, as it absorbs harmful ultraviolet (UV) radiation. Ozone is produced in the stratosphere by photochemistry, with strongest ozone production in the tropics. The distribution of ozone is, however, strongly influenced by dynamics. The dominant circulation that acts to redistribute ozone is the large-scale meridional circulation, the *Brewer-Dobson Circulation (BDC)*<sup>1</sup>, that transports air upward in the tropics, poleward from low to high latitudes and downward at high latitudes. This circulation is driven by momentum transfer from the troposphere to the stratosphere, i.e. the stratospheric dynamics are in parts controlled by tropospheric processes. In turn the troposphere is also influenced by stratospheric dynamics, for example by downward propagation of stratospheric anomalies into the troposphere (e.g. Baldwin and Dunkerton, 1999).

The BDC is responsible for the redistribution of ozone, leading to a maximum in total ozone column in the middle to high latitudes in spring/winter, despite the fact that ozone is mainly produced in the tropics. Tropical upwelling, the equatorward branch of the BDC, acts as the main pathway for transport of tropospheric air masses into the stratosphere. The stratospheric concentration of many trace gases with tropospheric

---

<sup>1</sup>This term and all other terms printed in italic upon their first occurrence are defined in Appendix A

sources depends strongly on the upward motion in the tropics (Holton et al., 1995). For example, the insertion of shortlived species, including bromine species that act to deplete ozone, depends on the upward advection in the tropics (e.g. Gettelman et al., 2009). Therefore, changes in tropical upwelling will alter the composition of stratospheric air and it is important to understand how tropical upwelling is influenced by changes in the climate system.

It is well established in today's scientific understanding that human activities do influence the climate system of Earth (IPCC, 2007). The emission of long-lived *greenhouse gases (GHGs)*, such as carbon dioxide ( $CO_2$ ), by humans is known to lead to substantial warming of the troposphere. The stratosphere is also directly affected by enhanced GHG concentrations. The stratosphere is cooling with enhanced GHG concentrations since GHGs emit more longwave radiation than they absorb in this layer. The direct radiational changes in both troposphere and stratosphere will affect dynamical balances. Therefore the entire circulation is expected to be influenced by *climate change*. The changes in stratospheric temperatures and circulation induced by climate change are also expected to impact the ozone layer. As these changes involve various processes and feedbacks, it is often not easy to identify the causes and effects of observed changes. Atmospheric models of various types can help to understand the causes and processes of climate change. In the stratosphere ozone acts as an important radiational active tracer that feeds back on climate. To study these feedbacks it is necessary to employ numerical models with a coupled chemistry scheme. These models are known as *chemistry-climate models (CCMs)*, and are commonly used in today's stratospheric research.

In the following sections, a short overview of the current state of knowledge regarding the subjects of this thesis, the Brewer-Dobson Circulation and stratospheric ozone, is given. Furthermore, the questions that remain to be solved are discussed.

## 1.1 State of the art

### 1.1.1 The Brewer-Dobson Circulation

The existence of a mean meridional circulation in the stratosphere was first proposed by Brewer (1949) and Dobson (1956) to explain observed water vapour and ozone distributions. Even though the chemical production of ozone maximises in the tropics, highest column values of ozone are observed in the mid-latitudes, which can only be explained by poleward transport of air from the tropics to high latitudes. The poleward transport is balanced by upward motion in the tropics and downward motion in the extratropics. This large-scale circulation is known as the Brewer-Dobson circulation. The BDC consists of two hemisphere-wide circulation cells, a broad high reaching circulation cell in the winter hemisphere, and a shallower cell in the summer hemisphere. Strongest upwelling in the *lower stratosphere* occurs in the tropical summer hemisphere. There is

no exact definition of what part of the meridional circulation is called Brewer-Dobson circulation. Here, and in the following, the *Brewer-Dobson circulation* is defined as the hemisphere-wide meridional circulation that is driven by the extratropical 'wave-pump' (see below). The term *meridional circulation*, or *residual circulation*, is used to describe the entire meridional circulation irrespective of its drivers and processes. In the course of this work, it will be shown that the hemisphere-wide BDC is superimposed by a shallow circulation in the lower stratosphere in the (sub-)tropics, which will be referred to as '*secondary circulation*'.

**Mechanism** The processes that drive the large-scale BDC in the extratropics are well understood. The transfer of momentum from the troposphere into the stratosphere by atmospheric waves implies a force on the zonal mean flow in the stratosphere which induces the meridional circulation.

Atmospheric waves are generally excited in the troposphere, for example by topography or land-sea differences in diabatic heating. In the stratosphere, mostly large-scale (*planetary*) Rossby-waves are of importance, but also smaller (*synoptic*) scale waves and gravity waves play a role. These waves can propagate vertically into the stratosphere, where they are subject to thermal damping and dynamical wave breaking (see below). Rossby-waves result from the beta-effect, i.e. from the increase of the Coriolis force towards the poles. They can penetrate vertically into the stratosphere if the zonal wind is positive and smaller than a certain critical velocity (Charney and Drazin, 1961; Holton, 2004). The critical velocity is proportional to the horizontal wave length, so that waves with larger scales can penetrate vertically at stronger zonal winds. Thus the waves found in the extratropical stratosphere are of relatively large scale (Haynes, 2005). For a wave of a certain phase speed, the line at which the background zonal wind field equals the critical velocity (hereafter referred to as critical line) acts as a boundary to its propagation (Randel and Held, 1991). Therefore, the phase speed of waves determines in which background winds they can penetrate. Once waves reach their critical line, nonlinear effects become important and wave breaking occurs. Near the critical line the wave perturbation becomes larger than the Doppler-shifted background velocity, which is zero at the critical line per definition. Rapid irreversible deformation of material contours occurs which is often called 'wave breaking'. The breaking or damping of waves leads to a momentum transfer from the wave to the zonal mean flow, i.e. the momentum that is transported by the waves is deposited in the regions of wave dissipation and a force is applied to the zonal mean flow.

The zonal mean general circulation in the stratosphere is often described with the transformed eulerian mean equations (TEM equations). They are obtained from the basic equations by zonal averaging and by introducing the modified meridional and vertical velocities  $\bar{v}^*$  and  $\bar{w}^*$ . The resulting meridional circulation is referred to as residual circulation. The transformation is described in Appendix B. In contrast to the conventional eulerian mean meridional circulation  $(\bar{v}, \bar{w})$ , the residual circulation

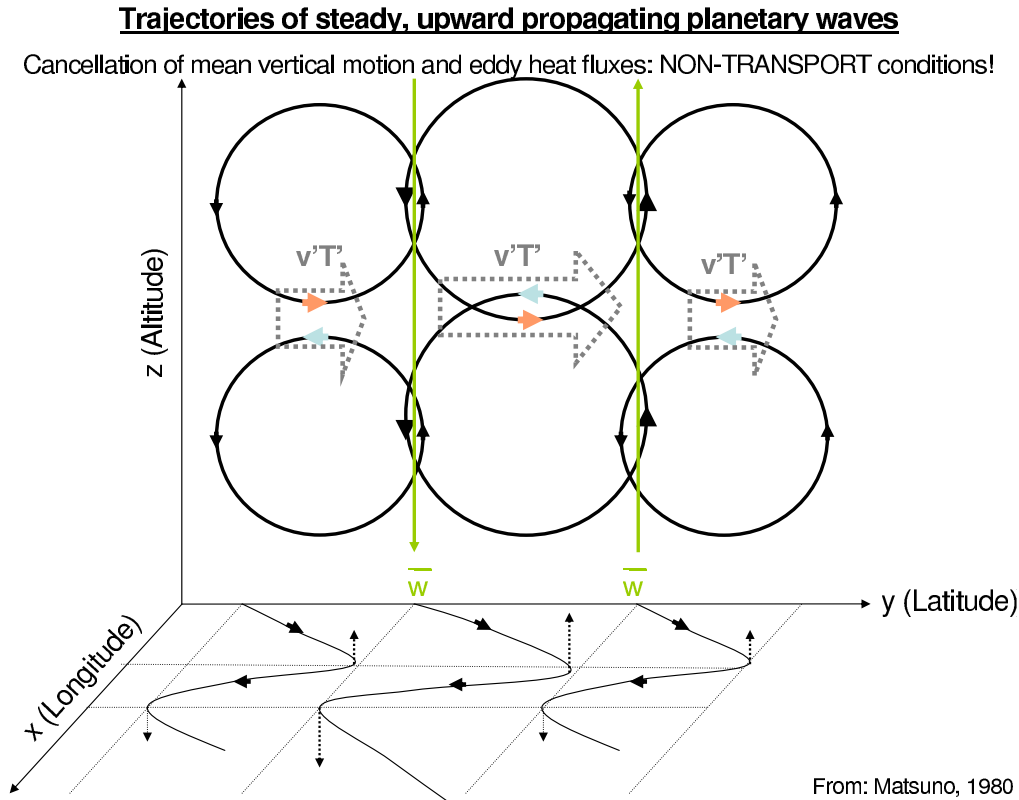


**Figure 1.1:** Schematic illustrating the Lagrangian air parcel movement for steady, non-dissipative waves. (Figure adapted from Matsuno, 1980, Figure 4).

eliminates the meridional motion induced by non-dissipative waves, which cancels the mean vertical motion. This can be understood when considering the circulation in a Lagrangian framework (Matsuno, 1980), as illustrated in Fig. 1.1: trajectories of steady, non-dissipative waves oscillate around a given latitudinal circle in the latitude-longitude plane, and form a circle in the meridional plane. Averaging the vertical velocity zonally, a meridional mean circulation with downward motion to the south of the wave amplitude maxima and upward motion to the north would be implied. Considering a background temperature gradient with temperatures decreasing with increasing latitude (as representative for the northern hemisphere), eddy heat fluxes as indicated by the grey arrows are implied. In the Eulerian framework, it is argued that the divergence (convergence) of eddy heat fluxes leads to cooling (heating) which implies downward (upward) motion. In the light of the Lagrangian motion it can be seen that this argumentation is somewhat artificial, and purely a result of the zonal averaging. As the trajectories describe circles (or rather inclined ellipses; Matsuno, 1980) in the meridional plane the individual air parcels have no mean motion, and thus no transport occurs. This illustrates the need to introduce a meridional circulation that actually describes the transport of air masses, which is obtained in the TEM framework.

The TEM equations form a set of equations for the four variables zonal wind,

potential temperature and the residual meridional and vertical velocities  $(\bar{u}, \bar{\Theta}, \bar{v}^*, \bar{w}^*)$ . The forcing terms of the physical system described by the TEM equations are due to momentum transfer by waves and heat transfer by diabatic heating. The momentum transfer can be divided into two parts: One part is the force applied on the zonal flow by dissipation of *resolved* waves described by the Eliassen-Palm (EP) flux divergence  $(\nabla \cdot F)$ . The second part is an additional forcing due to non-resolved waves as for example gravity wave forcing  $(\bar{X})$ . Diabatic heating  $(\bar{Q})$  is often parameterised as 'Newtonian cooling'  $\bar{Q} = \alpha(\bar{T} - \bar{T}_r)$ , i.e. being proportional to the deviation of the local temperature  $\bar{T}$  to the radiative equilibrium temperature  $\bar{T}_r$  with the thermal damping rate  $\alpha$ . Thus temperature perturbations induced by waves will be damped thermally. In the absence of wave forcing  $(\bar{X}, \nabla \cdot F = 0)$  a solution of the TEM equations is  $(\partial\bar{u}/\partial t, \partial\bar{\Theta}/\partial t, \bar{v}^*, \bar{w}^*) = 0$ , i.e. a steady state is reached with no meridional residual circulation. This is known as the non-acceleration or non-transport theorem (Charney and Drazin, 1961). It can be shown that steady, non-dissipative waves do always have zero EP flux divergence, and thus no transport is induced, in correspondence to the discussion on Lagrangian air parcel motion above (Fig. 1.1).

If the wave forcing is not zero, a meridional circulation will be implied. For example, when applying a periodic wave forcing of the form  $a_0 \exp(i\sigma t)$ , a solution for the meridional circulation can be found (see e.g. Haynes, 2005). The solution depends on the ratio of thermal damping ( $\alpha$ ) to the wave forcing period ( $\sigma$ ). It can be distinguished between an adiabatic solution ( $\sigma/\alpha \gg 1$ ), a solution where the ratio is about 1 and a steady-state solution ( $\sigma/\alpha \ll 1$ ). The meridional circulation increases in strength with a decreasing  $\sigma/\alpha$  ratio and has its largest latitudinal extent for medium values (see Fig. 1.2).

In the real atmosphere, breaking Rossby-waves exchange momentum with the mean flow and can therefore be associated with a westward force. The wave forcing is governed by the annual cycle, implying the build-up of a circulation cell in the winter hemisphere. With a thermal damping timescale of approximately 20 days, the ratio  $\sigma/\alpha \approx 0.3$  and the cell is of a form as in Fig. 1.2b.

This theory of a wave-driven circulation in the extratropics (often referred to as the extratropical 'wave-pump') is well established and explains large parts of the observed meridional circulation in the stratosphere. However, the observed strength of tropical upwelling in the lower stratosphere and the location of the upwelling maxima in the summer hemisphere can not be explained by extratropical wave forcing alone (e.g. Plumb and Eluszkiewicz, 1999). An additional force must be present that leads to upwelling in the tropics, and in particular in the summer (sub-)tropics. Some studies suggested that this additional force might be due to diabatic heating, i.e. a 'Hadley'-cell like circulation (Semeniuk and Shepherd, 2001; Plumb and Eluszkiewicz, 1999). However, they conclude that this can not explain tropical upwelling in the lower stratosphere. Rather, it was shown that wave forcing that is applied in the inner tropics close to the equator can quantitatively account for the observed upwelling (Semeniuk and

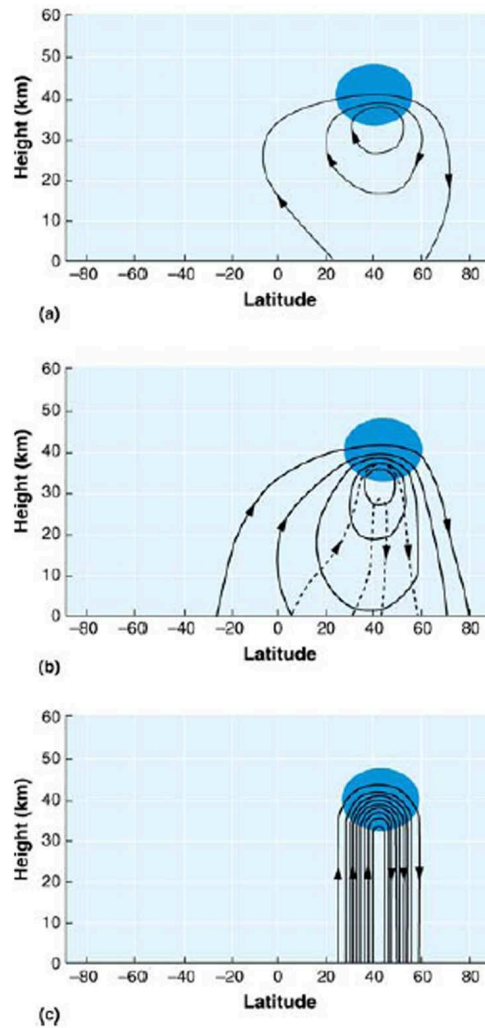


**Figure 1.2:** Solutions for the residual meridional circulation as response to westward wave forcing in the dark blue region. (a) Adiabatic solution ( $\sigma/\alpha \gg 1$ ). (b) Response for  $\sigma/\alpha \approx 0.3$  (corresponding to annual cycle in wave forcing and thermal damping timescale of 20 days), in phase with the forcing (solid line) and  $90^\circ$  out of phase with the forcing (dashed line). (c) Steady-state solution ( $\sigma/\alpha \ll 1$ ). (Figure from Holton et al., 1995).

Shepherd, 2001; Plumb and Eluszkiewicz, 1999). In fact, increasing evidence for the important role of wave forcing in the tropics in driving tropical upwelling was found recently. Some studies suggested that this wave forcing is due to both extratropical waves propagating equatorward and tropical planetary waves generated by latent heat release through deep convection (Boehm and Lee, 2003; Kerr-Munslow and Norton, 2006; Randel et al., 2008). It is one of the aims of this study to investigate and deepen the understanding of the driving mechanism for tropical upwelling.

**Long-term changes in the BDC** A large number of recent modelling studies show that the BDC, and in particular tropical upwelling in the lower stratosphere, is strengthening in a changing climate (e.g. Butchart et al., 2006; Garcia and Randel, 2008; Deckert and Dameris, 2008; McLandress and Shepherd, 2009). However, this strengthening of the BDC is still a subject of controversial discussion mainly due to the following open points: 1) the increase of tropical upwelling could so far not be verified from observations and 2) the mechanisms for the strengthening of the BDC in the models are not yet understood.

Concerning the first point, the main problem when attempting to investigate tropical upwelling in observations is the poor data basis for this quantity. As the vertical velocities in the tropics in the *upper troposphere and lower stratosphere* (UTLS) are very small (in the order of mm/s), tropical upwelling is hard to measure directly and only estimates of upwelling or derived quantities can be examined. Many recent studies tried to detect trends in upwelling using various methods. For example, Sinnhuber and Wohltmann (2010), who estimated the mean vertical residual velocity ( $\overline{w^*}$ ) from re-analysis data and ozone estimations, found no significant increases in tropical upwelling at 70 hPa over 40 years of data. Engel et al. (2009) used sulphur hexafluoride ( $SF_6$ ) and  $CO_2$  mixing ratios to derive mean age of air<sup>2</sup> (which is expected to decrease with increasing tropical upwelling) and found no significant changes in the 30 years of available data. However, the relationship between tropical upwelling and age of air might also be determined by other factors, so that an unchanged age of air does not necessarily contradict increased upwelling [E. Ray, personal communication]. Other studies found temperature changes in the tropical lower stratosphere (Thompson and Solomon, 2005; Fu et al., 2010) and in the extratropics (Lin et al., 2009) that are consistent with a strengthened BDC. However, given the poor observational data basis, especially in the tropics, and the rather short time periods that are available, it is not surprising that only weak evidence for changes in upwelling are found, especially given that the trend is small compared to the interannual variability. Also, the trend in upwelling might be sensitive to the latitude and height range as well as the season. Therefore, the results of the studies mentioned above might be different if other regions were considered. While models generally agree on a strengthening of tropical upwelling, they do not agree on

---

<sup>2</sup>The mean age of air measures the time an air parcel has spent in the stratosphere since entering it through the tropopause, see e.g. Hall and Plumb (1994)

the exact pattern of changes in the BDC (see below). Overall, it is noted here that even though the robust findings of climate models could not be approved by observations so far, the observational findings do not necessarily contradict the model results.

Many recent studies dealt with understanding the change in the BDC that are simulated by climate and chemistry-climate models. While most models show an increase in tropical upwelling in the lower stratosphere associated with increased downwelling in the subtropics (e.g. McLandress and Shepherd, 2009; Garcia and Randel, 2008; Deckert and Dameris, 2008; Sigmond et al., 2004; Fomichev et al., 2007; Oman et al., 2009), there is a wider spread in model results on changes in downwelling in the extratropics and high latitudes. Associated with the increase in tropical upwelling, a decrease in temperatures and ozone concentrations is simulated in the tropical lower stratosphere (e.g. Lamarque and Solomon, 2010). It has been found that the main forcing of BDC changes is an increase in *sea surface temperatures (SSTs)* as the indirect effect of increasing GHG concentrations (e.g. Fomichev et al., 2007; Sigmond et al., 2004; Oman et al., 2009). The overall picture arises that the changes in the circulation are driven by a combination of changes in resolved wave activity and orographic gravity wave drag (OGWD). Both McLandress and Shepherd (2009) and Garcia and Randel (2008) conclude that the effects of OGWD are important for changes in upwelling at altitudes above  $\sim 20$  to 25 km in the extratropics. In the tropical lower stratosphere, on the other hand, effects of changes in resolved waves, and in particular planetary waves prevail.

The increase in forcing by large-scale (resolved) waves in the tropical lower stratosphere might either be due to changes in the propagation properties of the waves or due to changes in the generation of either extratropical or tropical waves. Deckert and Dameris (2008) suggested that the enhanced wave forcing is a consequence of increased wave generation in the tropics. They argue that enhanced tropical SSTs leads to changes in deep convection, which in turn influences the emergence of tropical large-scale waves. They found increased wave fluxes and convergence in the summer hemisphere (sub-)tropics, coinciding with the region where strongest convection and strongest changes in convection take place. Also Calvo and Garcia (2009) showed indications of increased latent heat release by deep convection and argue that this process is important for the increase in wave forcing. However, they also found that changes in the refraction index lead to enhanced propagation of waves into the lower stratosphere. Overall, there is no consistent picture on processes that lead to enhanced wave forcing and thus tropical upwelling yet.

### 1.1.2 Stratospheric ozone

The stratosphere is home to the ozone layer, which is essential for protecting Earth's surface from harmful UV radiation and thus crucial for guaranteeing life in its current form. The ozone layer is determined by chemical processes, but ozone is also transported by the stratospheric flow and thus its distribution is influenced by dynamics.

**Stratospheric ozone chemistry** The theory of formation and destruction of stratospheric ozone involving only oxygen reactions was first proposed by Sir Sydney Chapman (1930). These reactions are commonly known as the Chapman cycle and lead to a steady-state ozone concentration in the stratosphere. In the first step, highly energetic solar rays break one oxygen molecule ( $O_2$ ) apart, resulting in two oxygen atoms ( $2O$ ). If an oxygen atom reacts with another oxygen molecule, they combine and form an ozone molecule ( $O_3$ ) in a second step. Ozone is mainly produced in the tropical stratosphere. The photolysis of  $O_3$  leads to the formation of molecular and atomic oxygen. Ozone can also recombine with atomic oxygen, forming two oxygen molecules. This reaction is strongly temperature dependent and provides a loss for  $O$  and  $O_3$  (odd-oxygen).

The Chapman cycle alone overestimates the amount of ozone in the stratosphere, so other chemical reaction cycles that destroy ozone must exist. These ozone destroying processes are catalytic cycles, which can be very effective, as the substance that acts as catalyst is not consumed. Therefore, only small amounts are needed compared to the amount of ozone destroyed. The catalytic cycles relevant in the stratosphere are described in the following:

The hydrogen cycle involves the so-called  $HO_x$  species ( $HO_x = H + OH + HO_2$ ). Hydrogen is transported into the stratosphere in the form of methane ( $CH_4$ ), water vapour ( $H_2O$ ) and molecular hydrogen ( $H_2$ ). There, these substances are chemically converted into  $HO_x$  species. As most water vapour is 'freeze dried' in the very cold tropopause region, the oxidation of methane is the main source of water vapour in the middle and upper stratosphere. The  $HO_x$  cycle is the dominating cycle at high altitudes (44 to 50 km).

Nitrogen oxides ( $NO_x = NO + NO_2$ ) are produced in the stratosphere mainly by the photolysis of nitrous oxide ( $N_2O$ ), which has tropospheric sources and is transported into the stratosphere. The chemical loss of ozone by the  $NO_x$  cycle is important in the lower and *middle stratosphere*.

Note that reaction rates of the catalytic cycles are strongly temperature dependent, leading to slower ozone destruction with lower temperatures (Portmann and Solomon, 2007).

In addition to the hydrogen and nitrogen catalytic cycles, cycles involving halogen (i.e. chlorine, bromine and fluorine) compounds have become increasingly important in the past due to the anthropogenic emission of *chlorofluorocarbons (CFCs)*. These cycles involve species of the odd-chlorine ( $ClO_x = Cl + ClO + 2ClOOCl$ ) and odd-bromine ( $BrO_x = Br + BrO$ ) family. The total amount of chlorine in the stratosphere is about 160 times larger than the amount of bromine, however, bromine is important as well, as it is about 50 times more effective (per atom) in destroying ozone (WMO, 2007).

In the polar regions, where temperatures are sufficiently low, additional processes lead to very effective ozone depletion, so that ozone concentrations can drop to very low values in the lower stratosphere (known as the 'ozone hole'). The key ingredients for strong ozone depletion are polar stratospheric clouds (PSCs) that form at very

low temperatures, which are only reached in the polar regions in winter and early spring. Reactions of inactive chlorine reservoir species such as  $HCl$  and  $ClONO_2$  on the surface of PSCs (heterogeneous chemistry) lead to an increase in  $ClO$  abundance, so that additional catalytic cycles involving  $ClO$  and  $BrO$  can become active. The dominant additional catalytic cycles are the so-called  $ClO$ -dimer cycle (Molina and Molina, 1987) and the  $ClO-BrO$  cycle, and these cycles are typically responsible for 55% to 70% of spring-time ozone loss in the Antarctic stratosphere (WMO, 2007). For these cycles to be active, sunlight is required so they can only destroy ozone once the sun returns to the polar regions. Therefore, the strongest ozone loss is observed in late winter/early spring, when sunlight becomes available but temperatures are still low. The necessity of very low temperatures in conjunction with sunlight for strong ozone depletion to occur is also the reason for much weaker ozone loss observed in the Arctic than in the Antarctic lower stratosphere. The polar vortex in the Arctic is disturbed more by planetary waves, that are excited preferentially in the northern hemisphere, compared to its southern hemisphere counterpart, and thus temperatures are usually not as low. An additional effect of low temperatures and PSC formation is the sedimentation of solid particles containing  $HNO_3$  (denitrification). As  $HNO_3$  acts to deactivate chlorine upon the return of sunlight, denitrification leads to even more effective ozone depletion in Antarctica. More details on ozone chemistry and other relevant processes can be found in Brasseur and Solomon (2005).

**Long-term changes in ozone** The stratospheric ozone layer is strongly affected by anthropogenic influences on the climate system. The most prominent and well-studied phenomena is the strong ozone loss through anthropogenic emission of CFCs, leading to the 'ozone hole' (Farman et al., 1985). The onset of ozone depletion is commonly dated back to some time in the 1980s, but recent studies show that already since the 1960s ozone was depleted by enhanced CFC concentrations (WMO, 2010). Thanks to the Montreal Protocol and its amendments and adjustments<sup>3</sup>, which regulates the emission of ozone depleting substances (mainly CFCs), the halogen loading of the stratosphere is expected to retreat again in the future (WMO, 2007).

Extensive studies on the CFC-induced depletion of ozone have been performed in the past on the basis of both observations and numerical models. The current state of knowledge is summarised every four years in the World Meteorological Organisation's ozone assessment (most recently in WMO, 2007). While the depletion of ozone by halogens in the past is well understood, the projection of the future development of the ozone layer is still a major challenge (Austin et al., 2010b). The ozone layer is not only affected by CFCs, but also by changes in the stratosphere related to the enhanced concentrations of GHGs, i.e. by 'climate change'. In the future, effects of decreasing CFC concentrations act at the same time as climate change, which makes the projection

---

<sup>3</sup>The 'Montreal Protocol on Substances That Deplete the Ozone Layer' that has been active since 1989 controls the emission of ozone depleting substances.

and assignment of future changes more challenging. As policy makers are interested in the impacts of the Montreal Protocol on ozone, it is a major scientific task to untangle the effects of CFCs from climate change in order to assess the impact of reduced CFC concentrations and thus the success of the Montreal Protocol.

In order to model past and future developments of the ozone layer, stratosphere-resolving CCMs with fully coupled chemistry schemes are used. The latest simulations with currently available CCMs project total ozone to recover in the 21st century in most regions of the atmosphere, but the return date of ozone to 1980 values depends strongly on latitude (Austin et al., 2010a). Austin et al. (2010a) showed that total ozone values in middle and high latitudes recover to 1980 values in the middle of the 21st century, with return dates in the northern hemisphere about 10 years prior to the southern hemisphere. In the tropics, on the other hand, ozone is projected to never return to 1980 values throughout the 21st century, but to retreat further. The return dates of stratospheric chlorine, on the other hand, are about the same throughout the stratosphere. Thus there is a difference between return dates of ozone and chlorine. It is known that this is due to the influence of enhanced GHG concentrations, and it has been shown by Eyring et al. (2010) that the recovery of ozone would indeed follow the retreat of CFC concentrations, were it not for the influence of climate change.

Climate change will lead to a reduction of stratospheric temperatures through radiative cooling with enhanced GHG concentrations. Also, the dynamically driven circulation of the stratosphere is subject to changes, and, as discussed above, models project the BDC to strengthen. The cooling of the stratosphere is expected to influence ozone chemistry, as reaction rates are temperature dependent, and ozone concentrations are expected to increase in a cooler stratosphere (e.g. Rosenfield et al., 2002). In the polar regions, however, lower temperatures might lead to more efficient ozone destruction, which would delay ozone recovery. The changes in the BDC, on the other hand, are expected to affect ozone by changes in transport (e.g. Oman et al., 2010), but so far it is not clear how important this effect is compared to the changes in chemistry.

## 1.2 Thesis Objectives and Outline

The work presented here aims to deepen the understanding of the processes responsible for the long-term changes in the meridional circulation in the stratosphere and its impact on the stratospheric ozone layer.

As described in section 1.1.1, the drivers of tropical upwelling in the lower stratosphere are not yet fully understood. As upwelling is projected to intensify by most models, it is crucial to understand the processes that drive upwelling. Is it wave forcing in the tropics, as suggested by recent studies (see above) that drives upwelling in the lower stratosphere? Can this explain the annual cycle in upwelling and thus tropopause temperatures? And if it is wave forcing, which kinds of waves are responsible for the wave driving and where do they originate? Ultimately, the question is what controls

the strength of tropical upwelling in the lower stratosphere in the past and in the future. The major aim of this work is to quantify, attribute and explain changes in the meridional circulation.

With changes in the meridional circulation in the stratosphere, the question arises as to how transport of trace gases, in particular ozone, will be affected. As discussed above, various factors will influence ozone in the future and it is essential to be able to attribute ozone changes to the relevant processes. In particular, the impact of changes in transport on ozone has so far mostly been qualitatively discussed, but not quantified (e.g. Eyring et al., 2010; Oman et al., 2010). In this work, a method is developed that allows to quantify the respective effects of transport and chemistry on ozone. Therefore, the question on how important changes in the BDC and thus transport are for future ozone changes can be answered.

These questions are addressed on the basis of simulations with a CCM. The strategy of this work is to analyse and try to understand the results from one model in depth, and gain a complete picture of this specific modelled atmospheric system. Even though the current work is almost entirely based on simulations with a single model, and thus the conclusions are limited to the ability of the model to simulate the real atmosphere, it is important to understand the processes that lead to changes in one consistent model system. As the data basis to analyse changes in the BDC from observations is hardly sufficient, it is important to understand why and where models do show changes due to two reasons: a) in order to know in which parameters similar changes could be detected in observations (i.e. know where we have to look for changes), and to b) understand why changes are not apparent in observations so far (see discussion above). Even if it would turn out that the strengthening of the circulation is not happening in reality, understanding the strengthening in the models would allow to detect model deficits and improve modelling capabilities.

This work is structured into four main chapters, each addressing a question on the changes in the meridional circulation in the modelled system used here:

**Chapter 3: WHAT kind of changes occur?** Firstly, it is important to quantify the changes in the particular model system used in this study. In this chapter, the long-term changes in the meridional circulation in the *transient* simulations are diagnosed.

**Chapter 4: WHY do these changes occur?** As the modelled system is driven by prescribed boundary conditions, any (deterministic) changes observed in the modelled atmosphere must stem from changes in the boundary conditions. This chapter aims to identify the causes of changes in the meridional circulation by analysing the separate effects of changes in various boundary conditions on the atmosphere.

**Chapter 5: HOW are these changes induced?** Even if the drivers and causes of

changes in the circulation are known, the processes that transfer the signal in the atmosphere are not necessarily easily accessible. In this chapter, the processes that drive the meridional circulation and changes therein are examined.

**Chapter 6: What are the IMPACTS of circulation changes on ozone?** After diagnosing and explaining the changes in the meridional circulation in the previous chapters, the impacts of these changes on transport of ozone are analysed here. This requires the development of a method that can be used to separate the effect of transport changes on ozone.

Preceding these main chapters, a description of the model system and the simulations used is given in Chapter 2. The thesis is completed with a conclusion on the main findings and an outlook for further work.



## Chapter 2

# Model description and simulation set-ups

### 2.1 Model description of E39CA

In this study, the CCM ECHAM4.L39(DLR)/CHEM/ATTILA (E39CA) is used. E39C is based on the spectral general circulation model ECHAM4.L39(DLR) (Land et al., 2002) and the chemistry-module CHEM (Steil et al., 1998). The spectral horizontal resolution of the model is T30, corresponding to approximately  $3.75^\circ \times 3.75^\circ$  on the transformed latitude-longitude grid. In the vertical, the model consists of 39 layers, extending from the surface to the uppermost layer which is centred at 10 hPa. The model is an updated version of ECHAM4.L39(DLR)/CHEM (E39C) (Hein et al., 2001; Dameris et al., 2005) with the former semi-Lagrangian advection scheme replaced by the fully Lagrangian advection scheme ATTILA (Reithmeier and Sausen, 2002). The mass of the model atmosphere is divided into approximately 500 000 air parcels of equal mass which are advected three-dimensionally using the actual model wind field. The use of the fully Lagrangian advection scheme ATTILA for tracer-transport improved the model performance substantially (Stenke et al., 2008; Stenke et al., 2009). The chemistry module CHEM is based on a generalised family concept and includes homogeneous and stratospheric heterogeneous ozone chemistry and the most relevant chemical processes for describing the tropospheric background chemistry. Orographic gravity wave drag is parameterised following Miller et al. (1989). Since non-orographic gravity waves are mainly important for the momentum balance in the upper stratosphere, the low upper boundary of the model (10 hPa) allows to neglect non-orographic gravity wave drag. For more details on E39CA, see Stenke et al. (2009).

The model version used here took part in the recent extensive inter-model comparison and evaluation project CCMVal-2 (SPARC-CCMVal, 2010). Overall, the performance of E39CA significantly improved compared to the predecessor version (E39C) due to the transition from a semi-Lagrangian to a fully Lagrangian transport scheme (see also Stenke et al., 2008; Stenke et al., 2009). It was found, that while the model

still has some dynamical biases especially in the middle stratosphere (presumably caused by the 10 hPa upper layer), it has an overall good performance in the upper troposphere/lower stratosphere, and simulates transport in this region well (SPARC-CCMVal, 2010; Gettelman et al., 2010; Hegglin et al., 2010). The good performance in this region is at least partly based on the very high vertical resolution between 400 hPa and 100 hPa with 16 model levels, i.e. pressure level intervals of as little as 15-20 hPa. As this study focuses on processes in the lower stratosphere and upper troposphere, the model is well suited for this purpose.

## 2.2 Simulation set-ups

A series of simulations with the CCM E39CA was designed and performed, and an overview of all simulations used in this study is given in Fig. 2.1 in a time-line diagram. The simulations include *transient* experiments, in which the temporal evolution of the atmosphere is simulated (REF-B1 and SCN-B2d; described in Sec. 2.2.1). In addition, simulations that resemble the state of the atmosphere at a certain point in time, i.e. with constant boundary conditions (so-called *time-slice simulations*) are performed, and indicated in the overview diagram with 10-year time slots. These simulations are described in Sec. 2.2.2. At the bottom of Fig. 2.1, two bars labelled 'PAST' and 'FUTURE' are shown. This division of the whole simulation period into the sub-periods from 1960 to 1999 ('past') and into 2000 to 2049 ('future') is used for the analysis in the following. This definition stems from the transition from observed to projected boundary conditions in the transient experiments in year 2000 (see below).

### 2.2.1 Transient simulations

The set-up of the transient simulations used in this study corresponds to the REF-B1 and the SCN-B2d scenario as defined for the next WMO ozone assessment (Eyring et al., 2008). The REF-B1 simulation is designed to closely resemble the climate of the past, while the SCN-B2d simulation is designed to model past and future development of the atmospheric system in a consistent manner. REF-B1 spans the period 1960 to 1999, and SCN-B2d spans years 1960 to 2049 (both following a 10 year spin-up). Both simulations include natural as well as anthropogenic forcings, which are described in the following.

In REF-B1, boundary conditions are deduced from observations. The sea surface temperatures (SSTs; including sea ice coverage) are given as monthly means from the HadISST1 data set provided by the UK Met Office Hadley Centre (Rayner et al., 2003, available via <http://hadobs.org/>). The data set is based on merged satellite and in situ observations.

The natural boundary conditions, namely the 11-year solar cycle, the quasi-biennial oscillation (QBO) and sulphate aerosol loadings and radiative effects of major volcanic

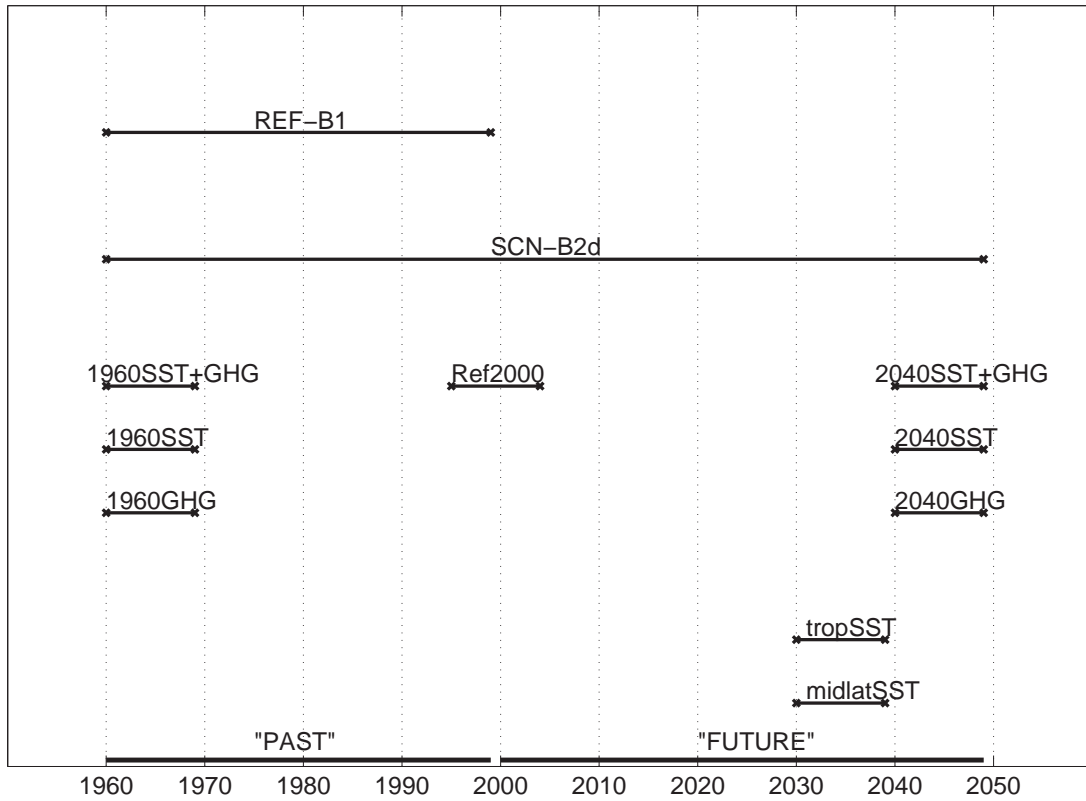


**Figure 2.1:** Overview of the simulations used in this study.

eruptions are prescribed to resemble observed natural variability. The QBO is forced by a linear relaxation ('nudging') of the zonal winds in the equatorial stratosphere to observed equatorial wind profiles. This assimilation is applied equatorwards of  $20^\circ$  latitude from 90 hPa up to the model top layer. The relaxation time scale is set uniformly to 7 days within the QBO core domain above 50 hPa and between  $10^\circ$  N and  $10^\circ$  S. Outside the core region the relaxation time depends on latitude and pressure (Giorgetta and Bengtsson, 1999). The influence of the 11-year solar cycle on photolysis is parameterised according to the intensity of the 10.7 cm radiation of the sun (Lean et al., 1997, data available via <http://www.drao.nrc.ca/icarus/www/daily.html>). The three major volcanic eruptions (Agung 1963, El Chichon 1982 and Pinatubo 1991) are taken into account through enhanced stratospheric aerosol abundances and additional radiative heating. The data set for the sulphate aerosol surface area densities follows satellite measurements and the additional heating rates are deduced from observations and model simulations (for more information on the volcanic parameters see Stenke et al., 2009).

The concentrations of long-lived greenhouse gases ( $CO_2$ ,  $CH_4$ ,  $N_2O$ ) are based on the values given by IPCC (2001), and concentrations of chlorofluorocarbons (CFCs) are prescribed following WMO (2003). The temporal evolution of GHGs and CFCs as prescribed in the simulations is shown in Fig. 2.2. Nitrogen oxide ( $NO_x = NO + NO_2$ )

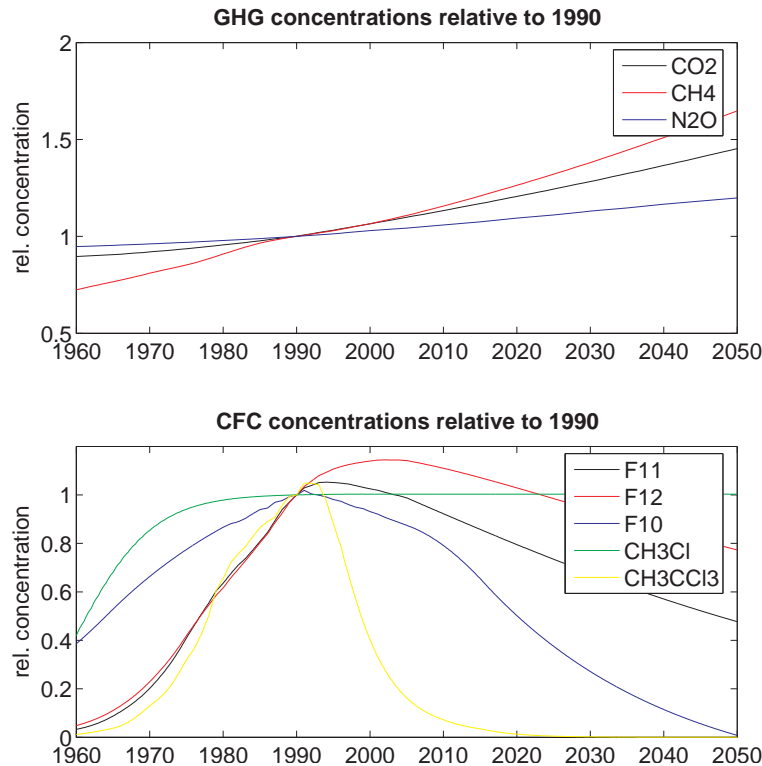


**Figure 2.2:** Temporal evolution of GHGs (top) and CFCs (bottom) as prescribed in the transient simulations. Shown are the global mean concentrations scaled to 1990 values.

emissions from several natural (lightning, biomass burning, soils) and anthropogenic (industry, aircraft, ships, surface transportation) sources are considered in the model simulation.  $NO_x$  emissions from lightning, soils, ships and aircraft follows the description in Dameris et al. (2005).  $NO_x$  emissions from industry, biomass burning and surface transportation are based on the RETRO emission inventory.

The SCN-B2d simulation, which spans years 1960 to 2049, is set up in the same way as the REF-B1 simulation for years 1960-1999 except for the prescribed SSTs. After 1999, the boundary conditions for the SCN-B2d simulation follow future scenarios. Instead of the HadISST1 data set, SSTs and sea ice in SCN-B2d are taken from the HadGEM1 general circulation model (Martin et al., 2006; Johns et al., 2006). The SSTs for 1960 to 1999 are from the HadGEM1 transient simulation with anthropogenic forcing only (Stott et al., 2006, 'ANTHRO' in their Table 1), i.e. excluding volcanic eruptions and the solar cycle. The future SST projections used for SCN-B2d (years 2000 to 2049) are from the SRES A1B run of HadGEM1, which is initiated from ANTHRO so that a consistent SST data set is obtained. These HadGEM1 simulations are part of the World Climate Research Programme's (WCRP's) Coupled Chemistry Climate Intercomparison Project phase 3 (CMIP-3) multimodel dataset used for the 4th Intergovernmental Panel on Climate Change (IPCC) Assessment Report and were provided by the Program for Climate Model Diagnosis and Intercomparison (PCMDI,

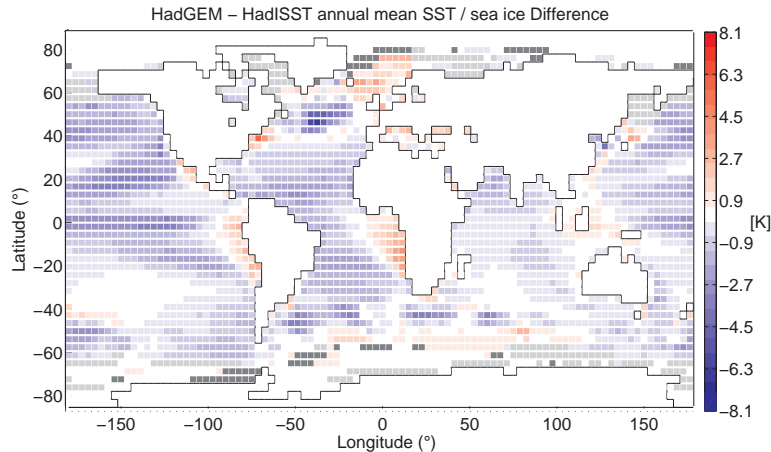


**Figure 2.3:** Difference of 1960 to 1999 annual mean sea surface temperatures [in K] from HadGEM minus HadISST. Differences in sea ice extent are shown in grey, where light grey areas correspond to more sea ice in HadGEM compared to HadISST, and dark grey regions to less sea ice in HadGEM. Here and in the following: positive latitudes denote 'degree north', negative latitudes denote 'degree south'.

available at [www-pcmdi.llnl.gov](http://www-pcmdi.llnl.gov)).

The natural boundary conditions in the future are extrapolated by repeating the solar cycle (from 1977 to 2007) and the QBO (from 1956 to 1999) periodically. It is assumed that no volcanic events are occurring in the future. The concentrations of long-lived greenhouse gases and natural as well as anthropogenic  $NO_x$  emissions follow the SRESA1B scenario given by IPCC (2001). The loading of ozone depleting substances (mainly CFCs), are based on the A1 scenario defined in WMO (2007) including the adjustments described in Eyring et al. (2008) ('adjusted A1 scenario').

After the initial spin-up period of 10 years in both simulations the equilibrium state is reached sufficiently well so that all variability and trends after 1960 are either forced by the prescribed boundary conditions or are due to internal variability of the atmospheric system. This is verified with water vapour at the uppermost model level (10 hPa), which shows an adjustment time to the underlying SSTs of about 6-7 years (not shown).

A comparison of the HadGEM1 and HadISST SST climatologies for the past is shown in Fig. 2.3 (see also Johns et al., 2006). The difference pattern is dominated by lower SSTs in HadGEM1 in the tropics, the subtropics and northern mid-latitudes, where the differences are up to 3 K. Smaller regions of higher SSTs in HadGEM1 are found on the west coasts of South America and Africa, as well as on the east coasts of North America and Asia in northern winter (i.e. the storm track regions). There are also large differences in sea ice extent, with generally more sea ice in HadGEM1. Time series of anomalies of global and hemispheric mean SSTs from HadISST and HadGEM1 are compared in Fig. 2.4. Both the global mean and southern hemisphere mean SSTs

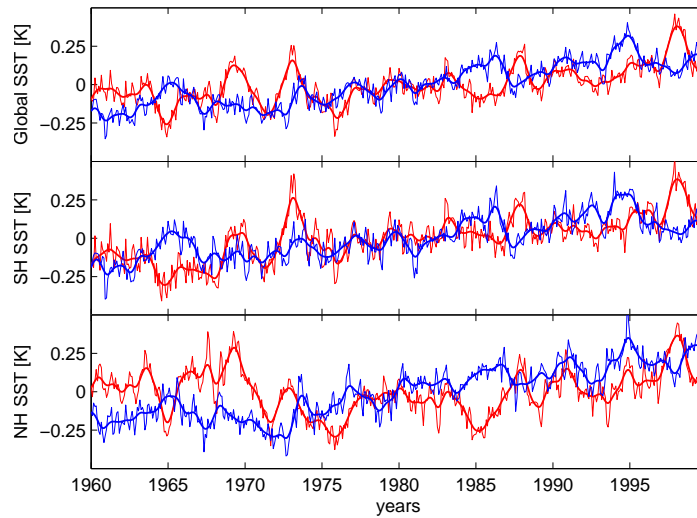


**Figure 2.4:** SST time series with the 1960-1999 mean annual cycle subtracted for REF-B1 (red) and SCN-B2d (blue) for global (top), southern (middle) and northern (bottom) hemisphere means. The thick solid lines are smoothed time series (by applying a 1-2-1 filter 20 times).

show generally rather constant values in the 1960s, and rising SSTs since about the mid-70s. However, in the northern hemisphere the SST data set deduced from observations show generally higher SSTs in the 1960s, a strong decrease in the 1970s and rising temperatures only after the late 1970s. The modelled time series does not reproduce this behaviour, here SST anomalies are negative throughout the 1960s. In terms of variability, the interannual variance due to the El Niño-Southern Oscillation (ENSO) is underestimated and the ENSO signal is too regular in the HadGEM1 model (Johns et al., 2006). A detailed study of annual and decadal variability of SST eigenmodes from both observations and several GCMs including HadGEM1 revealed large deficits of the models to capture the variability, and showed that the patterns are less persistent than in reality (Newman, 2007).

### 2.2.2 Sensitivity simulations

In addition to the transient simulations, multiple sensitivity simulations were performed. These simulations were run in the so-called *time-slice* mode, i.e. the mean climate state of one period is simulated by keeping the boundary conditions constant (only varying intra-annual). Each of the simulations spans 20 years, following a 5 year spin-up.

**Reference simulation.** As reference simulation, the mean state of the year 2000 was simulated, fixing boundary conditions at values representative for the year 2000. The

**Table 2.1:** Listing of the sensitivity simulations used in this study with the corresponding year of the GHG concentration and the SSTs used as boundary conditions. All other boundary conditions are identical as in the Ref2000 simulation (see text).

Run	GHGs	SSTs
Ref2000	2000	mean 1995-2004
1960GHG	1960	mean 1995-2004
1960SST	2000	mean 1960-1969
1960GHG+SST	1960	mean 1960-1969
2040GHG	2040	mean 1995-2004
2040SST	2000	mean 2040-2049
2040SST+GHG	2040	mean 2040-2049
tropSST	2000	mean 1995-2004 + anomaly
NHSST	2000	mean 1995-2004 + anomaly

prescribed SSTs are the 10-year climatological mean over 1995 to 2004 of the HadGEM SSTs. The simulation includes QBO nudging, with the cycles of years 1990 to 2009. The solar activity is held constant at a mean value.

**SST and GHG simulations.** A set of sensitivity simulations was performed in which only the lower boundary condition (SSTs) or only the long-lived GHG concentrations ( $CO_2$ ,  $CH_4$  and  $N_2O$ ) were changed. All other boundary conditions (e.g. CFC concentrations) remained as in the 2000 reference simulation. The disturbances were chosen to resemble mean conditions of the decades 1960-69 and 2040-49, i.e. the first and last decade of the transient simulation. A listing and details of the sensitivity simulations is given in Table 2.1.

**Idealised SST simulations.** Two additional, rather idealised sensitivity simulations were performed in order to quantify the effect of non-global changes in SSTs. In one simulation, SSTs were changed in the tropics only while in the other simulation changes in the SSTs in northern mid-latitudes were made. To capture the changes in SSTs that possibly drive long-term trends in the atmosphere, a mean trend in SSTs over years 1970-1999 was calculated for each month and added to the SSTs used in the reference time-slice simulation (Ref2000). The period from 1970 to 1999 was chosen because the increase in SSTs was weak in the 1960s compared to later decades (see Fig. 2.4). The mean trend was calculated by averaging over linear trends of 10 episodes of 20 years each from 1970-1989 to 1980-1999. In the tropical SST simulation, for latitudes of  $16.7^\circ S$  to  $16.7^\circ N$  the trend was added fully to the reference SSTs, while between  $20.4^\circ N/S$  and  $31.5^\circ N/S$ , the anomaly was added with a decreasing weight from 1 to 0. Additionally, a moving average smoothing function was applied to the anomaly field.

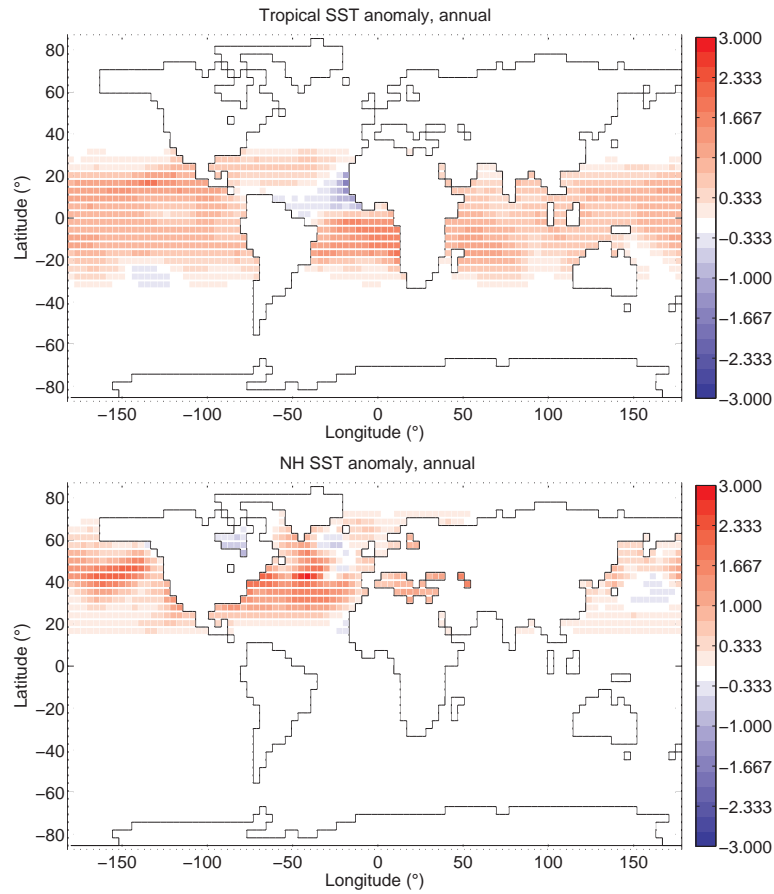


**Figure 2.5:** Annual mean anomalies in SSTs in K prescribed in the trSST (top) and NHSST (bottom) simulations.

In the mid-latitude SST simulation, the core region with a full anomaly spans from  $61.2^{\circ}\text{N}$  to  $31.5^{\circ}\text{N}$  and the 'sponge region' with decreasing percentage of the anomalies from  $64.9^{\circ}\text{N}$  to  $72.4^{\circ}\text{N}$  and from  $27.8^{\circ}\text{N}$  to  $16.7^{\circ}\text{N}$ . The anomalies at gridpoints where ice occurred in any years were assigned with a value of zero (since there the trend calculation is not correct). The anomaly pattern in SSTs of these simulations are shown in Fig. 2.5.

## Chapter 3

# Diagnosing changes in the meridional circulation

Simulations that are designed to resemble past climate and project possible future climate developments are performed with the chemistry-climate model E39CA. These transient simulations are used here to diagnose the state and the temporal development of the stratospheric meridional circulation. Firstly, the temporal evolution of the dynamical background in terms of temperature and zonal wind is analysed, since changes in the dynamical background state and the meridional circulation are closely coupled. To quantify the BDC, the residual meridional circulation as defined in the transformed eulerian mean concept (see Appendix B) is used. In addition, changes in this diagnostic are compared to changes in age of air.

### 3.1 Background state

Long-term trends in temperature and zonal wind are calculated from the REF-B1 and SCN-B2d simulations by applying a linear least square regression (see Appendix C). Fig. 3.1 shows the seasonal trends in temperature for past and future. As expected from GHG induced radiation effects, tropospheric warming and stratospheric cooling occurs in the modelled atmosphere. During all seasons, increases in temperature maximise in the tropical upper troposphere. The rate of tropospheric warming is generally higher in the future than in the past, which can be explained by the delay of the warming of the ocean (before about 1970 SSTs do not show a positive trend, see Fig. 2.4). In the lower and middle stratosphere, on the other hand, the cooling rates do generally not increase in the future compared to the past, but rather decrease. This is also as expected as ozone depletion in the second half of the 20th century leads to additional cooling of the stratosphere, while the recovery of ozone in the 21st century counteracts the GHG-induced cooling. Note that in the upper stratosphere, which is not captured by the model used here, the effect by GHGs is expected to dominate over the CFC-related temperature changes and thus cooling rates do not decline in the future compared to

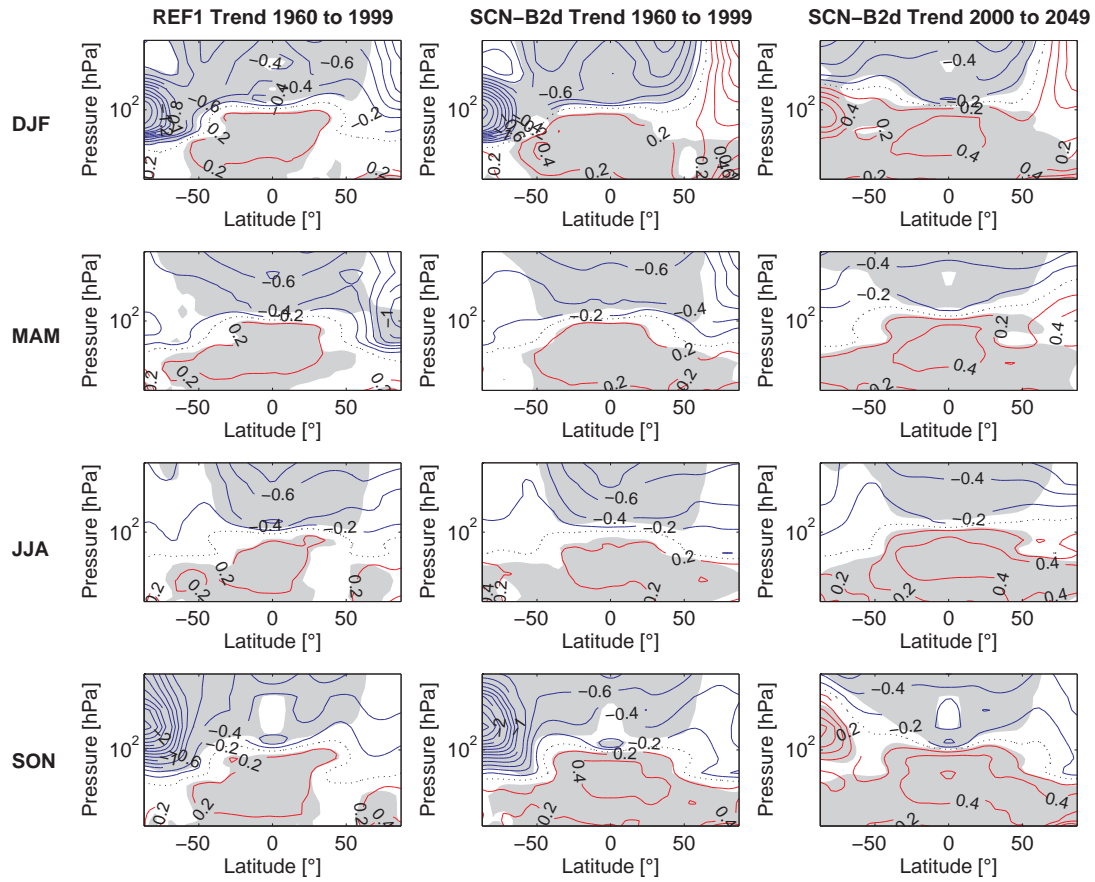


**Figure 3.1:** Linear trends in temperature in [K/dec] for 1960 to 1999 in REF-B1 (left), the same period in SCN-B2d (middle) and for 2000 to 2049 in SCN-B2d (right). The four panels show the trends for DJF, MAM, JJA and SON (top to bottom). Grey shading denotes significance on the 95% level.

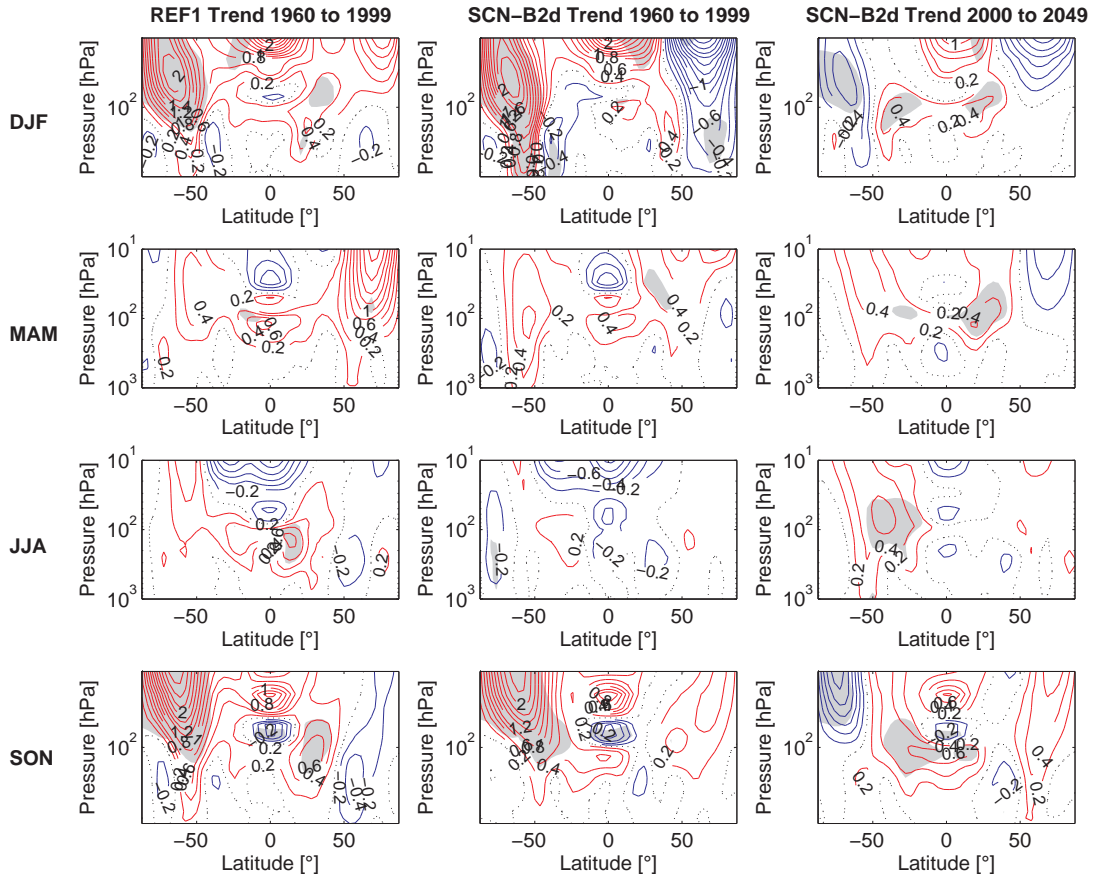


**Figure 3.2:** As in Fig. 3.1 but showing the linear trends in zonal winds in [m/s/dec].

the past. The effect of ozone depletion on temperature can also be seen clearly in the Antarctic lower stratosphere, where strong cooling takes place in spring and summer in the past, followed by warming in the future. Temperature trends in the Arctic are generally not significant due to the high interannual variability.

The linear trends in zonal mean zonal winds are calculated like the temperature trends and shown in Fig. 3.2. The most prominent feature in linear trends in zonal winds is the strengthening of the southern hemisphere polar jet in southern spring and summer for the period 1960 to 1999. In the future, the trend in the polar jet is reversed but decreases with a weaker rate. This is consistent with the temperature trends in southern high latitudes, since due to thermal wind balance changes in the meridional temperature gradient must induce changes in the zonal winds. In most seasons in the past, and more consistently in the future, positive trends in zonal wind in the region of the subtropical jets are apparent, suggesting a strengthening of the subtropical jets <sup>1</sup>. This strengthening of the jets can also be understood from thermal wind balance, as the temperature increase is strongest in the tropics and hence the meridional temperature

<sup>1</sup>Even though the QBO is accounted for in the regression used to determine the trends, remnants of it remain and the interpretation of zonal wind trends in the tropical stratosphere are critical.

gradient increases.

As the boundary conditions from REF-B1 and SCN-B2d differ only in the prescribed SSTs for 1960 to 1999, the comparison of the two simulations in this period reveals the influence of using different SST data sets on the climatology and on long-term trends. The modelled SSTs used in SCN-B2d have a relatively large cold bias (see Chapter 2), which leads to differences in climatological temperatures in the troposphere of up to 1.5 K (not shown). However, the crucial question is whether the long-term trends are comparable in the two simulations. If this was not the case, long-term projections, which are bound to use modelled SSTs, would be very questionable. As can be seen from Fig. 3.1 the trend pattern in temperature of the two transient simulations are very similar. In the annual mean, the temperature trends are significantly different (on the 95% level) only in the northern hemisphere mid-latitudes in the troposphere, consistent with weaker SST trends in the mean over the northern hemisphere in the HadISST data compared to HadGEM1. Trends in zonal mean winds are generally hardly significant in the past except for the southern polar stratosphere, where both simulations agree in the strong increase in the polar jet. The significant increase in the subtropical jet of the northern hemisphere in JJA and SON in REF-B1 is not apparent in SCN-B2d. As tropical temperatures and thus the subtropical jets are strongly influenced by tropical SSTs (see also later chapters), differences in the temporal evolution of the tropical SSTs in the two simulations are likely to cause this discrepancy in zonal wind trends.

## 3.2 Mean tropical upwelling

Mean upwelling in the tropics is commonly used as a diagnostic to quantify the strength of the meridional circulation. Tropical upwelling is calculated as mass-weighted integral of upward motion over the latitudes in which the vertical velocity point upward. Thus, tropical upwelling as calculated here gives the total mass flux of the upward branch of the residual circulation at each pressure level (for details on the calculation see Appendix B).

Linear trends in tropical upwelling calculated over the whole period 1960 to 2049 based on the SCN-B2d simulation are shown as a function of height in Fig. 3.3. The strongest signal with trends up to 3% per decade appears at levels around 150 hPa and is apparent in all seasons. Above 100 hPa a significant strengthening occurs mainly in SON and less so in DJF, and these seasons show similar behaviour with increases in tropical upwelling throughout the stratosphere. In JJA, on the other hand, the trend in upwelling is close to zero above 100 hPa and only becomes positive and significant again for the uppermost model layer.

To investigate the temporal evolution of tropical upwelling, in Fig. 3.4 timeseries from REF-B1 and SCN-B2d are shown for pressure levels of 131 hPa (where the strongest relative trend occurs) and at 76 hPa and 10 hPa.

In SCN-B2d, positive trends in upwelling are apparent in the lower stratosphere/

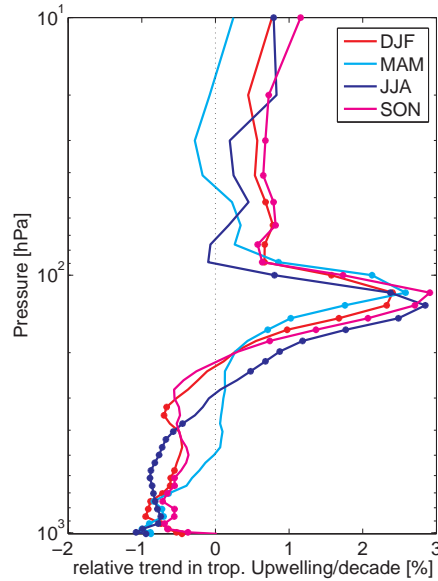


**Figure 3.3:** Relative trends in tropical upwelling [%/dec] from SCN-B2d over 90 years (1960 to 2049) for all seasons. Levels where the trend is statistically significant on the 95% level are indicated with a dot.

upper troposphere in all seasons. The trends remain similar in terms of magnitude in the future compared to the past period. Only in JJA, the trend is weaker in the first 40 years and increases in strength afterwards. In the REF-B1 simulation, the trend is as well positive but is significant only for JJA, contradicting the results for SCN-B2d, where JJA is the only season where the trend is not significant in the past. Note that the overall magnitude in upwelling in REF-B1 is slightly higher than in SCN-B2d, and also the variability is higher which leads to non-significant trends even though the magnitude of the trends is similar. This difference in mean upwelling and its variability can be explained by the difference in the prescribed SST data set. The modelled SSTs prescribed in SCN-B2d have a general cold bias, and the variability especially in the tropics is underestimated. As will be shown later on (Chapter 4) tropical SSTs are essential in determining the strength of tropical upwelling in the lower stratosphere, so that the difference in the prescribed SSTs does translate to the difference in tropical upwelling.

At 76 hPa, statistically significant trends over the 90 years of the SCN-B2d simulation occur in DJF and SON. The trends in SON are similar for past and future while in DJF, changes are stronger in the past than in the future. In MAM, tropical upwelling increases in the past period only, and for JJA no trend in upwelling is apparent for any period. In the REF-B1 simulation, trends are not significant in all seasons over the 40 years of simulation. However, in DJF a decrease over the first 20 years and an increase afterwards can be seen. The initial decrease in upwelling leads to a not-significant trend over the whole period.

At the uppermost model level, tropical upwelling increases significantly in JJA and

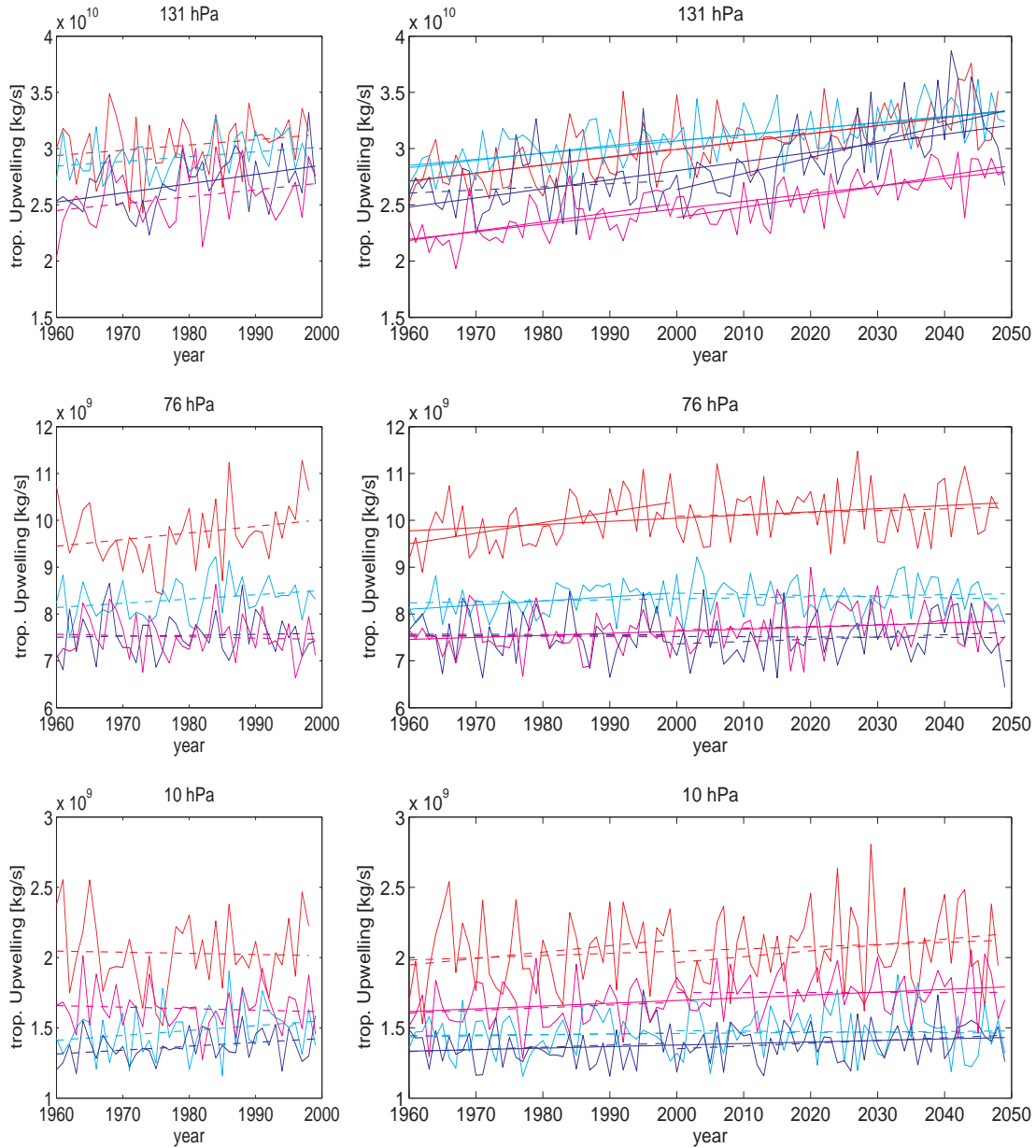


**Figure 3.4:** Timeseries of tropical upwelling at three pressure levels for REF-B1 (left panels) and SCN-B2d (right panels). The colours represent the seasons as in Fig. 3.3, i.e. DJF (red), MAM (cyan), JJA (blue) and SON (magenta). Linear Trends are shown together with the timeseries for different periods as solid lines for significant trends, otherwise dashed lines.

SON over 90 years in the SCN-B2d simulation, but trends are not significant for shorter periods in neither simulation. As noted above, the significant increase in JJA is confined to the 10 hPa level while during SON upwelling increases significantly throughout the stratosphere.

### 3.3 Residual circulation

The meridional circulation is quantified by the residual circulation from the TEM equations (see Appendix B), and trends are calculated using linear regression (see Appendix C) for each gridbox in the latitude-pressure plane. With this method, the patterns of changes in the meridional circulation can be identified.

The climatology of the residual circulation is shown together with its trends calculated for each season in Fig. 3.5. The seasonality with a stronger and wider circulation in the winter hemisphere and a weaker and shallower circulation cell in the summer hemisphere can be seen clearly from the climatologies.

The pattern in circulation changes found in most seasons both for future and past is an increase in upwelling around the equator in the lowermost stratosphere, consistent with the trends found in net tropical upwelling in the last section. The change in the circulation is mostly confined to the lowermost stratosphere. The increased upwelling, which occurs symmetrically around the equator, is balanced by downwelling at about 20-40° latitude. In the trend calculated over the whole simulation period of SCN-B2d it appears that the increase in the circulation is confined to below about 70 hPa in the summer hemisphere but extends to higher levels in autumn and winter in the northern and southern hemisphere, respectively. The significant increase in tropical upwelling extending up to the model top in SON seen in Fig. 3.3 is consistent with the increase in the circulation cell in the northern hemisphere in SON. Even though not significant for the past, the pattern remains similar for the different periods and simulations.

In the southern hemisphere in DJF, a strong hemisphere-wide increase in the circulation occurs in the past for both simulations and is counteracted by a decrease in the future period. This is in agreement with the trend in tropical upwelling at 76 hPa (see Fig. 3.4), which is strong for the past but almost zero for the future. In the future, a positive trend in the northern hemisphere seems to be counteracted by the decrease in circulation strength in the southern hemisphere so that the overall trend in upwelling is close to zero.

In the past period, the trend pattern in REF-B1 and SCN-B2d are fairly similar in MAM, JJA and SON.

In DJF, however, in SCN-B2d the increase in the northern hemisphere extends up to the top of the model domain (but is not significant), while in REF-B1 the strength of the residual circulation is rather decreasing. As noted for the tropical upwelling timeseries in the last section, upwelling decreases in the first half of the REF-B1 simulation and increases only in the second half. These decadal variations result in the differences

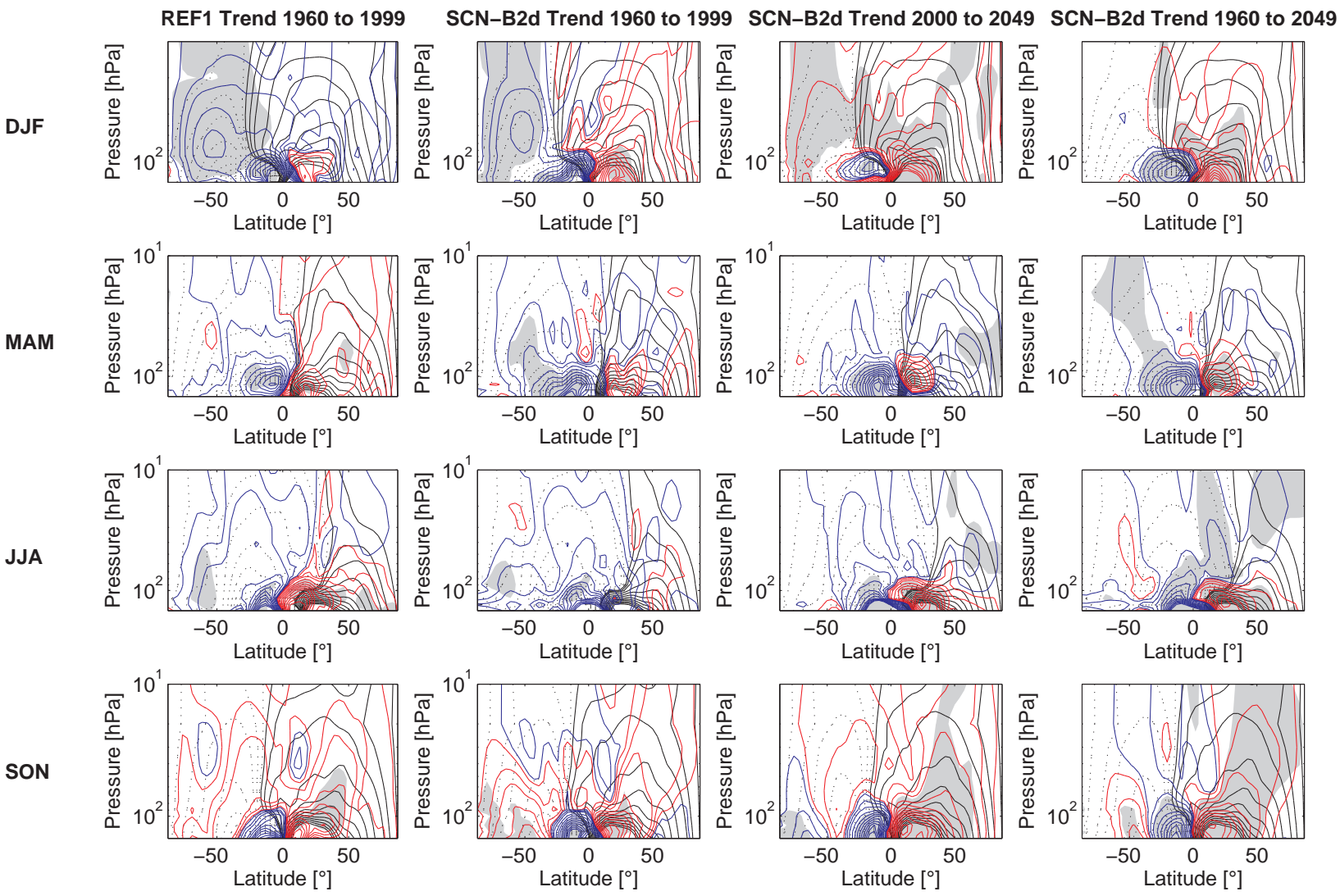


**Figure 3.5:** Climatology of the residual mass-weighted streamfunction (in black contours, solid for positive, dashed for negative values, contour interval  $1 \times 10^9 \text{ kg/s}$ ) and its trends (red contours for positive, blue for negative values, interval  $5 \times 10^6 \text{ kg/s/yr}$ ) for different periods and seasons as denoted by the labels. Grey shading denotes significance on the 95% level.

between the two simulations in the trends calculated over the past period. In Garny et al. (2009), the causes of the different temporal behaviour of the tropical upwelling timeseries were investigated and it was found that the negative trends in upwelling in years 1960 to 1979 in REF-B1 originates from wave flux trends indicative of less planetary wave generation in the extratropical troposphere. The period of decreases in wave fluxes in the troposphere coincides with a decrease in northern hemisphere mean SSTs over the same period. This suggests some evidence that the trend in upwelling is indeed forced by the SSTs and not an artefact of this particular realisation. However, one major problem of trying to attribute the changes to SST trends is the lack of understanding of how extratropical SST anomalies can affect the excitation of planetary waves (Kushnir et al., 2002). Peng et al. (1995) and Peng and Whitaker (1999) showed that the response to SST anomalies is highly sensitive to the background state, i.e. the response to the same anomaly might be of different nature for different month, but also appears different when using different models. Another possibility is that the extratropical anomaly in wave generation is forced by tropical SST variation. Unlike for the extratropics, the effects of tropical SST anomalies and namely of ENSO on extratropical waves (Ineson and Scaife, 2009), and subsequently modulation of the planetary wave flux into the stratosphere and the BDC (Hardiman et al., 2007; García-Herrera et al., 2006) are well studied. A detailed analyses of the response of the model atmosphere to ENSO showed that these relationships also hold in the simulations used here (Leuthold, 2010). In the mid-1970s, two strong negative ENSO events occurred, indicative of weakened wave activity. Leuthold (2010) showed that along with these ENSO events tropical upwelling was weakened. Therefore, modulation of extratropical wave activity by ENSO is likely to be the cause of the weak BDC in the 1970s in REF-B1. However, the deficit of only having one ensemble member of each model simulation available inhibits the attribution of the differences found in the trends to SST differences. The results can rather be seen as tests of robustness of the trends both against the SSTs and the internal variability.

### 3.4 Age of Air

Mean age of stratospheric air is an often used quantity that measures the time an air parcel spent in the stratosphere after entering it through the tropopause (e.g. Hall and Plumb, 1994). Age of air is thus a useful measure of transport processes, describing the integrated effect of the circulation on an air parcel since entering the stratosphere. However, not only the large-scale meridional circulation affects age of air, but also mixing of air masses (e.g. Hall and Plumb, 1994). In the present study the calculation of the age of air is not based on inert tracers like  $SF_6$  or  $CO_2$ , which are commonly used to determine age of air, but on the Lagrangian trajectories that are available from the advection scheme ATTILA. After a sufficiently long spin-up time (approx. 10 years) the age spectrum at a certain point in the stratosphere is simply calculated by sampling

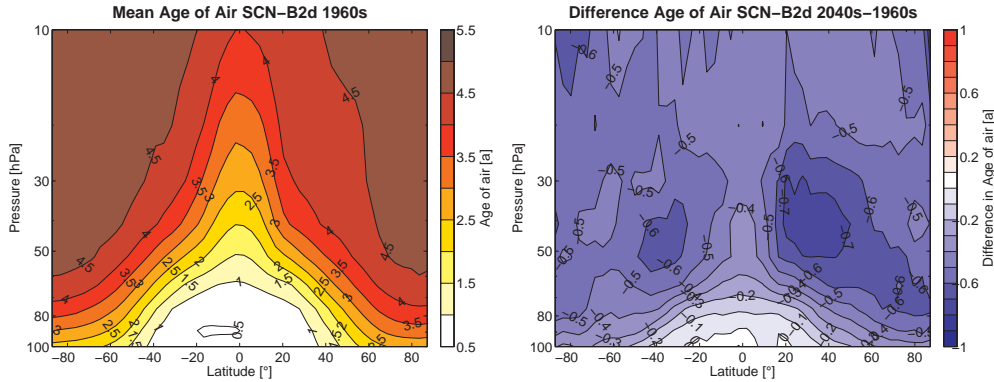


**Figure 3.6:** Mean age of air climatology from SCN-B2d for the 1960s (left) and the difference of the decades 2040s minus 1960s (right).

the trajectories around that point with respect to their transit time since entering the stratosphere. In order to calculate the mean age of air, each air parcel was furnished with a clock, which was held at zero in the troposphere and thus measured the time elapsed since an air parcel (in the stratosphere) crossed the tropopause.

The climatology of mean age of air from the SCN-B2d simulation is shown in Fig. 3.6. The well-known shape of relatively young air in the tropics and longest transit times to the polar stratosphere is apparent.

The difference in mean age of air between the decades 2040s and 1960s (right panel in Fig. 3.6) shows a decrease in the age of air in the entire stratosphere. The maximal decrease of about 0.7 years occurs around 50 hPa and 40° latitude in both hemispheres, with a larger difference in the northern than in the southern hemisphere. The general decline in age of air implies that the transport time from the tropopause to the stratosphere is decreasing in a changing climate. In the upper stratosphere, age of air is changing at a rate that is similar across latitudes and levels, implying that no local circulation change occurs here, but the air is younger due to the faster entry and transport in the lower stratosphere. However, an additional local maxima in the absolute change of age of air occurs in the polar stratosphere at 10 to 20 hPa, indicating faster transport from the tropics to high latitudes. Overall the changes in mean age of air are consistent with the changes in the residual circulation. Enhanced upwelling in the tropics and transport to the subtropics reflects in shorter transport times especially in the (sub-)tropical lower stratosphere. Even though the changes in the meridional circulation are largely confined to the lower stratosphere, age of air is reduced throughout the stratosphere as the reduction in transit time in the lower stratosphere will reduce the age of air at any point in the atmosphere the air parcel travels to later on. The fact that the change in age of air is constant in most of the middle stratosphere also shows that transport is not changed here, but the reduction is a result of the faster transport in the lower stratosphere. As mentioned above, irreversible mixing processes also cause transport, and changes therein might also be important to changes of mean age of air.

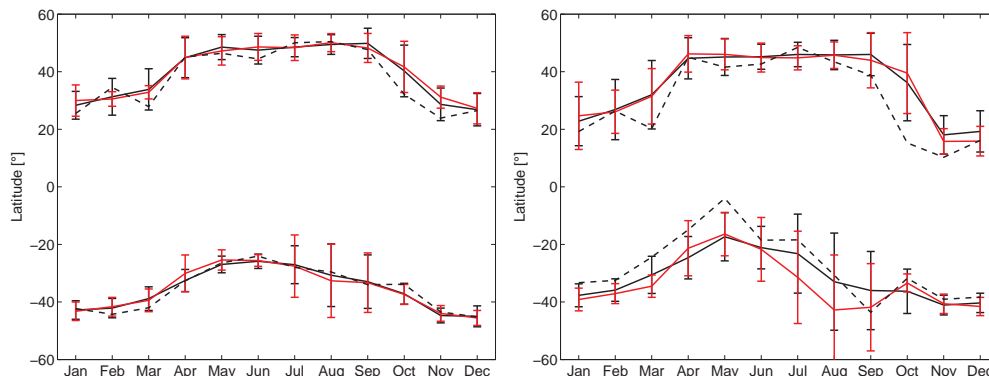


**Figure 3.7:** Mean annual cycle in the turnaround latitudes at 76 hPa (left) and 100 hPa (right) from REF-B1 (red) and SCN-B2d (black). The average is taken over the 1960s. The vertical bars denote the standard deviation of the turnaround latitudes. The dashed lines show the change of the position of the turnaround latitudes over 90 years in SCN-B2d.

### 3.5 Width of the upwelling region

Not only the strength of tropical upwelling but also the location or the width of the region of upwelling might be subject to changes. If, for example, the region of upwelling broadens this might cause an increase in total upwelling even though the vertical velocities do not change. The width of the tropics is defined here as the region between the turnaround latitudes, i.e. the latitudes within the tropics where the residual vertical velocity points upward. Note that in other studies, the 'width of the tropics' is often defined by e.g. tropopause heights (e.g. Seidel and Randel, 2007). This 'width' does not necessarily relate to the region of upwelling as analysed here, and it needs to be clarified if and how they correlate (see also discussion in Chapter 7).

The location of the upwelling region has a pronounced annual cycle and is shifted into the respective summer hemisphere both at 76 hPa and 100 hPa, as is shown by the mean annual cycle of the turnaround latitudes in Fig. 3.7. The variability in the position of the turnaround latitudes is largest in winter and especially in early spring, while in summer the position is more stable at a similar latitude each year.

The timeseries of the width of the upwelling region is shown in Fig. 3.8. The width is decreasing both in REF-B1 and over the 90 years of simulation in SCN-B2d at 76 hPa and even stronger at 100 hPa. The linear trends over 90 years calculated for each month individually and added to the mean annual cycle (see dashed lines in Fig. 3.7) show that the decrease at 100 hPa mainly results from an equatorward shift of the edge of the upwelling region in late summer and autumn, indicating an earlier and faster transition into winter conditions. At 76 hPa, this is apparent only for the northern hemisphere, while in the southern hemisphere the turnaround latitude is shifted poleward in February and March.

The trend towards a narrower band of upwelling is consistent with the trend pattern in the residual circulation, which indicates stronger upwelling at the equator but less

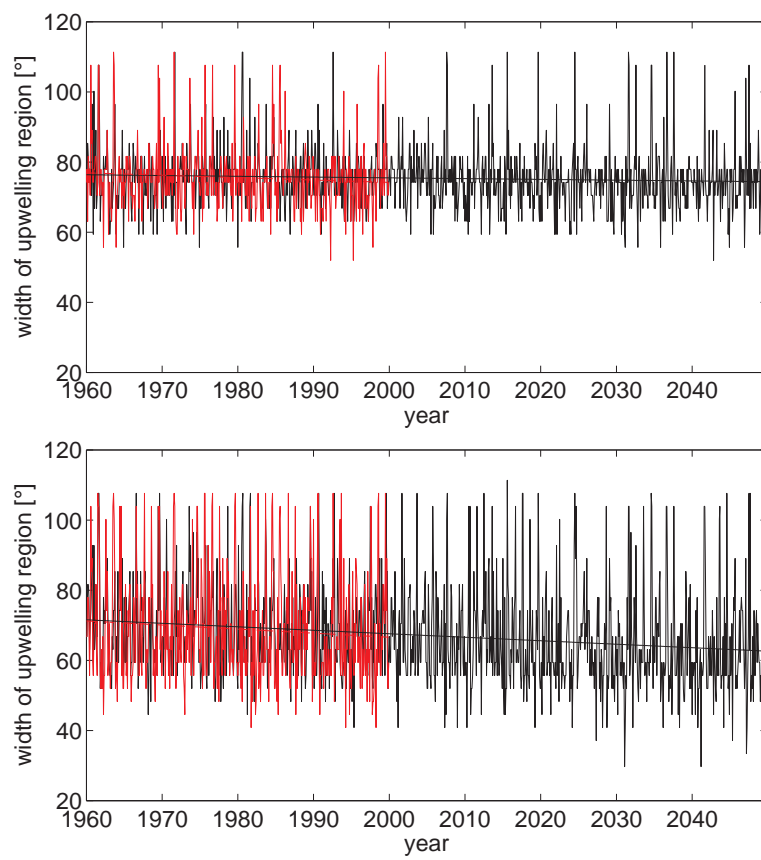


**Figure 3.8:** Monthly time series of the width of the upwelling region from REF-B1 (red) and SCN-B2d (black) at 76 hPa (top) and 100 hPa (bottom).

upwelling poleward of about  $20^\circ$  to  $30^\circ$  latitude. This decreased upwelling (or increased downwelling) in the subtropics leads to a narrower region of upward mass flux.

### 3.6 Summary

In this chapter, the transient model simulations were analysed in terms of trends in temperature, zonal winds and the meridional circulation. Generally, the changes detected in REF-B1 and SCN-B2d are similar (except in DJF in the northern hemisphere), and so are the major changes found in the past and in the future (except for the changes in the BDC in DJF in the southern hemisphere). As the high variability causes the trends to be most prominent for the whole 90 year period in SCN-B2d, in the following the analyses of mechanism for the trends will mostly focus on this period if appropriate.

The key findings from the analyses of the transient simulations are as follows:

#### I) Background State

**Temperature** The trends in temperature show warming in the troposphere and cooling in the stratosphere as expected in response to increasing GHG concentrations. In DJF, a strong cooling before 2000 and subsequent warming after 2000 is apparent in the Antarctic lower stratosphere.

**Zonal wind** In response to the changes in meridional temperature gradient, the strength of the subtropical jets increases. The polar jet increases before 2000 and decreases after 2000 in the southern hemisphere in DJF, as well consistent with the temperature trends.

#### II) Residual circulation

**Tropics, lower stratosphere** The most prominent feature in the meridional circulation trends is increased upwelling in the lower tropical stratosphere and downwelling in the subtropics. This feature is apparent in all seasons and time periods. The downwelling trend in the subtropics leads to a decrease in the width of the upwelling region.

**Tropics to mid-latitudes** During autumn and winter, the increase in the circulation in the tropics extends up to higher levels, in particular during SON in the northern hemisphere and during JJA in the southern hemisphere. However, these increases are mostly only barely significant and not always consistent over different periods.

**Southern high latitudes** During DJF, a hemisphere wide strengthening of the meridional circulation is apparent before 2000 and a weakening after 2000.



## Chapter 4

# Drivers of circulation changes

The climate state in a numerical model is determined by the prescription of external boundary conditions. Also deterministic changes in the climate state must be forced by changes in the external boundary conditions. In the atmospheric model system used here, the principal boundary conditions that control the climate are the SSTs and the concentrations of GHGs. In addition, concentrations of CFCs are prescribed, which have the main effect of destroying ozone and therewith feedback on the climate as ozone is a radiatively active gas. However, CFCs do also act as greenhouse gases. As the changes to the climate state in the model are known to be forced by the boundary conditions, appropriate simulations can be designed to separate the effects of the individual boundary conditions on the climate. In this chapter, a set of sensitivity simulations will be used in order to disentangle the impact of changes in the climate-controlling boundary conditions of SSTs and GHGs. The aim is to identify the drivers of changes in the residual circulation.

In the first section, the response to changes in GHGs, SSTs and CFCs is analysed, attempting to reproduce and explain the changes in the transient simulations as shown in the last chapter. In the second section, more idealised simulations are used in order to study the impact of SST changes in different regions. Namely, the impact of changes in SSTs in the tropics and in the northern mid-latitudes are investigated.

### 4.1 Impact of changes in GHGs, SSTs and CFCs

#### 4.1.1 Utilisation of the simulations to assign changes to the boundary conditions

A set of sensitivity simulations was performed in order to untangle the effects of changes in the different boundary conditions. Namely, the boundary conditions are divided into chlorofluorocarbons (CFCs), long-lived greenhouse gases (GHGs) and sea surface temperatures (SSTs) as described in Chapter 2 (see also Appendix A). Enhanced abundance of CFCs lead to increased ozone destruction, and it is known that the

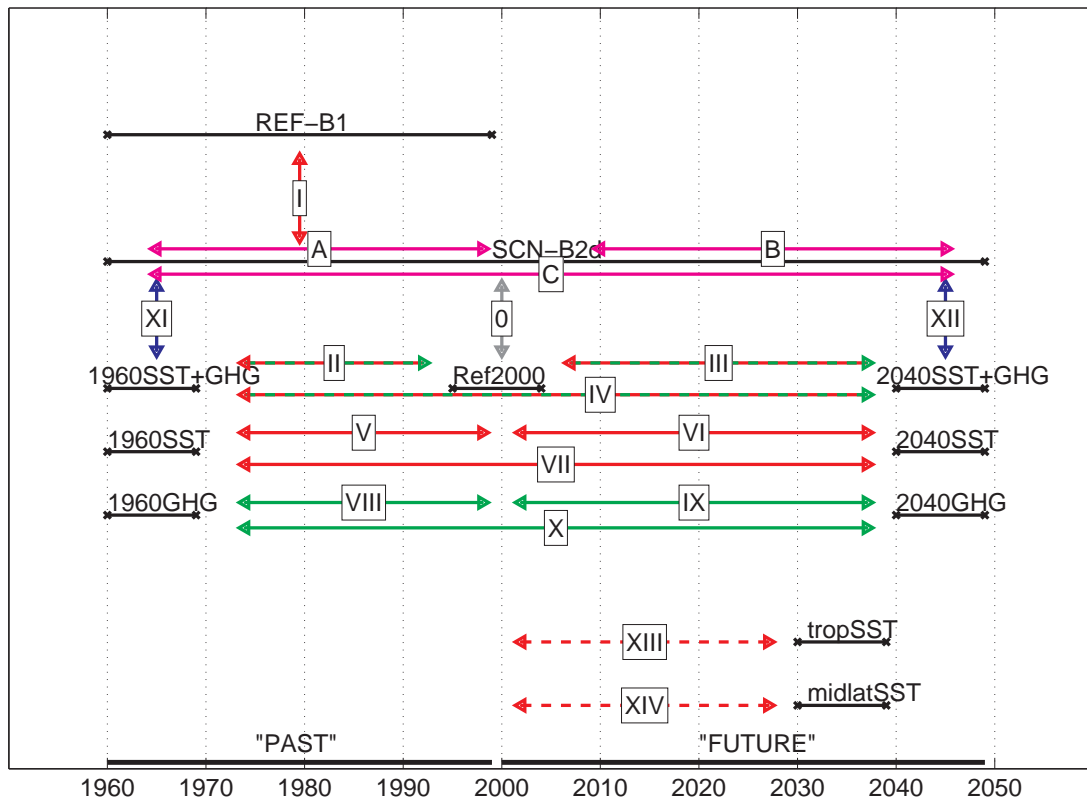


**Figure 4.1:** Overview of all simulations used in this study with arrows indicating the differences in boundary conditions: no differences (grey), differences in CFCs (blue), in SSTs (red) and in GHGs (green). The pink arrows indicate differences taken from episodes of the transient simulation SCN-B2d and therefore include changes in all boundary conditions. The numbers on the arrows are used as identifiers later on.

strong ozone depletion that occurred in Antarctica feeds back on the climate through radiative cooling. However, CFCs also act as greenhouse gases. The category of long-lived GHGs is defined here as the combined effect of  $CO_2$ ,  $CH_4$  and  $N_2O$  and they effect the atmosphere through trapping of longwave radiation in the troposphere and enhanced infrared emission in the stratosphere. Since SSTs are prescribed and not interactively coupled in the model, they can be regarded as separate forcing. In reality, the changes in SSTs are caused by the effects of GHGs and the two forcings are not necessarily distinguishable. Earlier studies suggest that the main climate effect on the troposphere is forced by the SSTs rather than by the direct effect of changes in GHG concentrations (Fomichev et al., 2007). Therefore, changing either SSTs or GHGs might be regarded as changing the climate in either the troposphere or the stratosphere separately. This gives insights into the processes that drive changes, but care has to be taken in the interpretation since the atmosphere-ocean interaction is neglected.

While in the transient simulations SCN-B2d and REF-B1, the boundary conditions do change over the course of the simulation, the time-slice simulations are designed to model the mean state of the atmosphere under certain conditions. By incorporating changes in only one of the prescribed boundary conditions, the response of the atmosphere to changes in this particular boundary condition can be determined. The set-up of all simulations performed was described in Chapter 2. Fig. 4.1 shows the overview of the simulations repeated from Fig. 2.1, but here including arrows indicative of the differences in boundary conditions between the simulations or between periods within simulations. The response on SSTs, GHGs and CFCs can be obtained by the following comparisons:

#### i) Response to SSTs

**V: 2000-1960** Time-slice Ref2000 minus 1960SST gives the response of the atmosphere to changes in the SSTs from mean 2000 to 1960 conditions, while all other boundary conditions remain at a mean level of year 2000.

**VI: 2040-2000** As above, but difference between time-slice 2040SST minus Ref2000, i.e. giving the response to changes in the SSTs from mean 2040 to 2000 conditions.

**VII: 2040-1960** As above, but difference between time-slice 2040SST minus 1960SST, i.e. giving the response to changes in the SSTs from mean 2040 to 1960 conditions.

#### ii) Response to GHGs

**VIII: 2000-1960** Time-slice Ref2000 minus 1960GHG gives the response of the atmosphere to changes in the GHG concentrations from 2000 to 1960 values, while all other boundary conditions remain at a mean level of year 2000.

**IX: 2040-2000** As above, but difference between Time-slice 2040GHG minus Ref2000, i.e. giving the response to changes in the GHG concentrations from mean 2040 to 2000 conditions.

**X: 2040-1960** As above, but difference between Time-slice 2040GHG minus 1960GHG, i.e. giving the response to changes in the GHG concentrations from mean 2040 to 1960 conditions.

### iii) Response to CFCs

**XI: 2000 - 1960** By comparing the time-slice with 1960s conditions in SSTs and GHG but CFC concentrations of the year 2000 with the period 1960-1969 from SCN-B2d, the effect of changes in CFCs from 1960 to 2000 values can be obtained. Note that here the SSTs and GHG concentrations are transient in one case and stationary in the other and therefore are not identical. However, both episodes represent the state of the atmosphere of the 1960s except for the CFC concentrations in 1960SST+GHG, so that the differences can be assumed to be largely due to the differences in CFCs.

**XII: 2040 - 2000** As above, but comparing the time-slice with 2040s conditions in SSTs and GHG but CFC concentrations of the year 2000 with the period 2040-2049 from SCN-B2d, showing the effect of changes in CFCs from 2040 to 2000 values.

### iv) Linearity of GHG+SST

**IV = VII + X** Since individual simulations were performed with changing only SSTs, only GHGs and both simultaneously to 1960 conditions and to 2040 conditions, the comparison of the sum of the response of the changing SSTs and GHGs only to the combined simulation can give a measure on whether the effects of GHGs and SSTs are adding linearly.

## 4.1.2 Background state

Using the sensitivity simulations as described above, the response in temperature and zonal wind to individual forcings can be compared to the combined effect of all forcings in the transient simulations. The temperature response is shown in Fig. 4.2. In the past (top row), the response to changes in SSTs mainly leads to strong warming in the troposphere, while the changes in GHG concentrations cause stratospheric cooling and only weak warming in the tropical troposphere. This shows that the stratospheric cooling is due to the direct radiative effect of GHGs. In the troposphere, on the other hand, the main effect on temperature is due to the indirect warming by the ocean. The sea surface is warmed by the radiative effect by enhanced GHG concentrations as infrared radiation is trapped in the troposphere. The increase in temperature in the

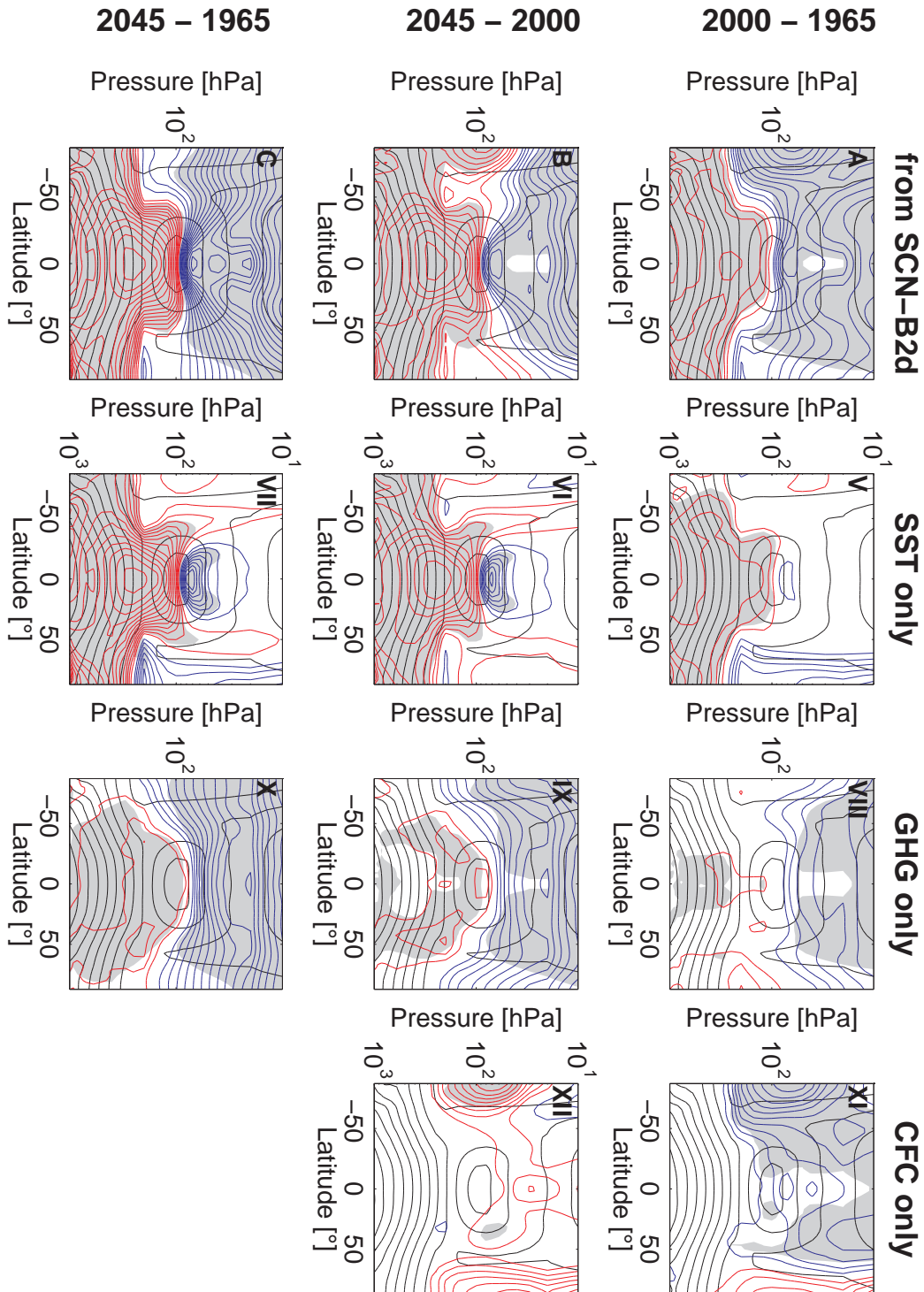


**Figure 4.2:** Annual mean response of zonal mean temperature to changes in all boundary conditions (left), to SSTs only (middle left), to GHGs only (middle right) and to CFCs only (right). The three column show differences from periods 2000 - 1960s (top), 2040s - 2000 (middle) and 2040s - 1960s (bottom). The number in the upper left corner of each panel refers to the differences as defined in Fig. 4.1. Black contours show the climatologies (contour interval 10 K, ranging from 200 to 290 K), red and blue contours denote positive and negative responses, respectively (contour interval 0.25 K, ranging from -4.5 to +3.5 K), and grey shading significance on the 95% level.

troposphere is then transferred from the sea surface by convective processes. Therefore warming maximises in the tropical middle troposphere, where deep convection transports latent heat which is released there.

The effects of CFC concentration changes in the past on temperature are strongest in the Antarctic lower stratosphere, consistent with strong ozone depletion and radiative cooling in this region. However, almost the entire stratosphere shows a significant decrease in temperatures due to the increase in CFC concentrations, with maxima in the mid-latitudes at 10 hPa of up to 1 K. This is probably caused by enhanced ozone destruction as a consequence of higher CFC concentrations also in mid-latitudes via homogeneous chemistry. In addition, CFCs also act as greenhouse gases by emitting infrared radiation in the stratosphere.

In the future, the pattern of the response of temperatures on SSTs is similar as in the past but the absolute values are higher. The tropospheric warming clearly maximises in the tropics at around 300 to 200 hPa. The cooling in the tropical lower stratosphere is significant for this period. Also the response to increased GHG concentrations shows a similar pattern as for the past, but absolute values increase.

The response to CFC concentration changes in the future is reversed in southern high latitudes compared to the past. Also in the remainder of the stratosphere temperatures increase with decreasing CFC concentrations, but the differences are significant only in the Antarctic lower stratosphere.

The changes in zonal wind in the period 1960 to 2000 are hardly significant in the annual mean, only an increase in the strength of the southern hemisphere polar jet is apparent (see Fig. 4.3). This increase is largely caused by changes in CFC concentrations, which lead to a strong cooling in the polar stratosphere and therefore increase in temperature gradient and thus thermal wind. The increase in the jet is strongest in southern summer (as shown in Fig. 3.1) and when regarding DJF only, the strengthening can clearly be attributed to changes in CFC concentrations (not shown).

In the future, the increase in the strength of the subtropical jets is significant and appears similarly strong for the difference from the transient simulation than for the difference forced by SSTs only. The increase in the strength of the subtropical jets can be explained by enhanced meridional temperature gradients as the tropical upper troposphere warms strongest, and due to thermal wind balance the vertical gradient in zonal wind must increase. As response to GHG concentration changes, there are no significant changes in the mean zonal winds. Again, when regarding DJF only, the decrease in the southern polar jet is stronger and can more clearly be attributed to changes in CFC concentrations.

Figure 4.4 analyses the linearity of the additive response to GHGs and SSTs. It can be seen that the sum of the temperature response to GHG and SST changes equals the combined response almost in the entire domain, only in the polar regions deviations are apparent. Zonal wind is as well to a good approximation responding to GHGs and SSTs linearly additive. The deviations from linearity in the polar jets in the stratosphere

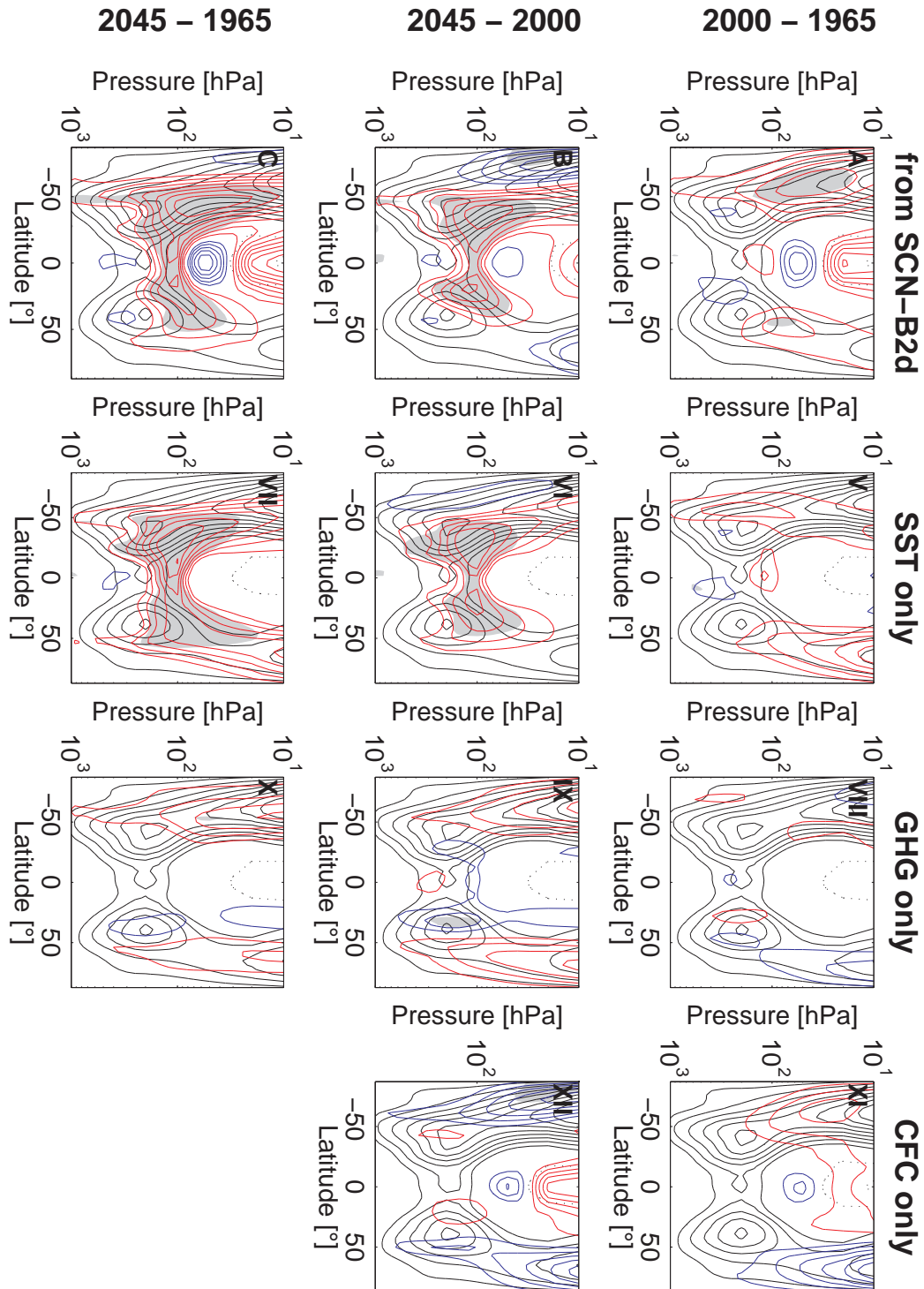


**Figure 4.3:** As in Fig. 4.2, but for zonal wind. The contour interval for the climatology is 5 m/s, values ranging from +40 to -5 m/s. The contour interval for the differences is 0.5 m/s, values range from +3.5 to -1.5 m/s.

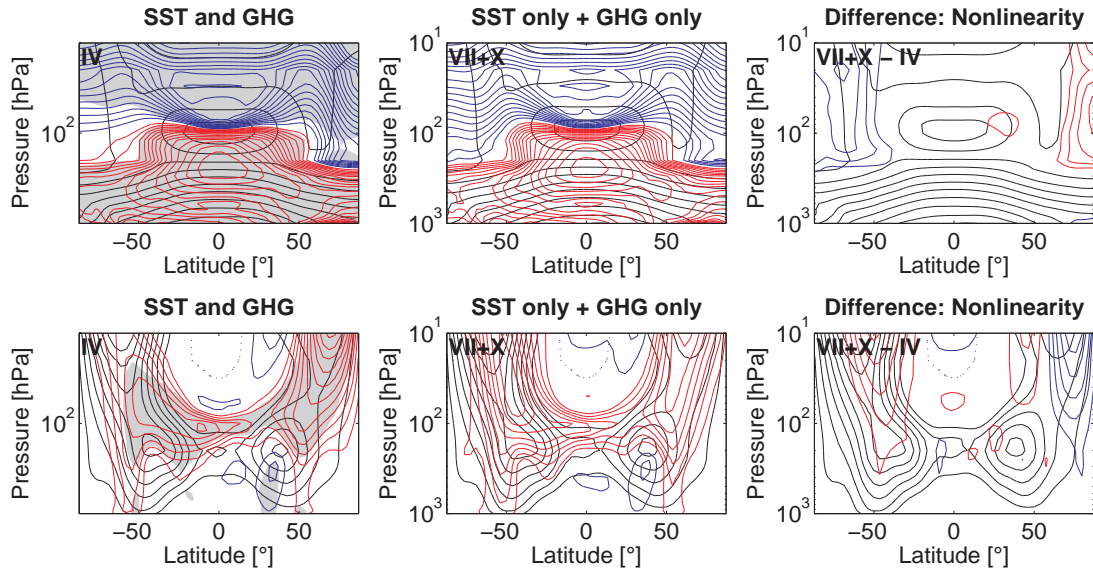


**Figure 4.4:** Temperature (top) and zonal wind (bottom) response to changes in SSTs and GHGs (left) and to SSTs only plus GHGs only (middle). The right panels show the difference between the two other ones, indicating the nonlinearity in the response to the two boundary conditions. Contours and contour intervals as in Fig. 4.2 and Fig. 4.3. Tests on significance are shown only for the left panel.

are consistent with the deviation in temperature. Since the variability is highest in the polar regions the difference in the residual is probably due to internal variability and not to a nonlinearity in the effects of SSTs and GHGs.

The atmospheric response to SST and GHG concentration changes as shown here is in good agreement with previous studies with simulations with similar set-ups, like Fomichev et al. (2007) and Sigmond et al. (2004). In the study by Sigmond et al. (2004) not the GHG and SST boundary conditions but GHG concentrations in the troposphere and stratosphere are changed separately (allowing to adjust the SSTs to the respective radiative forcing). Their simulation with tropospheric GHG changes results in a very similar response as the simulation with SST changes shown here, and the simulation with stratospheric GHG changes responds as the simulation with GHG changes only. This shows that changing either SSTs or GHG concentrations can be regarded to a first approximation as changing the climate in either the troposphere or the stratosphere separately.

### 4.1.3 Residual Circulation

In Chapter 3 it was shown that in the model system used here, the residual circulation is strengthening in the tropical lower stratosphere in a changing climate. Here, the sensitivity simulations are used to explore the causes of the circulation changes in the model. The enhancement of the circulation in the tropical lower stratosphere is also apparent in the annual mean decadal differences shown in Fig. 4.5 (first column).

The response to changes in SSTs only in the meridional circulation is similar in shape and magnitude to the full response. Especially in the tropical lower stratosphere, the increased circulation is clearly driven by SST changes both in the past and in the future. Changes in GHG concentrations have generally little impact on the circulation strength, only weak strengthening of the northern hemisphere meridional circulation in the annual mean appears in the past.

In the southern hemisphere, a strengthening in the residual circulation for 1960 to 2000 was found in southern summer, followed by a weakening after 2000. This pattern is not apparent in the annual mean, but when considering DJF only, the change can clearly be attributed to changes in CFC concentrations as shown in Fig. 4.6.

The test for linearity of the addition of the forcing by SSTs and GHGs shows generally good agreement between the combined and individually forced anomalies. The combination of the individual forcings does over predict the changes in the residual circulation slightly, especially in the southern hemisphere. This implies that the opposing effect of GHGs on the meridional circulation compared to SSTs (see Fig. 4.5 panel VII and X) is slightly stronger when considering both forcings at the same time. However, there seems to be no fundamental nonlinearity in the response to the forcings.

## 4.2 Impact of tropical versus extratropical SSTs

In this section, the sole effect of changes in SSTs in particular regions of the globe is analysed. In the last section, it was shown that changes in SSTs lead to tropospheric warming, enhancement of the subtropical jets and a strengthening in the residual circulation in the tropical lower stratosphere. In the following it will be investigated whether these changes can be assigned to changes in SSTs in the tropics or in the extratropics. A detailed description of the sensitivity simulations used here is given in Chapter 2.

In response to enhanced tropical SSTs (Fig. 4.8) the temperature in the troposphere increases, with strongest warming in the tropical upper troposphere. The pattern in temperature changes is similar to the response to changes in global SSTs (see Fig. 4.2). However, differences do occur in the extratropics, where the troposphere is warmed as response to global SST changes but not to tropical SST changes only. The cooling in the tropical lower stratosphere, on the other hand, does also occur in response to tropical SST changes only. As the additional energy introduced by warmer tropical SSTs is redistributed to higher altitudes by convective processes in the tropics, the troposphere-wide response in temperature to tropical SSTs is as expected.

Extratropical SST changes in the northern mid-latitudes do affect atmospheric temperatures only locally, the warming is confined to the region of SST changes and in the vertical to the troposphere. In the stratosphere, there is a small region of a negative temperature response at around 100 hPa.

The response in zonal wind to tropical SST changes is again similar to the response to global SST changes (see Fig. 4.3) with an increase in the strength of the subtropical

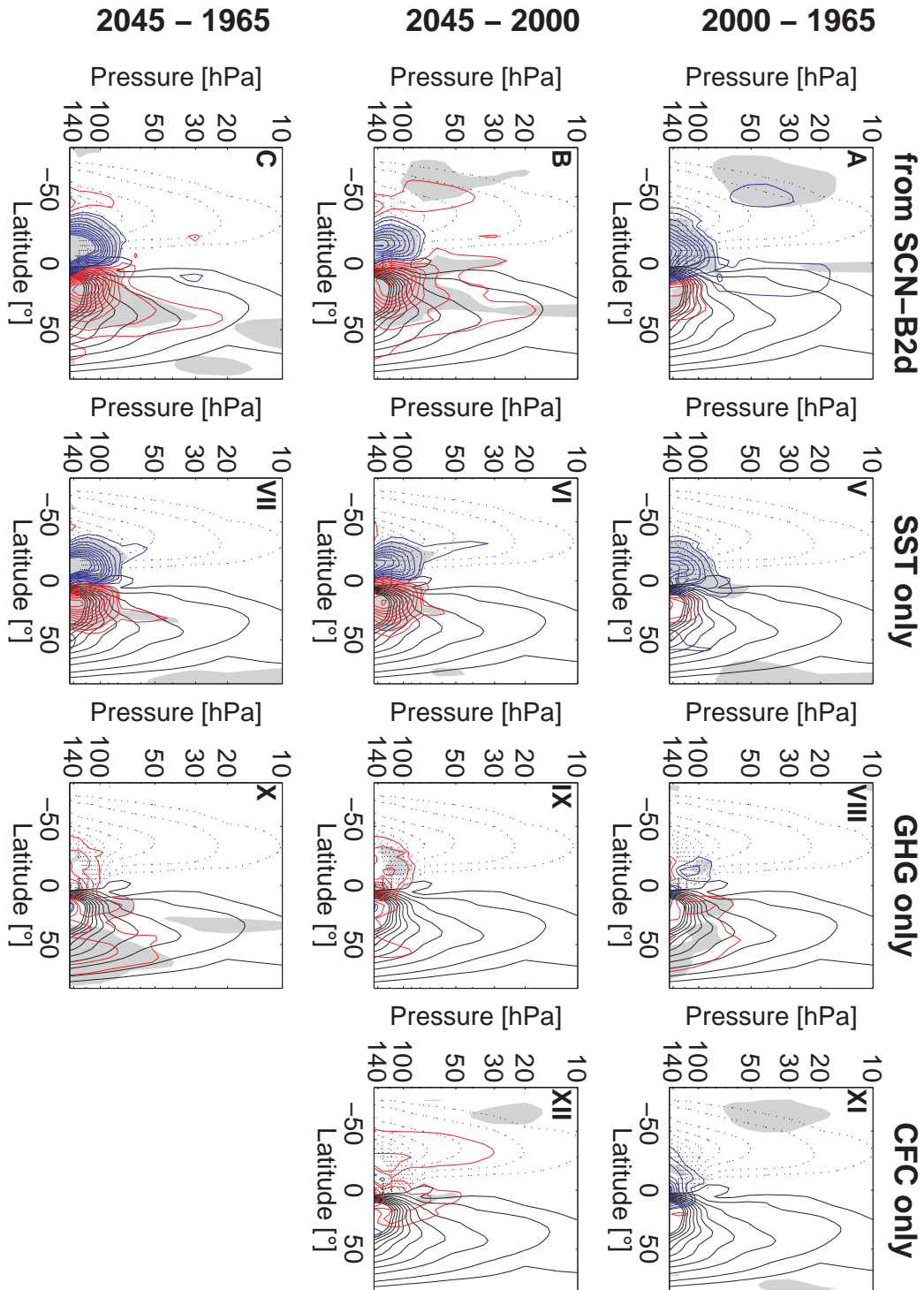


**Figure 4.5:** As in Fig. 4.2, but for the residual circulation. The contour interval for the climatology is  $1 \times 10^9$  kg/s, values ranging from  $-10$  to  $10 \times 10^9$  kg/s. The contour interval for the differences is  $2 \times 10^8$  kg/s, values range from  $+20$  to  $-20 \times 10^8$  kg/s.

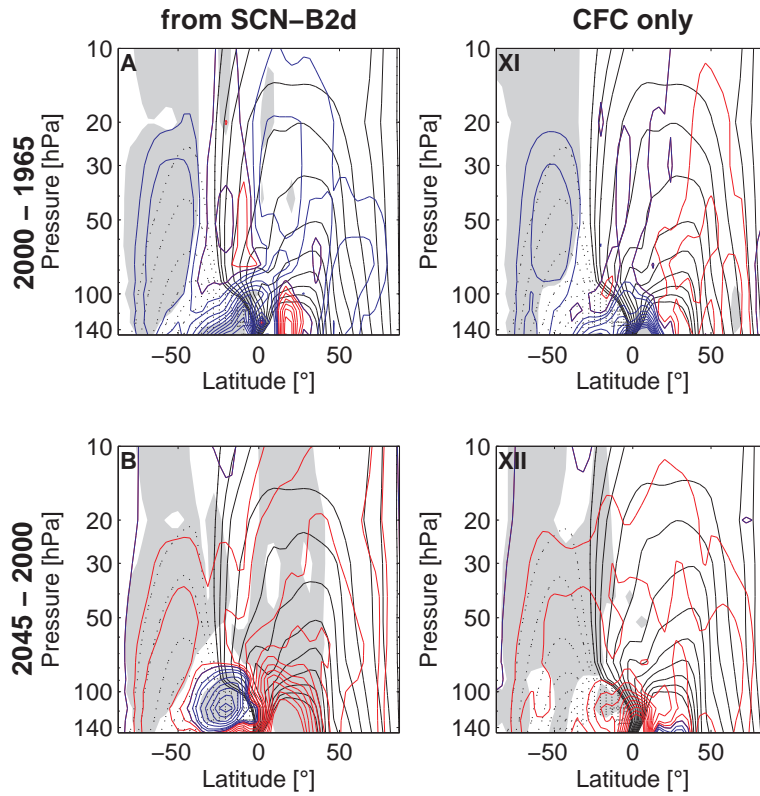


**Figure 4.6:** As in Fig. 4.2, but for the residual circulation in DJF and the response to CFCs only. Contours and intervals are as in Fig. 4.5.

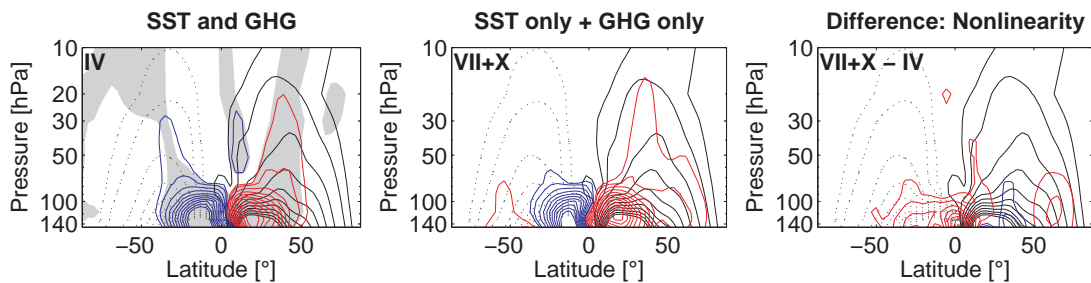


**Figure 4.7:** As in Fig. 4.4, but for the residual circulation. Contours and intervals are as in Fig. 4.5.

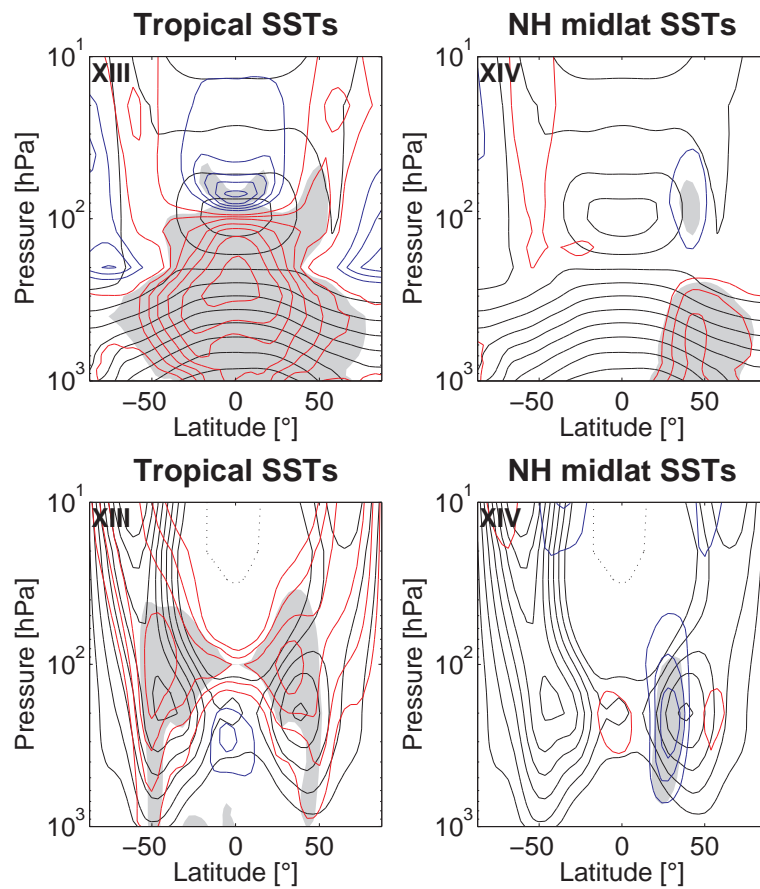


**Figure 4.8:** Differences in temperature (top) and zonal wind (bottom) for changes in tropical (left) and NH middle latitude SSTs (right). Contours and intervals are as in Fig. 4.2 for temperature and as in Fig. 4.3 for zonal wind.

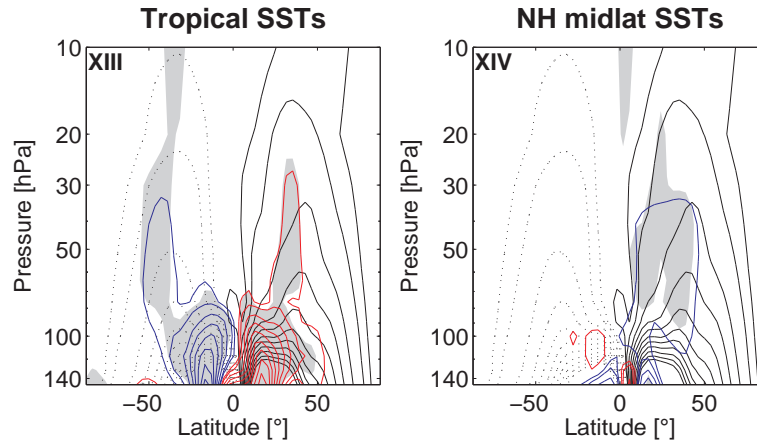


**Figure 4.9:** As in Fig. 4.8, but for the residual circulation. Contours and intervals are as in Fig. 4.5.

jets. This can be expected as the increase in the jets occurs as response to the enhanced meridional temperature gradient. The significant increase in the subtropical jets in the tropical SST simulation extends all the way to the surface and is stronger than in response to global SST changes in the past (which the tropical SST anomalies are based on). This is mostly due to the fact that by changing SSTs in the tropics only, the meridional temperature gradient is in addition artificially enhanced compared to the full SST change, especially in the extratropical troposphere. The increase in mid-latitude SSTs, on the other hand, leads to a decrease in tropospheric temperature gradients and consequently to a slight decrease in zonal winds equatorward of the jet maxima.

The response in the residual circulation to changes in tropical and mid-latitude SSTs, respectively, is shown in Fig. 4.9. The residual circulation is increasing in the tropical lower stratosphere with increased tropical SSTs. The anomaly pattern is similar to changes in the residual circulation as forced by globally increased SSTs (see Fig. 4.5). The response to increased mid-latitude SSTs in the residual circulation is weaker, but a significant response of the northern hemisphere circulation cell is apparent. The enhancement of the mid-latitude SSTs leads to a slight weakening of the meridional circulation in the northern extratropical stratosphere.

As discussed above, the modification of SSTs in one latitudinal region only does lead to an artificial modification of the meridional temperature gradient. In the case of the tropical SST anomaly, the meridional equator-to-pole temperature gradient is enhanced, but a change of the same sign occurs when changing the SSTs globally, i.e. the effect is intensified but qualitatively the same as for full forcing. In the case of mid-latitude SST anomalies, on the other hand, the temperature gradient from the equator to middle latitudes is decreased, which is not the case for global SST trends, i.e. an artefact is introduced. The slight weakening of the northern hemisphere meridional circulation in response to extratropical SST changes does not reproduce changes in either the transient simulation or the global SST simulations, and can be regarded as

artefact probably resulting from the modified temperature gradient. Overall, the non-global SST sensitivity simulations show that the changes in the residual circulation in the transient simulation are reproduced in response to tropical SST changes, while extratropical SSTs do not act to drive changes in the stratosphere that can explain the simulated long-term changes.

### 4.3 Summary

The attribution of changes in temperature, zonal wind and the meridional circulation to changes in boundary conditions gave the following results:

**Temperature** Tropospheric temperatures change largely in response to SST changes, while stratospheric temperatures decrease due to enhanced GHG concentrations. The pattern of temperature changes in response to global SST changes with strongest warming in the tropical troposphere and cooling in the tropical lower stratosphere is reproduced when changing tropical SSTs only. In addition, the temporal development of CFC concentrations evokes a temperature response in the Antarctic lower stratosphere.

**Zonal Wind** The changes in the meridional temperature gradient that is responsible for the strengthening of the subtropical jet is mainly due to changes in tropospheric temperatures. Therefore, the changes in jets are reproduced in response to both global and tropical SST changes. As response to CFC concentration changes, the southern polar jet strengthens before 2000 and weakens afterwards.

**Residual Circulation** The changes in the meridional circulation in the tropical lower stratosphere are driven by changes in tropical SSTs. In response to GHG concentration changes, on the other hand, no consistent changes in the residual circulation were found. Changes in CFC concentrations mainly drive the hemisphere-wide strengthening of the southern hemisphere meridional circulation in summer in the past and weakening in the future.

## Chapter 5

# Wave forcing of the meridional circulation and tropical upwelling

It was shown in the preceding chapters that the meridional circulation and tropical upwelling are subject to changes in a changing climate. The findings suggest that the long-term changes in tropical upwelling in the lower stratosphere are induced by enhanced tropical SSTs, while changes in the southern hemisphere circulation are caused by changes in CFC concentrations. By attributing the trends to changes in boundary conditions, the causes can be revealed, but the mechanisms are not necessarily easily assessable. The aim of this chapter is to investigate the mechanism that lead to enhanced tropical upwelling and to changes in the BDC. The trends in the tropical lower stratosphere were found to occur robustly throughout the simulation periods of both REF-B1 and SCN-B2d in past and future. Therefore, the analyses of processes related to this intensification are performed for the full 90-year period in SCN-B2d, but are generally valid also for sub-periods. The changes in the southern summer BDC, on the other hand, are of different sign in past and future, so that these sub-periods are considered to study the causes for this change. In this Chapter, the analyses are limited to the SCN-B2d simulation, but as shown in Chapter 3 and in Garny et al. (2009) long-term trends in REF-B1 are generally not distinguishable from SCN-B2d.

It is well known that the BDC is driven by wave drag of both planetary and synoptic scale waves as well as gravity waves.<sup>1</sup> However, as discussed in the introduction, the mechanisms that are responsible for the strength, location and annual cycle of tropical upwelling in the lower stratosphere are still under discussion. Using the theoretical framework of downward control (see Appendix B), the wave driving of the BDC and of tropical upwelling is investigated, and both the climatology and changes are attributed to wave forcing in Section 5.1.1. This study focuses on the role of planetary and synoptic scale waves (i.e. waves that are explicitly resolved in the model, referred to as resolved waves). To understand the origin of wave fluxes that drive the circulation and

---

<sup>1</sup>The classification of waves according to their scale, period or treatment in the model is given in Appendix A.

changes therein, climatologies and trends in Eliassen-Palm (EP) fluxes are analysed in Section 5.1.2. The definition and theory of EP fluxes is given in Appendix B. At the end of the chapter, the findings are discussed in terms of the evidence that is found to explain the climatology of tropical upwelling and to explain the origin of wave flux changes that lead to changes in the meridional circulation.

## 5.1 Wave forcing of tropical upwelling

### 5.1.1 Downward control

The downward control (DC) principle (Haynes et al., 1991) is used here to calculate the residual circulation that is forced by resolved waves. For details on the calculation see Appendix B. Fig. 5.1 shows the annual mean residual streamfunction both directly calculated and as forced by resolved waves assuming downward control. As the meridional gradient of angular momentum is close to zero in the inner tropics, downward control can not be applied there, and the DC streamfunction is only shown for latitudes greater than  $20^\circ$  latitude. The residual after subtracting the DC streamfunction from the directly calculated streamfunction is shown on the right in Fig. 5.1, and this difference is a measure to what degree the circulation can be explained by resolved wave forcing. If the meridional circulation was entirely driven by resolved waves, and the assumptions of downward control hold, this difference would equal to zero everywhere. The climatological circulation is shown to be largely driven by resolved waves, only in the northern hemisphere in mid-latitudes a considerable part is not captured by DC. Other forcings than resolved wave drag must play a role here, mostly likely orographic gravity waves that are excited mostly in the northern hemisphere. As shown in the last chapters, the residual circulation is increasing in strength in the tropical lower stratosphere as response to climate change. These changes in the circulation from the 1960s to the 2040s are largely captured by the DC streamfunction, and can thus be attributed to resolved wave forcing. In the northern hemisphere the changes are underestimated by DC, which is most likely also due to orographic gravity wave forcing. However, the largest part in changes in the residual circulation can be explained by changes in resolved waves.

As shown in Chapters 3 and 4, the BDC in the southern hemisphere in summer is strengthening in the past and weakening in the future. This was shown to be driven by the CFC-induced ozone depletion. In order to investigate whether this anomaly is also due to changes in resolved wave forcing, Fig. 5.2 shows the changes in the residual circulation for the past (1990s-1960s) and for the future (2040s-1990s) in DJF. It can clearly be seen that both the strengthening and the subsequent weakening of the BDC is reproduced using DC and thus forced by resolved waves. Only the extension of the circulation changes into the (sub-)tropics is slightly underestimated, but the strength of the changes in the mid-latitudes overestimated (leading to the positive-negative

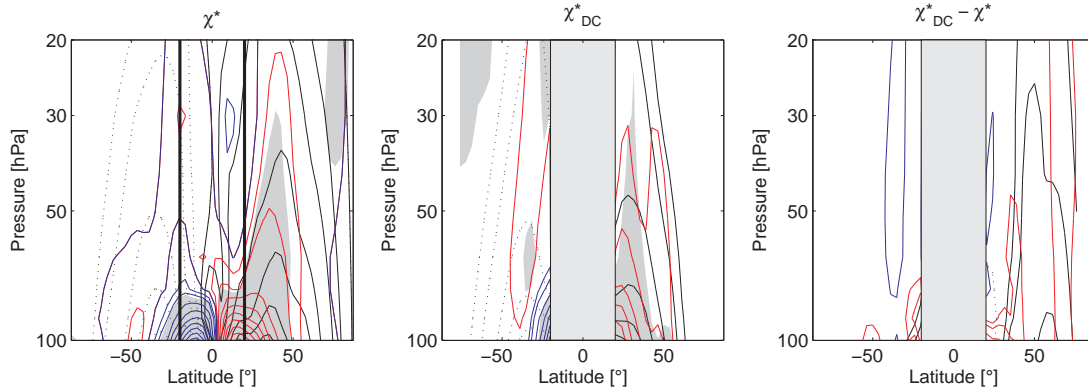


**Figure 5.1:** Climatology (black contours) and differences between the decades 2040s - 1960s in SCN-B2d (coloured contours) in the annual mean residual streamfunction. The left panel shows the directly calculated residual streamfunction, the middle panel the streamfunction calculated using downward control with resolved waves as forcing, and the right panel the difference between the middle and left panels. Conventions of contours and contour intervals as in Fig. 4.5.

pattern in middle/low latitudes in the residual on the right, which is reversed in the future). This difference in the extension of the circulation change might be caused by the assumption of stationary conditions in the downward control calculation. Transient conditions can lead to a broader extension of the induced circulation (Holton et al., 1995, see also Introduction).

As mentioned above, the residual circulation can not be calculated by the DC principle in the inner tropics. However, as mass conservation guarantees that mass that is transported horizontally across one latitude must be balanced by vertical motion, the difference between the streamfunction at two latitudes must be the net upwelling in between these latitudes (for details see Appendix B). This allows to calculate the mean tropical upwelling between two latitudes that is forced by resolved waves. As the strongest and most robust long-term changes in the meridional circulation are found in the tropical lower stratosphere, in the following mean tropical upwelling across the 100 hPa surface will be investigated. While the total mass flux integrated between the turn-around latitudes was used in Section 3.2, here the mean of the vertical residual velocity ( $\overline{w^*}$ ) over a certain fixed latitude band is used as measure of upward motion in the tropics. In Section 3.2 it was intended to show changes in the total mass transported upward, while in the following the dynamical causes of changes in the vertical velocity should be determined. For this purpose, fixed latitudinal boundaries are considered appropriate, and are used here as problems occur in the downward control calculation when using the turn-around latitudes (the latitudinal structure of  $\overline{w^*}$  is somewhat patchy and therewith the turn-around latitudes very variable).

The climatological values of  $\overline{w^*}$  averaged over 20°S to 20°N are shown for the model results in Fig. 5.3. Here, the model results are compared to reanalysis data from

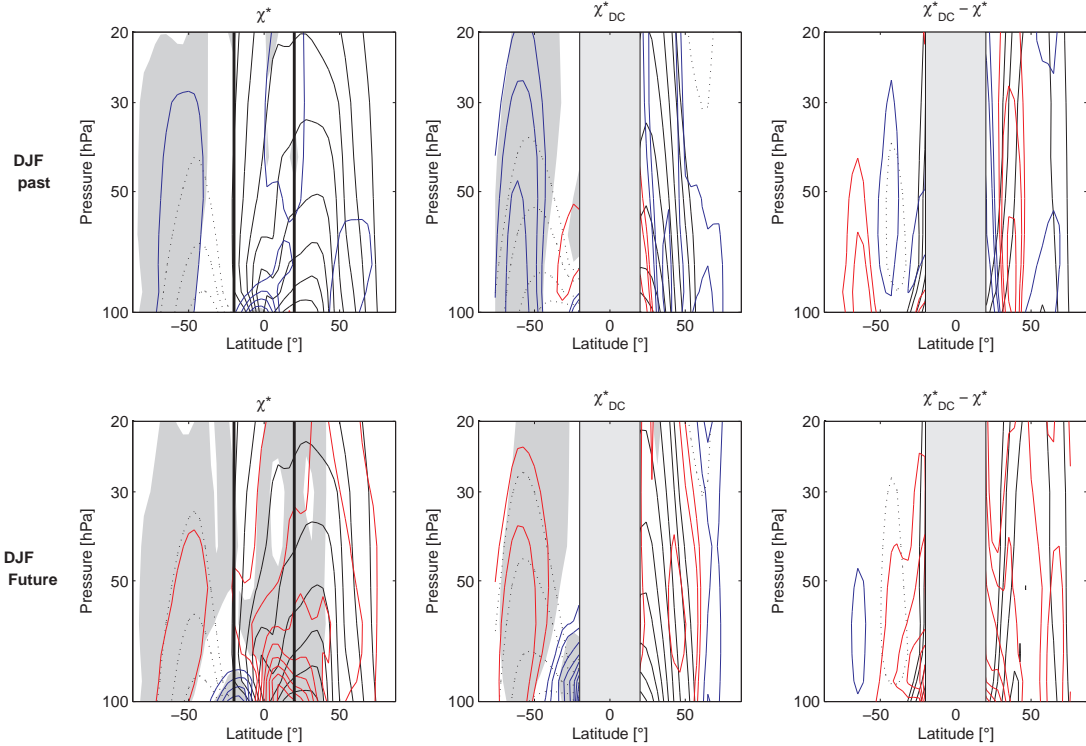


**Figure 5.2:** As in Fig. 5.1, but for DJF and the difference 2000 - 1960s (top) and 2040s - 2000 (bottom). Conventions of contours and contour intervals as in Fig. 4.5.

ERAInterim<sup>2</sup> in order to evaluate whether the mechanism of tropical upwelling in the model are well simulated. The absolute values and the annual cycle in  $\overline{w^*}_{DC}$  of E39CA are fairly similar to ERAInterim. However, the directly calculated  $\overline{w^*}$  is lower than  $\overline{w^*}_{DC}$  in the model but higher in the reanalysis. Also for the direct  $\overline{w^*}$  the annual cycle matches quite well between model and reanalysis with minimum values in July and maximum values in northern spring. In both cases the minimum in  $\overline{w^*}$  occurs about 1-2 months earlier than in  $\overline{w^*}_{DC}$  and also the maximum in spring is absent in  $\overline{w^*}_{DC}$ . As  $\overline{w^*}_{DC}$  is only taking resolved waves into account, the common features in  $\overline{w^*}$  might be due to the additional forcing by orographic gravity waves (which are parametrised in both cases). The discrepancy between the absolute values in  $\overline{w^*}$  in E39CA compared to the reanalysis might arise from non-orographic gravity wave forcing which is neglected in E39CA, or also from orographic gravity wave drag that occurs at different locations due to different background zonal winds. Also, differences in orographic gravity waves might occur due to the low horizontal model resolution in E39CA (T30), which leads to rather flat and low mountains. However, the DC analyses show that upwelling in the tropics can at least in large parts be explained by forcing of resolved waves.

In E39CA as well as in ERAInterim, both transient and stationary waves contribute with similar amounts to the wave forcing within  $\pm 20^\circ$  latitude. Stationary wave forc-

<sup>2</sup>ERAInterim is a reanalysis product of the ECMWF. The data span years 1989 to the present. For a description of the data set and details see Simmons et al. (2006).

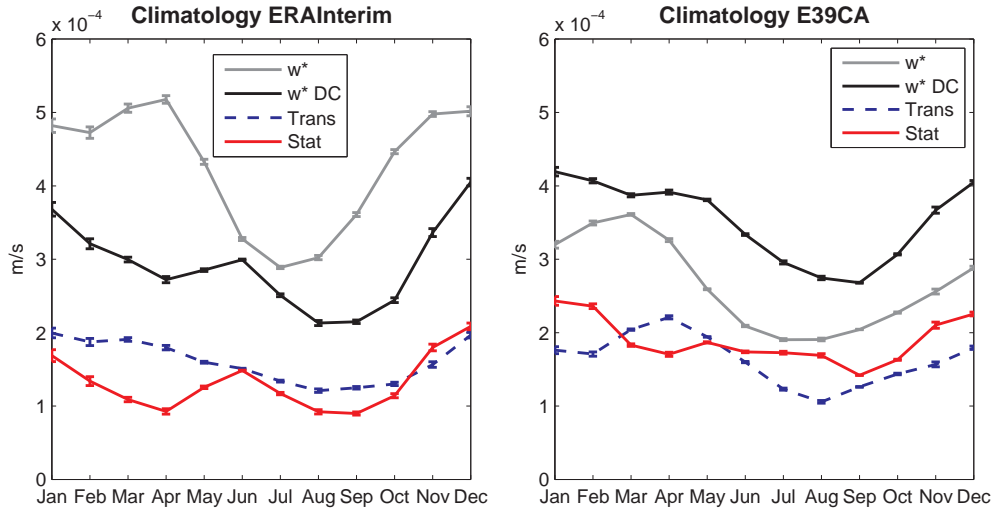


**Figure 5.3:** Annual cycle in mean  $\overline{w^*}$  between  $20^\circ\text{N}$  to  $20^\circ\text{S}$  (grey line),  $\overline{w^*}_{DC}$  from downward control using EP fluxes as forcing (black line),  $\overline{w^*}_{DC}$  from downward control using only stationary (red solid) and only transient (blue dashed) wave components. The left panel shows the ERAInterim climatology (years 1989-2008), the right panel shows the E39CA climatology (years 1960-2049 from SCN-B2d).

ing is stronger in the solstice seasons than in the transition seasons, and the forcing is stronger in northern winter than in southern winter. In the transition seasons, the relative importance of transient wave components is enhanced, and transient wave forcing minimises in August both in the model and the reanalysis. Only the maximum in northern spring in E39CA is absent in ERAInterim. Also, the overall relative contribution of transient waves is slightly higher in ERAInterim compared to E39CA. However, the relative contribution of stationary versus transient waves is dependent on the choice of the latitude bounds. Fig. 5.4 (left) shows  $\overline{w^*}_{DC}$  as a function of the latitude bounds, ranging from about  $\pm 15^\circ$  to  $\pm 32^\circ$ . For lower latitudes than about  $15^\circ$  the downward control can not be applied anymore (as the meridional gradient of angular momentum becomes zero) while for higher latitudes than about  $35^\circ$  the averaging would be done over regions of up- and downwelling, and thus would not be meaningful. As Fig. 5.4 (left) shows,  $\overline{w^*}_{DC}$  forced by stationary waves increases with decreasing latitude bounds, doubling within  $\pm 15^\circ$  latitude compared to  $\pm 30^\circ$  latitude. The annual cycle remains similar when averaging over different latitude bands. The forcing by transient waves on the other hand increases only slightly with decreasing latitude bounds, so that equatorward of about  $25^\circ$  the stationary wave forcing exceeds the transient wave forcing. This shows how sensitive the contribution of different wave types to forcing of tropical upwelling is to the latitudinal average region chosen.

The contribution to the forcing of upwelling of waves of different horizontal wavenumber is investigated in Fig. 5.5. Forcing by both planetary stationary waves (left) and synoptic-scale transient waves (right) has a semiannual-like cycle. The forcing by plan-

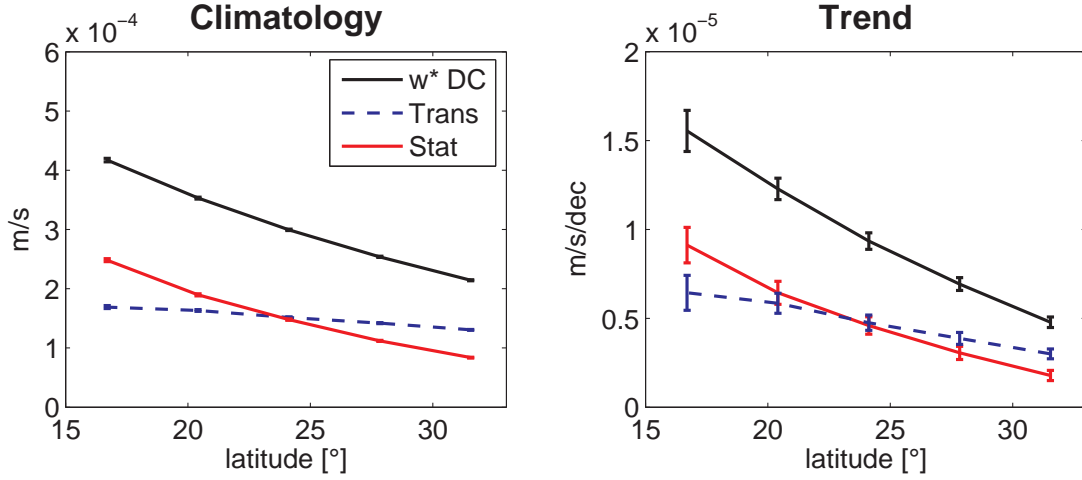


**Figure 5.4:** Annual mean  $\overline{w^*}_{DC}$  calculated via the downward control principle as a function of the averaging latitude bounds. Shown is  $\overline{w^*}_{DC}$  with stationary waves as forcing only (red solid), with transient waves only (blue dashed) and the sum (black). Climatology from SCN-B2d over 90 years (left) and the trend calculated over these 90 years (right).

etary stationary waves is strongest in the solstice seasons, with both wavenumber 1 and 3 being of importance in northern winter while in southern winter the forcing is almost entirely due to wavenumber 1 waves. Forcing of upwelling by transients is dominated by synoptic scale waves ( $WN \geq 4$ ), maximising in the transition seasons.

Next to the climatology of upwelling, the long-term changes in upwelling are investigated using E39CA. The reanalysis data are not available over a sufficiently long period to analyse long-term trends. The 90-year trend in mean  $\overline{w^*}$  is positive throughout the year (Fig. 5.6 left panel), with largest increases around northern winter and smallest increases in northern summer. The relative trend is largest in October (about 5%/decade) and smallest in August (about 1.5%/decade) while it lies around 3.5%/decade through the rest of the year. The mean  $\overline{w^*}_{DC}$  also shows a positive trend of comparable size to the directly calculated  $\overline{w^*}$ , showing that changes in upwelling are driven by changes in resolved wave forcing. Both stationary and transient waves play a role in forcing the changes in upwelling, and trends in both are strongly seasonally dependent. In solstice seasons, the relative contribution by stationary waves is largest. The changes in the forcing by transient waves has a semiannual-like cycle with strongest increases in the transition seasons (especially in northern spring, while the second peak is shifted towards late autumn). The dependence of trends in forcing on the latitudinal bounds behaves as in the climatological mean, with increasing importance of stationary waves towards lower latitudes (see Fig. 5.4 right panel). The fact that the structure of the trend is the same as the climatology shows that the forcing is enhanced equally strongly for both wave classes, and not one of them becomes more favoured in a future climate.

The contribution to wave forcing of upwelling of planetary waves 1, 2 and 3 and of synoptic scale waves ( $WN \geq 4$ ) is shown in Fig. 5.5. Here the first and last decade of the

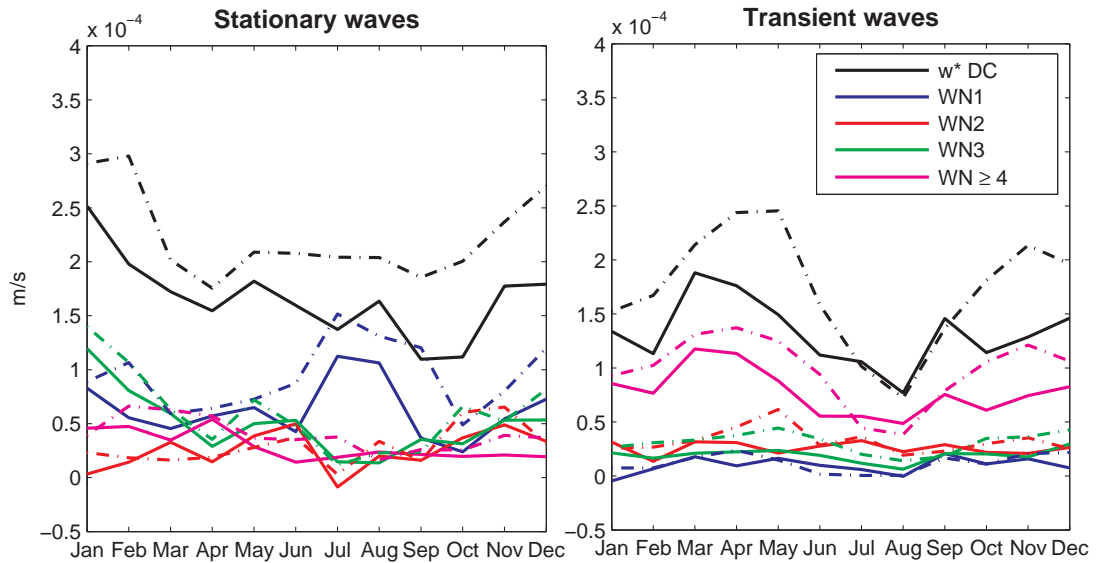


**Figure 5.5:** As in Fig. 5.3 (right), but for stationary waves only (left) and transient waves only (right) and for individual wave numbers 1 to 3 and wave numbers  $\geq 4$ . Solid lines are 1960-69 climatological values, dash-dotted lines 2040-49 climatological values from the SCN-B2d simulation.

transient simulation SCN-B2d is compared, as EP fluxes decomposed into wavenumbers were calculated for these time periods only (note that the results of Fig. 5.6 remain qualitatively valid for the decadal difference). It can be seen that the forcing by stationary waves with wavenumber 3 and 1 increase in the 2040s compared to the 1960s in DJF. In JJA, the wave driving by almost solely waves with wavenumber 1 also increases, while the smaller scaled waves remain unimportant. In the transition seasons, the increase in upwelling is driven in large parts by transient waves (especially in the MAM season). This increase is due to an increase in wave driving mainly by synoptic scale waves (wave numbers  $\geq 4$ ).

It was found in Chapter 4, that the response of the residual circulation to changes in tropical SSTs resembles the long-term trends, and it was concluded that changes in tropical SSTs drive the long-term changes in the transient simulations. Therefore, the trends in the dynamical forcing of upwelling are compared here with the response of the forcing to tropical SST changes. The differences in tropical upwelling as forced by increases in tropical SSTs are shown in Fig. 5.6. As in the transient simulation, upwelling increases throughout the year and the increase is forced by resolved waves. Also the magnitude of the change rate is similar. However, the seasonal dependence of the relative contribution of stationary versus transient waves is not reproduced in the tropical SST simulation. Here it is found that stationary waves account for most of the wave forcing in most months, only in September to October transients are of importance. Note that the anomaly in SSTs in the tropical SST simulation is based on the linear trend in SSTs over 1970 to 1999, while the linear trends from SCN-B2d

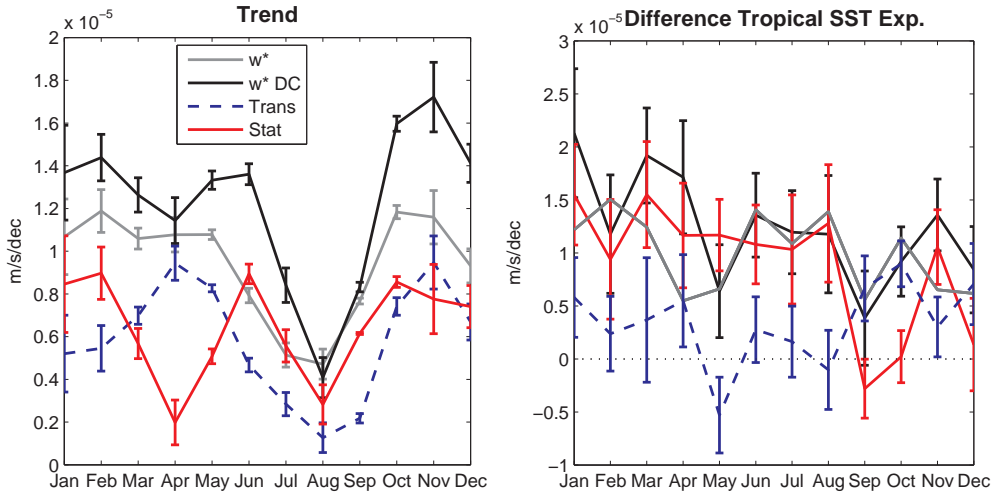


**Figure 5.6:** As in Fig. 5.3 but showing the linear trend from the SCN-B2d simulation over 1960-2049 (left) and the response to changes in tropical SSTs (right; shown is the difference tropSST-Ref2000 scaled to change per decade). The errorbars denote the  $1\sigma$  uncertainty in the trends and the differences, respectively.

are calculated over the full 90 years. Therefore, the pattern of the SST disturbance is different in the two cases. The trends in wave forcing over 1970 to 1999 from SCN-B2d do also not show the pronounced seasonality of changes in stationary and transient wave forcing. However, the response in tropical upwelling in wave fluxes in the tropical lower stratosphere is robust for the sensitivity simulation and for sub-periods in the transient simulations. This indicates that the relative contribution of transient versus stationary waves might not be crucial in determining the response in tropical upwelling.

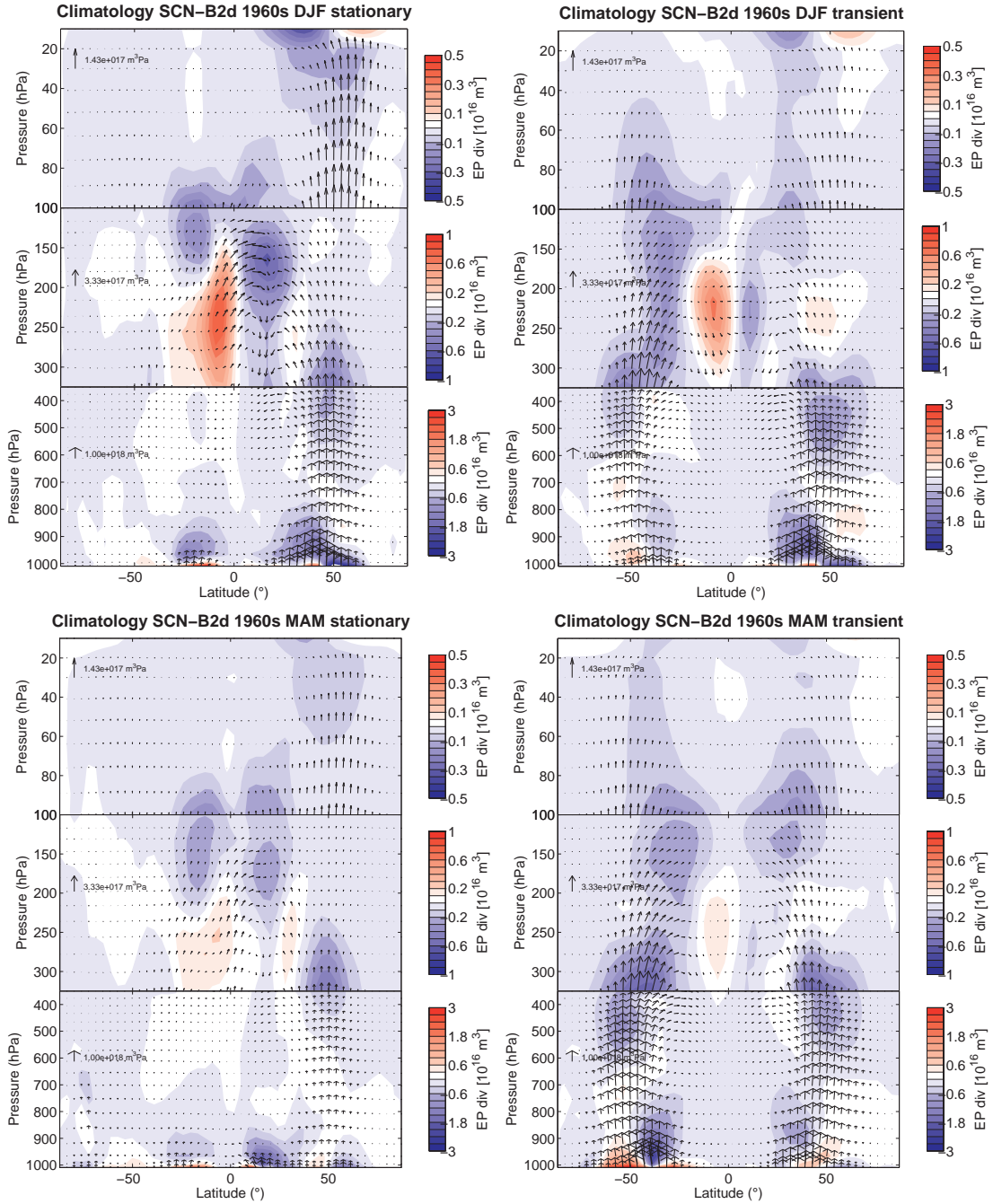
### 5.1.2 EP fluxes

It was found in the last section that tropical upwelling in the lower stratosphere is largely driven by resolved wave forcing from both stationary and transient waves. Also the increase in upwelling and the changes in the southern hemisphere BDC are due to changes in resolved wave forcing. Therefore EP fluxes are analysed in the following to investigate the origin of the waves causing the forcing in the (sub-)tropics, and the changes in wave forcing. The first subsection focuses on the solstice seasons, and the second subsection focuses on the transition seasons. The climatologies from E39CA are compared to the EP fluxes from ERAInterim.

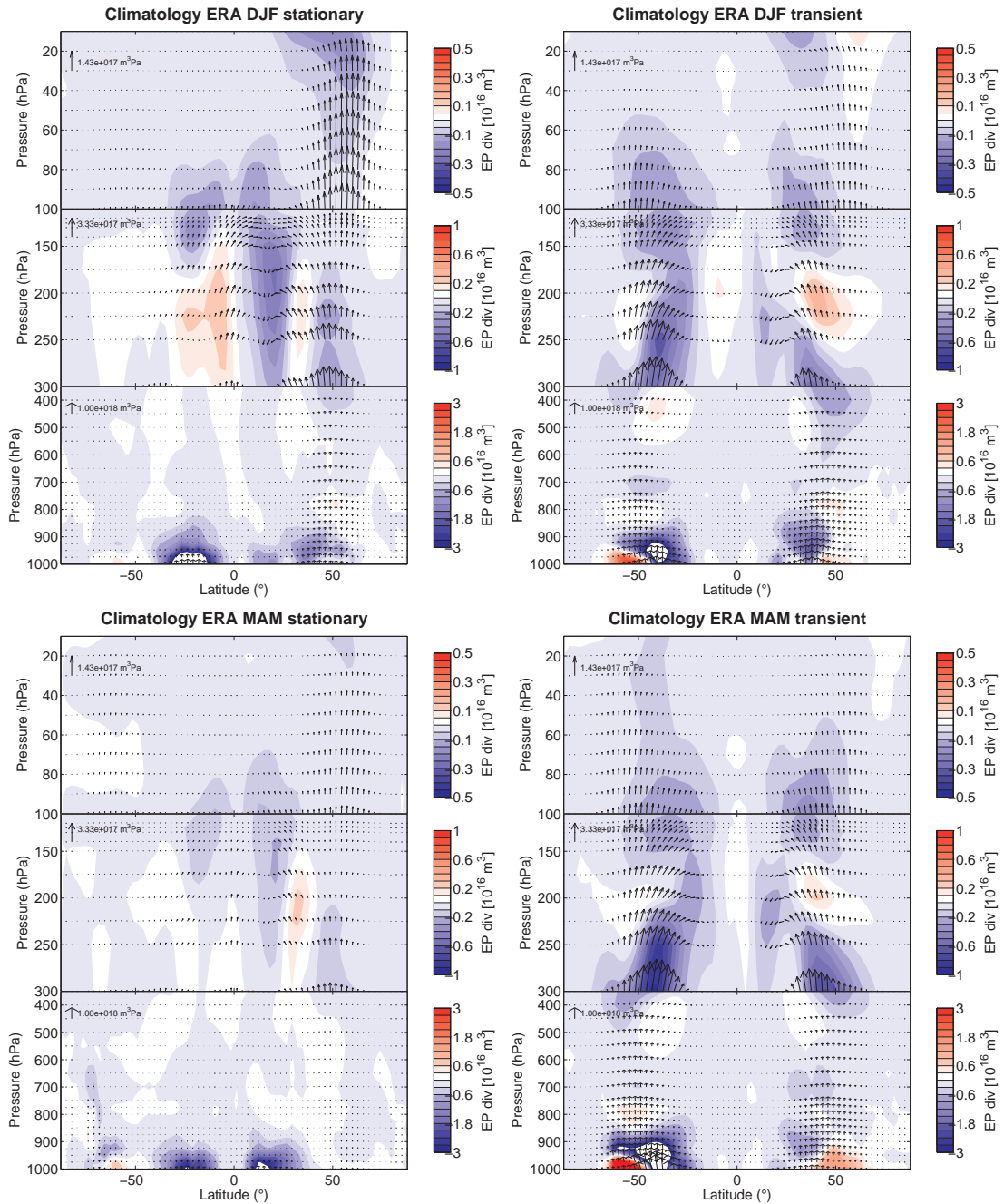
#### Solstice seasons

Fig. 5.7 (top) shows the climatology in EP fluxes for northern winter (DJF) for stationary and transient waves for E39CA. The pattern is similar but mirrored about the equator in northern summer (not shown).

In the tropical lower stratosphere EP fluxes propagate upward from the troposphere



**Figure 5.7:** Climatologies (1960-69 from SCN-B2d) of EP fluxes (black arrows) and EP divergences (coloured) for three different height regions with different scaling. The scaling of the EP fluxes and divergences is indicated by the scale arrow and the colourbar in each panel. The upper panels show EP fluxes of stationary (left) and transient (right) waves, the lower panels show MAM climatologies.



**Figure 5.8:** As in Fig. 5.7 but for the ERAInterim climatology over 1989-2008.

but can not propagate far in the vertical in the mean. This leads to EP convergence in the tropics and subtropics at levels below 80 hPa. Zonal winds in the tropical stratosphere are oscillating from west to east phases with a biennial period (Quasi-biennial oscillation, QBO), but as the wind speeds in easterly phases are higher as in westerly phases, zonal winds are easterly in the climatological mean. This leads to the inhibited vertical wave propagation. The modulation of vertical wave propagation by the QBO is also discussed below in Section 5.2.3. The climatology of EP fluxes shows that waves propagating into the tropical lower stratosphere are both of tropical and extratropical origin. The extratropical contribution consists mostly of transient waves, that propagate upward in the mid-latitudes in the troposphere and are refracted towards the equator. In the upper troposphere in the summer hemisphere a region of EP divergence is apparent to the south of the equator. This source region is indicative of generation of tropical waves. It is known that latent heat release in the upper troposphere by convection triggers planetary scale Rossby and Kelvin waves (see e.g. Gill, 1980). On the winter side of the equator, a local maximum of EP convergence by stationary waves is found at around  $10^{\circ}$ - $20^{\circ}$  latitude and 200 hPa. This region of strong EP convergence is due to both dissipation of the tropical generated waves and to dissipation of equatorward refracted mid-latitude generated waves. However, in the tropical lower stratosphere stronger EP convergence of stationary waves occurs in the summer hemisphere compared to the winter hemisphere (this is also true in JJA, not shown). The decomposition of the EP fluxes into stationary and transient waves shows that the strong EP convergence in the summer subtropics is mainly due to stationary waves that origin in the tropics (i.e. are generated in the region of EP divergence in the tropics) and propagate upward. Transient waves account for wave fluxes in mid-latitudes and contribute to EP convergence in the subtropics.

For comparison, the climatology of EP fluxes from ERAInterim is shown in Fig. 5.8. Generally, both the pattern and the magnitude of EP fluxes and the associated forcing agree very well. The region of generation of stationary waves in the tropics is apparent in ERAInterim at a similar location to E39CA, although the magnitude is somewhat smaller. Tropical waves do partly propagate upward on the summer side of the equator and lead to EP convergence in the lower stratosphere, and partly contribute to EP convergence in the winter (sub-)tropics. Also the contribution of transient waves of E39CA closely resembles ERAInterim, with mainly extratropical wave fluxes and contributions to EP convergence in the subtropics.

Fig. 5.9 (top) shows the long-term trend in the stationary component of the EP fluxes for both solstice seasons. It was found that increases in the wave forcing in large-scale stationary waves occur in the solstice seasons, and the stationary waves are shown in order to investigate the origin of changes in these wave fluxes. Significant increases in EP flux convergence in the lower stratosphere (sub-)tropics of the summer hemisphere are found in both seasons. The strong increase in convergence stems from stronger upward EP fluxes around 100 hPa in the summer hemisphere.

In DJF, in the tropical upper troposphere, both regions of increases and decreases in EP divergence are apparent. In the region of wave source (marked in the figure with the dashed contour), decreases of EP divergence occur at lower levels (around 275 hPa) and close to the equator, but also a small region of increases in EP divergence is apparent at latitudes around 20°S and at around 225 hPa. This trend pattern suggests a shift in the region of wave generation towards the subtropics in DJF. The region of positive trends in EP divergence around 10°N and 200 hPa lies in a region of climatological EP convergence, so that it indicates reduced EP convergence (waves are damped less strongly and can therefore propagate higher up, apparent as upward EP flux trends).

Also in JJA EP fluxes show significant trends in the upper troposphere. Here, in the region of climatological wave generation the trend is mostly significant and negative, i.e. indicating less generation of wave activity especially at lower altitudes. Only in the upper levels around 150 hPa EP divergence is enhancing, i.e. the source region of EP divergence is slightly shifting upwards in JJA.

The extratropics, on the other hand, show no considerable changes in EP fluxes in the stratosphere both in DJF and JJA over the 90-year period. This strongly suggests that the increase in wave forcing by stationary waves is due to changes in the generation or propagation properties of tropical waves, while extratropical waves play a minor role.

As it was shown in Fig. 5.3 also transient waves have a contribution to the increase in the forcing of upwelling, especially in northern winter. Also for transient waves, the trend pattern in EP fluxes (not shown) suggest that changes in the upper tropical troposphere lead to the increased wave drag in the lower stratosphere subtropics while extratropical waves show no significant trends.

The trend pattern in EP fluxes from the transient simulation are compared to the response in EP fluxes to changes in tropical SSTs (Fig. 5.9 bottom). The increase in upward EP fluxes and convergence in the summer subtropics in the lower stratosphere in both seasons as response to higher tropical SSTs closely resembles the trends in the transient simulation. Also here, the increased EP flux into the stratosphere seems to originate from the tropics. In the extratropics a considerable response to tropical SST changes occurs only in the northern mid-latitudes in DJF, where upward EP fluxes are reduced in troposphere and stratosphere. This might well be due to the artificially enhanced meridional temperature gradient (as only SSTs in the tropics are enhanced), and should have no relevance for the problem studied here, so will not be considered further.

In DJF, the difference pattern in the tropical upper troposphere broadly resembles the trend in the transient simulation. However, the wave source region is weakened in a larger region here, and an increase of EP divergence occurs only at upper levels (around 200 to 150 hPa) close to the equator. In JJA, on the other hand no considerable changes are found in the wave source region. Here, the only changes in the troposphere are a decrease of the EP divergence around 150 hPa and 25°N. The response in the lower stratosphere does, however, occur irrespective of the absence of changes in wave

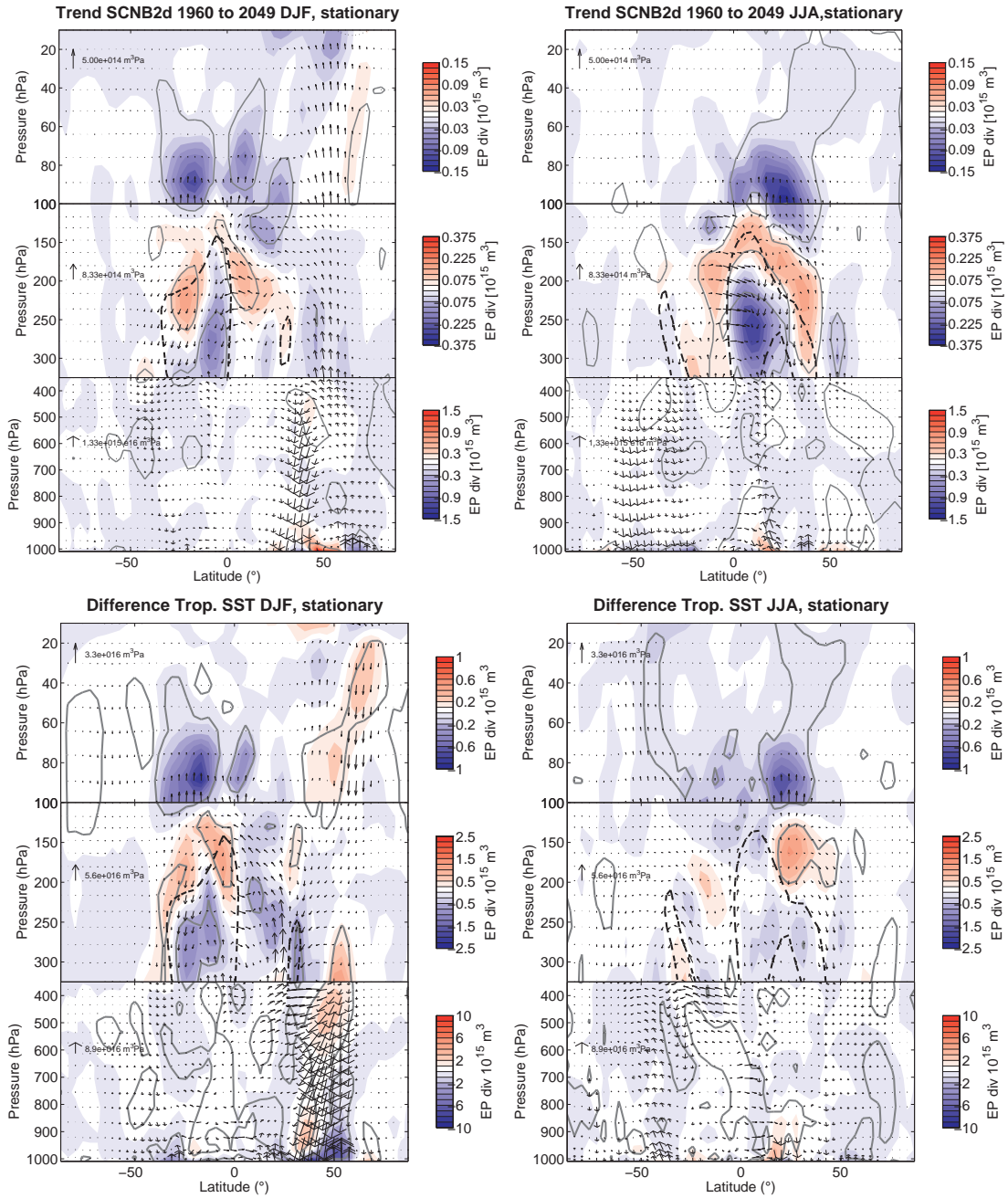


**Figure 5.9:** As in Fig. 5.7 but showing trends per decade in EP fluxes of stationary waves over 1960-2049 in the transient simulation (top) for DJF (left) and JJA (right). The lower panels show the response to changes in tropical SSTs (difference tropSST-Ref2000). Changes or trends in EP divergence are significant within the grey contours. The black dashed contour signifies regions of climatological EP divergence (contour line at  $0.1 \times 10^{16} m^3$ )

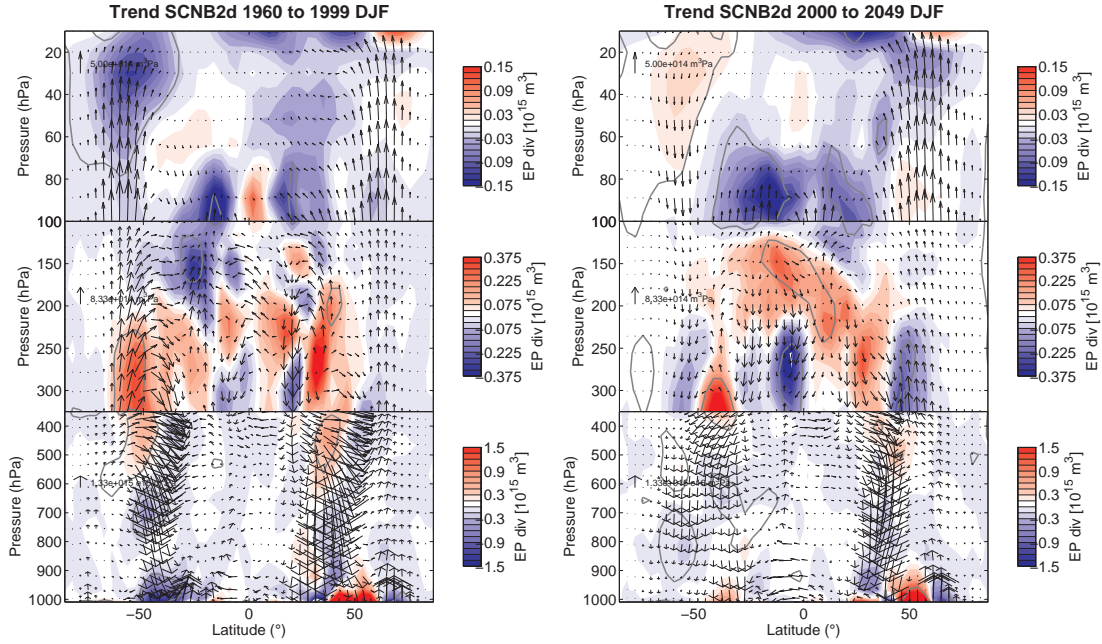


**Figure 5.10:** As in Fig. 5.9 but showing trends in EP fluxes for DJF for the past (1960 to 1999, left) and the future (2000 to 2049, right).

generation and closely resembles the trend in the transient simulation.

Overall the response of EP fluxes to tropical SSTs shows the same signature in the lower stratosphere than the trends in the transient simulation, but the changes in tropical wave generation do not occur in the same manner. Especially in JJA, the increase of EP fluxes into the lower stratosphere occurs here solely coincidental with a decrease in dissipation in the upper troposphere.

In addition to the 90 year long-term trends, Fig. 5.10 shows the trends in EP fluxes for sub-periods of the simulation, namely for 1960 to 1999 and 2000 to 2049 for DJF. As shown earlier, an increase in the southern hemisphere BDC in summer occurs in the past and is reversed in the future, and these changes are shown to be driven by changes in resolved wave forcing in Section 5.1.1. Indeed, the trends in EP fluxes show enhanced wave propagation and thus dissipation in the southern extratropics in the past, and changes of reversed sign in the future. The trends in wave drag (EP divergence) in the southern middle stratosphere are significant, and consistent with the circulation changes. It can be seen that the enhanced wave flux in the stratosphere does not result from more wave generation near the surface, but seems to be linked to changes in the dissipation in the upper troposphere. Note that in southern summer, winds are easterly in the stratosphere and wave propagation is inhibited. The mechanism for changes in the wave fluxes are discussed in detail below.

### Transition seasons

Representative for the transition seasons, the climatology of EP fluxes for northern spring (MAM) is shown in Fig. 5.7. Again the pattern for SON is mirrored about the equator but otherwise qualitatively similar (not shown). The wave forcing in the lower stratosphere is, however, weaker in SON. The pattern in the transition seasons is mostly symmetric about the equator, with about equally strong wave fluxes in the extratropics in both hemispheres, being refracted towards the equator in the upper troposphere. In the transition seasons the region of strong EP divergence (i.e. wave generation) in the tropical upper troposphere is much weaker than in the solstice seasons, but weak wave generation remains in the autumn hemisphere. This weak generation of stationary waves leads to weak EP convergence in the inner tropics in the lower stratosphere, while transient waves contribute to EP divergence at subtropical latitudes. The weaker generation of tropical waves explains the relatively weaker forcing by stationary waves in the transition seasons compared to the solstice seasons (see Fig. 5.3).

Also in MAM EP fluxes from E39CA agree quite well with ERAInterim. In both cases the transient waves show strong fluxes in both hemisphere in mid-latitudes. The tropical wave activity of stationary waves is reduced compared to DJF, more so in ERAInterim than in E39CA. This explains the more pronounced seasonality of wave forcing of upwelling by stationary waves in ERAInterim compared to E39CA (as it was shown in Fig. 5.3).

The long-term trends in wave forcing of tropical upwelling in the transition seasons was found to be due to transient waves in large parts (especially in northern spring). In particular, small-scale waves have a local maxima in forcing upwelling in the transition seasons, and the forcing is enhanced in a future climate.

Fig. 5.11 shows the trends in EP fluxes of transient waves in the transition seasons. Clearly, an increase in upward fluxes and therefore EP convergence in the lower stratosphere subtropics can be seen in both hemispheres both in MAM and SON. In the upper troposphere (around 200 to 150 hPa), some regions of decreased EP convergence (i.e. decreased dissipation) are apparent. The wave fluxes in the extratropical lower troposphere are decreasing, so that the increase in tropical wave fluxes can not be attributed to increased wave generation in the extratropical lower troposphere.

## 5.2 Discussion

In this section, the results of the previous sections are synthesised and possible mechanism for both the climatological wave driving of tropical upwelling and changes found in this forcing are discussed. The discussion on processes that might change wave activity is subdivided into a part discussing changes in wave generation and a part discussing changes in wave propagation and dissipation.

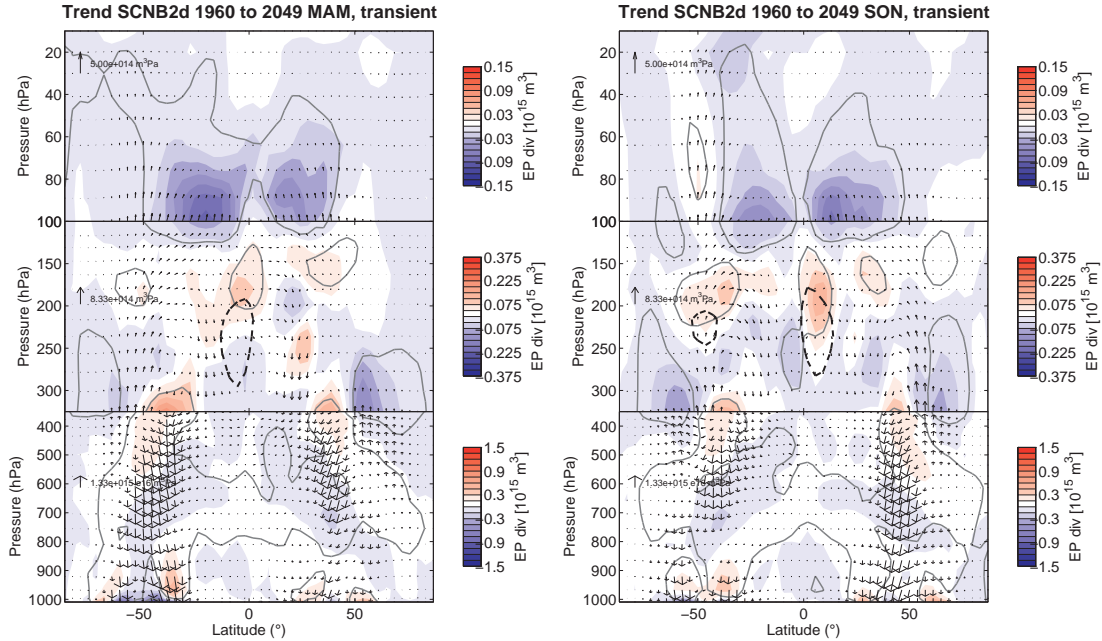


**Figure 5.11:** As Fig. 5.9, but trends in EP fluxes of transient waves for MAM (left) and SON (right).

### 5.2.1 Climatological forcing of tropical upwelling

The results presented in this study show that the residual circulation in the model is largely driven by resolved wave forcing, confirming the well-known mechanism of the BDC (e.g. Holton et al., 1995). However, it is also known that the extratropical wave-pump can not fully explain tropical upwelling, and here it was shown that tropical upwelling in the lowermost stratosphere is largely driven by local wave forcing in the (sub-)tropics. It could be shown that resolved wave forcing accounts for both the strength and the annual cycle in tropical upwelling. Both stationary and transient large-scale waves are important in contributing to the wave forcing, with the relative importance of stationary waves increasing towards the equator. Tropical upwelling forced by resolved waves in E39CA agrees quite well with ERAInterim reanalysis, but a discrepancy occurs between the strength of directly calculated mean vertical velocities in E39CA and ERAInterim. As discussed above, this discrepancy might be due to additional forcing by (non-orographic) gravity waves which are not considered in E39CA. However, processes related to resolved waves in the tropical troposphere and lower stratosphere are simulated adequately by the model.

It was found that wave convergence in the tropics occurs both due to the equatorward refraction of transient waves originating from the extratropical troposphere and due to the upward propagation of tropical waves that are generated in the upper troposphere. The relative importance of the two components varies with season. Stationary tropical waves lead to a stronger forcing in the solstice seasons, and the forcing is stronger in DJF compared to JJA. This is well understood since these waves

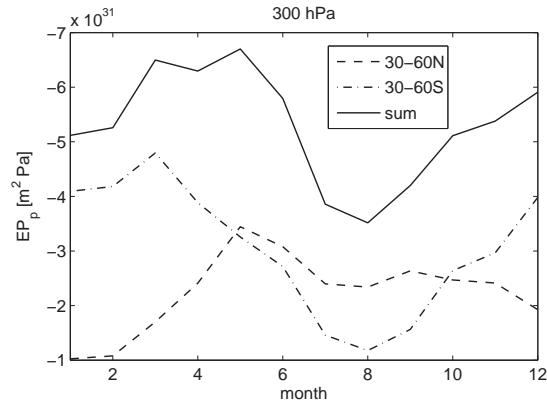


**Figure 5.12:** Climatological mean (1960-2049) of the annual cycle of vertical EP fluxes of transient waves at 300 hPa in the extratropics averaged over 30-60°N (dashed), 30-60°S (dash-dotted) and the sum of both (solid).

are generated by latent heat release through convection, which is strongest in the solstice seasons. The tropical waves are mostly confined to the lower stratosphere as low frequency waves are rapidly damped (Garcia and Salby, 1987, see also discussion below). The climatologies of EP fluxes confirm that generation of stationary waves in the tropics is strongest in the solstice seasons.

Also the transient wave forcing shows a seasonal cycle with weakest forcing in northern summer. It was shown that the transient waves are mostly of synoptic scale and that they originate from the extratropics, propagate upward and are refracted towards the equator so that they contribute to wave forcing in the subtropics. The seasonality in the forcing might arise from a) a seasonal cycle in extratropical wave generation or b) a seasonal dependence of the ability of transient waves to propagate into the tropics. To shed light in this question, Fig. 5.12 shows upward EP fluxes at 300 hPa averaged over 30-60°N/S. If a) was true, we expect a similar seasonal cycle in the upward propagation in the extratropics than in tropical wave fluxes. Indeed, the sum of wave fluxes from both hemispheres (which act together to drive tropical upwelling) shows lowest values in August and a maximum in northern spring, as does the wave forcing of tropical upwelling by transient waves (Fig. 5.3). Therefore, the seasonal cycle in wave forcing by transient synoptic-scale waves can be explained by the seasonal cycle in the amount of wave activity propagating upward from the lower troposphere. Seasonal differences in the local conditions that influence wave propagation (hypotheses b) can not be excluded to contribute to the annual cycle, but are not necessary to explain the seasonality.

## 5.2.2 Changes in wave generation

**a. Tropical waves** Enhanced wave driving in the solstice seasons is caused by increases in wave convergence in the summer hemisphere lower stratosphere. The in-

creased upward EP flux is clearly originating from tropical waves. As discussed in Section 5.1.2, in the transient simulation, the increase of EP divergence in the upper troposphere is showing changes in the wave generation of tropical waves. While the generation is inhibited in large parts, a shift of the region of wave generation towards the subtropics is found in DJF, and a shift towards higher altitudes in JJA.

Large-scale tropical waves are forced by the zonally asymmetric heating by deep convection (e.g. Gill, 1980). It can be expected that changes in convective latent heat release drive changes in wave generation. As shown by Runde et al. (2010), who uses the same simulations as in this study, changes in tropical SSTs lead to changes in the pattern of occurrence of deep convection. The total number of convective events was shown to decrease with increasing SSTs, but the individual event is strengthening (i.e. the single events have a stronger mean cloud updraft). The changing pattern in, for example, convective precipitation (which is positively correlated to the number of convective events) is strongly dependent on the particular change pattern in SSTs, and therefore varies for different seasons and periods. These changes in properties of convection, along with a general increase of the evaporation of water on the surface due to higher SSTs, is likely to modify strength and location of latent heat release. As wave generation is sensible to the location of latent heat release (Norton, 2006), a shift in the region of strong deep convection is likely to modify the tropical wave response.

The sensitivity simulation in which only tropical SSTs are modified showed a response in the tropical lower stratosphere which resembles closely the long-term trend in the transient simulation. This allows to conclude that processes associated with the tropospheric warming by tropical SSTs are responsible for the increase in the wave fluxes in the lower stratosphere. However, the pattern indicative for changes in wave generation were found to be different in this simulation. While in DJF, tropical wave generation appeared to be largely suppressed by higher tropical SSTs, but is at the same time shifted slightly towards higher levels, in JJA no changes in tropical wave generation were found. The different behaviour in the tropical upper troposphere in the transient and sensitivity simulations arises presumably from the different underlying time period and therewith different changing pattern in the SSTs. Analysing trends from the transient simulation for sub-periods of the whole simulation also reveals different behaviour in the wave fluxes in the upper troposphere. However, the signal in the lowermost stratosphere appears to be very robust and occurs irrespective of the nature of the changes in the upper troposphere. This suggests that changes in wave generation are not the determining factor in controlling changes in the wave flux into the lower stratosphere.

As the driver of changes in wave fluxes and hence tropical upwelling is found to be changes in tropical SSTs, additional evidence on the mechanisms that lead to changes in wave fluxes by modifications in tropical SSTs might be deducible from the internal variability in tropical SSTs, namely in response to ENSO. Fig. 5.13 (left) shows the response of EP fluxes to ENSO by comparing years with ENSO positive phases to years

with ENSO negative phases (for more details on the calculation see Leuthold, 2010). The response in the lower stratosphere resembles the trend pattern with enhanced wave propagation into the lower stratosphere and hence enhanced EP convergence. Tropical wave generation (indicated by the dashed line in Fig. 5.13) is clearly weakened in ENSO warm phases compared to ENSO cold phases, and so are the regions of wave dissipation at around 150 hPa and 20°N/S. It seems somewhat surprising that the convective wave generation is weaker in ENSO warm than ENSO cold phases, as higher SSTs in ENSO warm phases should lead to enhanced convection in the ENSO region and thus enhanced latent heat release. Indeed, in the simulation used here, both the number of convective events and the strength of individual events (i.e. the mean updraft per event) intensifies in the eastern pacific in ENSO warm phases, and no other significant changes in convective events occur (as shown in Runde, 2009). The decrease in wave generation in spite of more and stronger convective activity might be caused by the change in the horizontal distribution of latent heat release: with increased convection in the eastern pacific in addition to the maximum in convection over Indonesia, the distribution of latent heat release is extended over a broader range of longitudes, i.e. more zonally symmetric, which might lead to a less pronounced wave excitation (e.g. Norton, 2006). The crucial result here is that as response to ENSO, less tropical waves are generated, less dissipation is occurring in the upper troposphere (which is partly due to less wave generation, i.e. less wave energy that can be damped) but still more wave energy reaches the tropical lower stratosphere. This supports the findings from in the sensitivity simulation that enhanced wave fluxes in the lower stratosphere are occurring irrespective of the changes in wave generation in the tropical troposphere.

**b. Extratropical waves** Extratropical waves contribute to the wave forcing of tropical upwelling, especially synoptic scale transient waves that are refracted towards the equator and dissipate in the subtropics. It was shown that the annual cycle in climatological transient wave forcing could be explained by the seasonality of mid-latitude wave fluxes. The changes in extratropical wave fluxes at 300 hPa are, however, not consistent with the increased forcing in the tropics. Indeed, both transient and stationary upward wave fluxes averaged over 30–60° latitude of each hemisphere show no significant changes from 1960 to 2049 throughout the year. Therefore we conclude that the increases in wave forcing in the tropical lower stratosphere can not be attributed to changes in extratropical wave activity in the troposphere. Also the changes in EP fluxes in the southern hemisphere extratropics associated with the CFC-induced ozone depletion are not due to changes in wave generation in the troposphere, but rather to changes in the propagation, as it is apparent from Fig. 5.10.

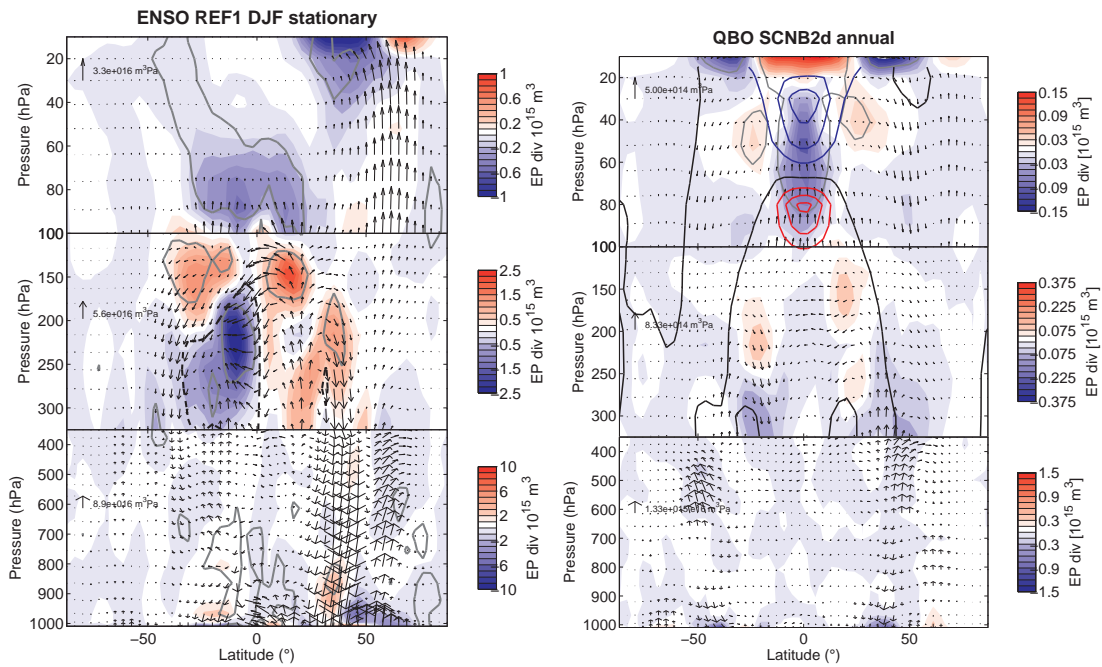


**Figure 5.13:** As in Fig. 5.9 but showing the response to ENSO in DJF in REF-B1 (left) and to the QBO in the annual mean in SCN-B2d (right). The ENSO response is calculated as composite of years with positive ENSO events minus years with negative ENSO event. A positive or negative ENSO event is defined if the nino3.4 index differs from its mean by more than one standard deviation (see Leuthold, 2010). The QBO response is calculated with linear regression and the annual mean response is shown. Together with the QBO response in EP fluxes, the associated vertical shear  $dU/dz$  anomaly is shown as contours (red: positive, blue: negative, black: zero line).

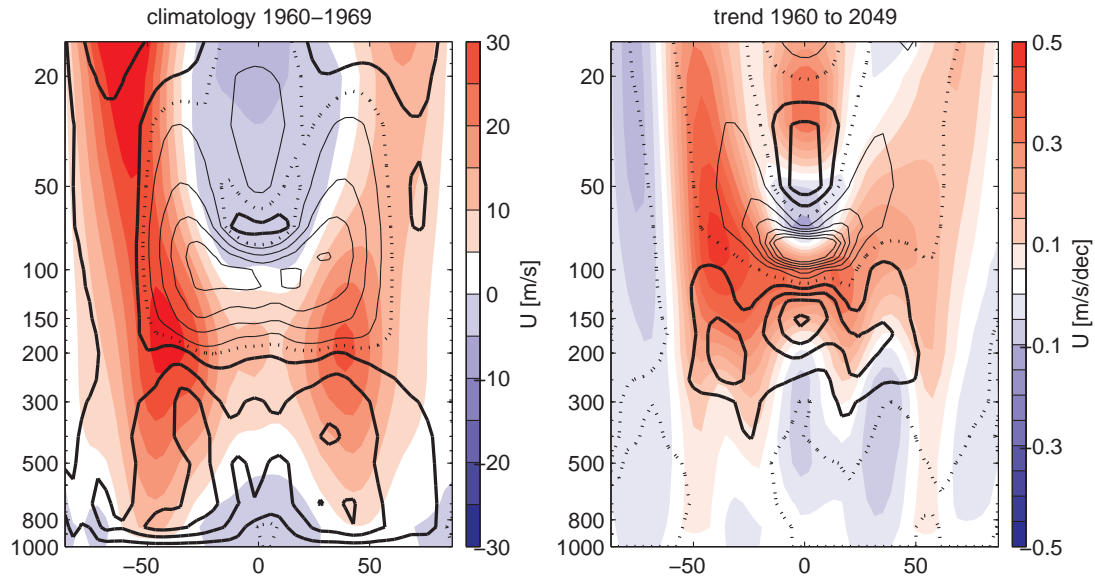


**Figure 5.14:** Left: Climatological (1960-2049) annual mean of the zonal mean zonal wind (colour) with the vertical shear  $dU/dz$  superimposed as contours. Thick (thin) lines denote positive (negative) values, the dotted line is the zero contour, contour intervals are  $0.5 \times 10^{-3}/s$ . On the right the long-term trend (1960 to 2049) in the zonal wind and the vertical shear is shown. Contour intervals for the vertical shear are  $2.5 \times 10^{-5}/s/dec$ .

### 5.2.3 Changes in wave propagation

**a. Tropical waves** Not only enhanced wave generation can increase the EP convergence in the lower stratosphere, but also changes in the ability of waves to propagate into this region. Both in the transient simulation and in the sensitivity simulations where the SSTs are modified, the zonal wind increases just above and equatorward of the subtropical jets. The modification of the background zonal winds is likely to modify propagation and dissipation of waves.

Garcia and Salby (1987) used a simplified model to characterise the wave response to latent heating. According to the arguments presented in their study, the damping of tropical waves is basically determined by the ratio of the time scale of the wave (i.e. the frequency of the wave) to the time scale of thermal relaxation (parametrised there as Newtonian cooling). Therefore wave damping is acting stronger on waves with low intrinsic frequencies. The background zonal mean wind acts to Doppler shift the frequency of the waves, and therewith either enhances or inhibits damping. For westward propagating waves, easterly winds act to reduce the frequency and therefore enhance wave damping while westerly winds inhibit wave damping. If the wind is decreasing with height, i.e. in regions with easterly shear, the frequency of westward propagating waves decreases with height and therefore vertical wave propagation is inhibited.

In the climatological mean the zonal mean wind is increasing with height below the

level of the subtropical jets and decreasing above, with a transition to easterly winds in the tropics in the lower stratosphere at about 100 hPa (see Fig. 5.14). This leads to strong damping of tropical waves in the lower stratosphere, and suppression of vertical wave propagation to altitudes above about 80 hPa in the tropics in the climatological mean. As stated above, the subtropical jets increase and are shifted equatorward and upward in a changing climate. Winds become more westerly in the lower stratosphere and the zero wind line as well as the region of easterly shear is shifting to higher levels (shown in Fig. 5.14 right). Therefore, wave frequencies are Doppler-shifted to higher frequencies and wave damping is inhibited in the region of enhanced westerlies. Vertical wave propagation in the upper troposphere and lower stratosphere is favoured due to the upward shift of the easterly shear zone. All in all this leads to less wave dissipation in the upper troposphere, therefore enhanced wave propagation to higher levels and enhanced damping in the lower stratosphere.

In Fig. 5.14 only the annual mean trend is shown, but changes are consistent throughout the seasons. The trend in the zonal winds in each hemisphere is stronger in the respective winter and spring hemispheres, but a trend towards stronger westerlies and the upward shift in the easterly shear zone occurs in all seasons.

The changes in the subtropical jets as response to tropical SST enhancement resembles the trend in the transient simulation, and also the difference pattern in the vertical shear of the zonal wind shows the same upward shift of the easterly shear zone as in the transient simulation (not shown). As the QBO phases in the two time-slice simulations compared here (tropSST-Ref2000) are identical, the difference pattern is purely due to the enhancement in tropical SSTs. The trend from the transient simulation might still show remnants of the QBO (even though the QBO was accounted for as a basis function in the trend estimation using linear regression). The changes in the zonal wind and its vertical shear are robust features in both the transient and sensitivity simulations.

As shown in the discussion of tropical wave generation, in response to ENSO a similar signal in EP fluxes in the tropical lower stratosphere is observed as for the long-term trend despite less wave generation in the tropical troposphere (see Fig. 5.13 left). So what is the mechanism for enhanced wave fluxes entering the lower stratosphere in ENSO warm phases? As for the trend, tropical tropospheric temperatures are enhanced during ENSO warm phases, which leads to a strengthening and upward shift of the subtropical jets. Thus with the ENSO response another case is presented in which enhanced wave propagation occurs in conjuncture with enhanced and shifted subtropical jets, and for this case wave generation can clearly be excluded as cause of enhanced wave activity reaching the lower stratosphere.

Note that the control of vertical wave propagation in the tropics by zonal wind shear is basically the same mechanism that is acting to drive the QBO. Even though the QBO is not generated internally in the model used here but prescribed by nudging of tropical zonal winds, we expect to see a response of the wave fluxes to the QBO. The

response of EP fluxes to the QBO was extracted by running a linear regression model (see Appendix C) and is shown in Fig. 5.13 (right). Indeed, vertical wave propagation is enhanced in anomalous westerly shear, and waves dissipate once they reach levels of easterly shear. The behaviour of the wave fluxes as response to the QBO confirms the important role vertical zonal wind shear plays in controlling the vertical propagation of tropical waves in the model.

**b. Extratropical waves** As it was shown in Fig. 5.10, changes in extratropical wave fluxes are responsible for the changes in the southern hemisphere BDC in summer. In the climatological mean, winds in the southern summer stratosphere are weak and turn easterly in the middle stratosphere (see Fig. 5.15). The strong radiative cooling due to ozone destruction (or rather the lack of radiative warming) caused by CFCs leads to a strongly enhanced meridional temperature gradient in the southern hemisphere. This in turn causes a strong increase in zonal mean winds (see Section 3.1). Therefore, the weak westerlies are strengthened, and the zone of easterlies is shifted upward by ozone depletion, i.e. in the period 1960 to the present. As it is shown in Fig. 5.15 the upward shift of the zero wind line is clearly linked to an upward shift of the region of EP convergence. As winds are more westerly, wave propagation is favoured which causes waves to propagate to higher levels and dissipate there. Hence the change in resolved wave forcing as response to ozone depletion can clearly be linked to changes in the background state in the stratosphere.

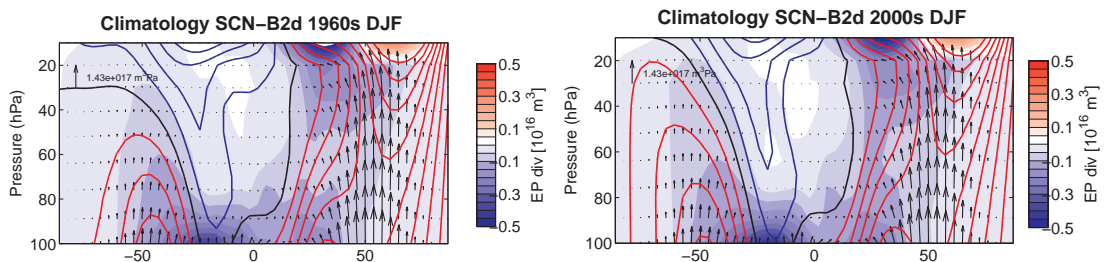


**Figure 5.15:** Mean EP fluxes and divergence for 1960-69 (left) and 1995-2004 (right) in DJF. Superimposed is the zonal mean zonal wind (blue solid lines negative, red solid lines positive and black line zero wind line. Contour intervals are 5 m/s.)

### 5.3 Summary

In this chapter, the climatology and changes in wave driving of the meridional circulation and in particular of tropical upwelling in the lower stratosphere was investigated. The key findings are:

**Climatology** As expected, the BDC is found to be largely driven by resolved wave forcing. Only in the northern mid-latitudes, other forcings play a role, most likely

orographic gravity waves that are excited preferably in the northern hemisphere. Also tropical upwelling in the lowermost stratosphere was found to be driven by resolved wave forcing that is applied locally in the (sub-)tropics. Waves that lead to the forcing in the (sub-)tropics originate both from the inner tropics (planetary large scale waves that are excited by convection and are stronger in the solstice seasons) and from the extratropics (synoptic scale waves that are generated in the mid-latitudes and refracted towards the equator).

**Trends in tropical upwelling** The increase in tropical upwelling in the lower stratosphere throughout the year can be explained by an increase in resolved wave forcing in the (sub-)tropics. While convective wave generation is modified and might contribute to the change in wave forcing, evidence was presented that suggests that the main mechanism for enhanced wave drag in the lower stratosphere is enhanced wave propagation into this region caused by changes in the background winds.

**Trends in the southern summer BDC** The changes in the BDC in the southern extratropics were shown to be driven by resolved wave forcing, that enhances in the past and reduces in the future. This is linked to changes in the zonal mean winds in the stratosphere that are influenced by ozone depletion and lead to enhanced (inhibited) wave propagation in the past (future).

## Chapter 6

# Impact of changes in the stratospheric circulation on transport and ozone

The atmospheric ozone layer was strongly influenced by anthropogenic emissions of CFCs over the last decades. The Montreal Protocol and its amendments and adjustments has led to a significantly reduction of emissions of CFCs and halogen levels are now decreasing (e.g. WMO, 2007). In the 21st century, ozone concentrations are expected to return to 1980 levels. However, not only changes in the halogen loading but also in GHG concentrations will impact the ozone layer, and thus alter the return date of ozone. It is known that enhanced GHG concentrations lead to a cooling of the stratosphere. This will in turn influence chemical reactions as many ozone destroying reaction rates are temperature depended (e.g. Portmann and Solomon, 2007). Furthermore, changes in dynamics might alter transport and hence influence the distribution of ozone. The meridional residual circulation was found to strengthen in the tropical lower stratosphere in a changing climate in the model simulations used in this study, as shown in the previous chapters. This is likely to influence the redistribution of ozone, in particular in the dynamically controlled lower stratosphere. These changes are superimposed on the enhancement of ozone concentrations expected in the middle (and upper) stratosphere driven by the climate-change related cooling of the middle stratosphere. In order to be able to assess the future development of the ozone layer, it is important to understand the impact of climate-change on ozone. In particular, it is desirable to untangle in which parts the simulated ozone recovery can be attributed to the decline in halogen concentrations and in which parts to GHG-induced climate change. Therefore it is crucial to be able to distinguish between different chemical and dynamical processes that act on ozone. The aim of this chapter is to separate and quantify the influence of changes in the meridional circulation on stratospheric ozone, and evaluate its importance compared to changes induced by chemical processes.

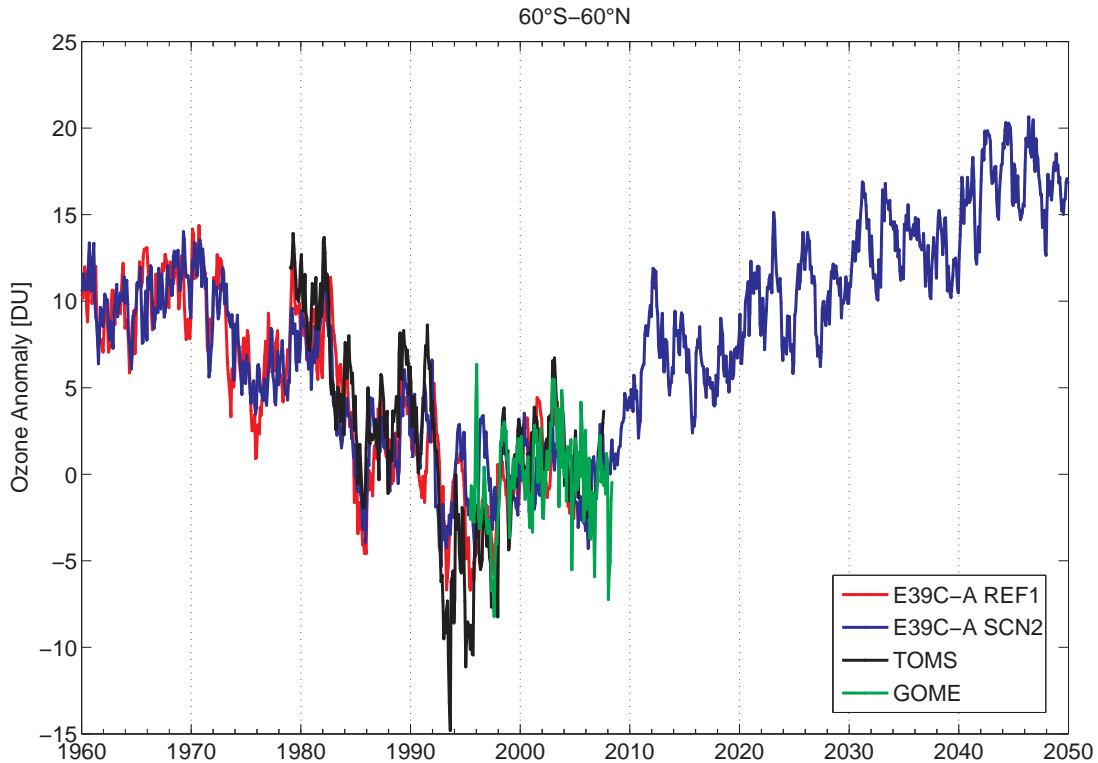


**Figure 6.1:** Time series of the near-global mean ( $60^{\circ}\text{S}$  to  $60^{\circ}\text{N}$ ) total column ozone anomalies (with the mean annual cycle of 1995–2004 subtracted) for REF-B1 (red), SCN-B2d (blue), and for TOMS (black) and GOME (green).

In the first section, the temporal evolution of the atmospheric ozone layer in the model simulations used here will be described briefly. Then, the sensitivity simulations as utilised in Chapter 4 will be used to identify drivers of ozone changes. In the second part of the chapter, a new method will be introduced which allows to attribute changes in ozone to changes in chemistry and in transport. This method also enables to quantify ozone fluxes between different regions of the atmosphere. At the end of the chapter, the results will be discussed and summarised.

## 6.1 Evolution of atmospheric ozone

### 6.1.1 Trends in ozone

The two transient simulations REF-B1 and SCN-B2d (see Chapter 2) are designed to simulate the long-term evolution of the atmosphere in the past and future. Here, the long-term trends in ozone as simulated by E39CA are analysed.

To characterise the temporal evolution of the ozone layer, in Fig. 6.1 the time series of the near-global mean ( $60^{\circ}\text{S}$ – $60^{\circ}\text{N}$ ) of total column ozone is shown for the two transient simulations with E39CA. The well-known strong depletion of ozone and subsequent recovery are apparent. These long-term changes are, however, superimposed

by anomalies forced by natural variability like the 11-year solar cycle and the QBO (e.g. Dameris et al., 2005; Steinbrecht et al., 2006). Therefore it is not straight forward to determine the onset of ozone depletion and recovery. For example, the increase in near-global ozone from the mid-1990s to the mid-2000s might be interpreted as onset of ozone recovery, but it is known that this increase is at least partly due to the solar cycle (Dameris et al., 2005). Together with the two transient simulations, total ozone time series from the satellite instruments TOMS and GOME are shown here (for details see Loyola et al., 2009). The anomalies in total ozone agree remarkably well between observations and model. A detailed evaluation of total ozone from the model simulations used here is given in Loyola et al. (2009). It is shown that not only the temporal evolution of total ozone but also the global distribution is well simulated, despite an offset in total column ozone in the model of about 40 DU. The reasons for this offset, which is nearly constant across latitudes and seasons, is not clarified so far. However, as the model simulates the ozone distribution and especially the temporal evolution of ozone well otherwise, it is assumed that this deficit is not affecting the results of this study to a large extend. In the following height-dependent trends of ozone mixing ratios are investigated. Even though the exact point in time at which ozone starts to recover is hard to determine, using year 2000 as division between the period of ozone depletion and ozone recovery seems appropriate. Therefore, the approach of dividing the simulation period into a past period from 1960 to 1999 and into the future from 2000 to 2049 is adapted here, following the division used in the previous chapters.

The seasonal trends in ozone mixing ratio for past and future are shown in Fig. 6.2. The trends are calculated by applying a linear regression model as described in Appendix C. The trends in the past are dominated by strong ozone loss in the stratosphere, while ozone mixing ratios increase in the troposphere. Strongest negative ozone trends are found in Antarctica at around 70 hPa in spring, showing that the model captures the well-known strong ozone depletion by heterogeneous chemistry. For the past period, trends from REF-B1 are compared to SCN-B2d, and it can be seen that the trend estimations from the two simulations agree very well despite offsets in the climatology (see discussion in Chapter 2).

In the future (years 2000 to 2049), ozone concentrations increase both in the troposphere and in the stratosphere, the only exception is a small region in the tropical lower stratosphere. Here, negative ozone trends are found throughout the year, strongest in DJF and weaker and not significant in JJA. In spring in the lower stratosphere over Antarctica, the strong negative ozone trend of the past is reversed and ozone recovers as the CFC loading decreases in the future.

### 6.1.2 Drivers of ozone changes

As discussed in Chapter 4 the sensitivity simulations are designed to disentangle the effects of the different boundary conditions that are prescribed in the model on the

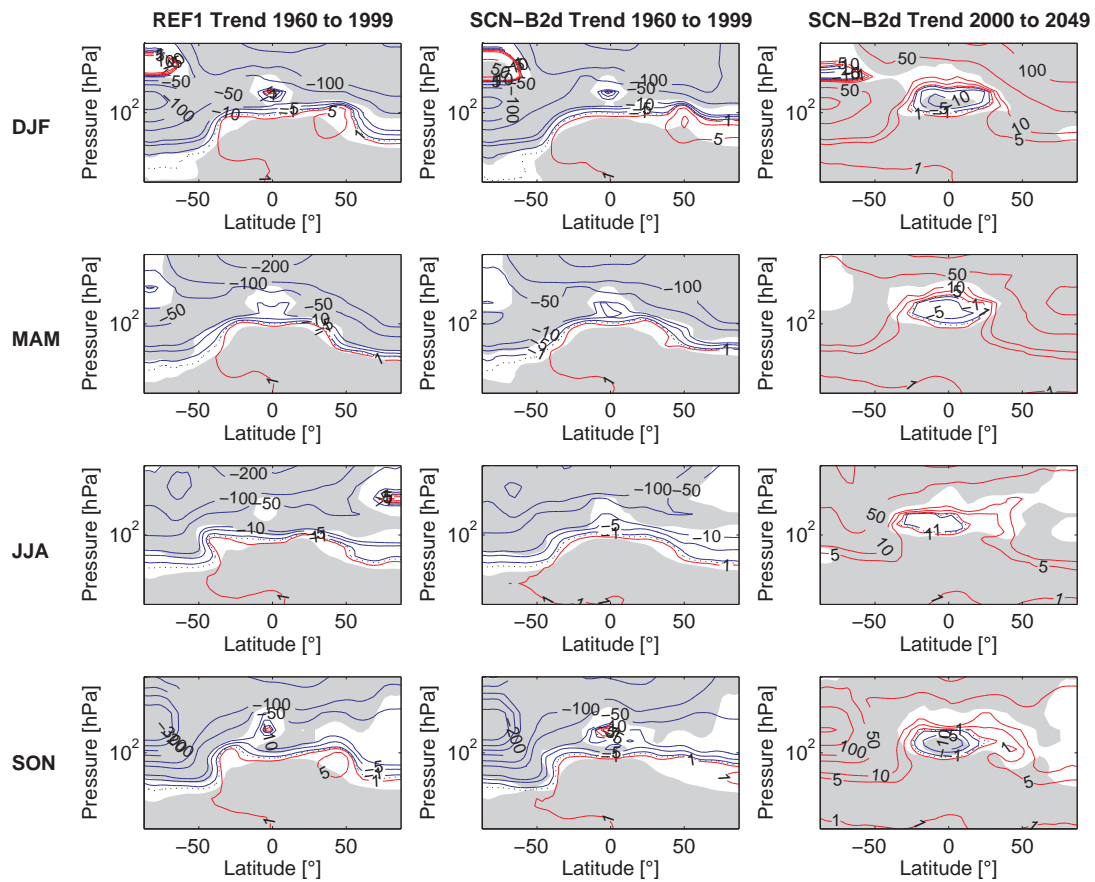


**Figure 6.2:** Long-term linear trends in ozone volume mixing ratio [ppb/decade] for years 1960 to 1999 in REF-B1 (left), in SCN-B2d (middle) and for years 2000 to 2049 in SCN-B2d (right). Trends are significant on the 95% level in the regions of grey shading.

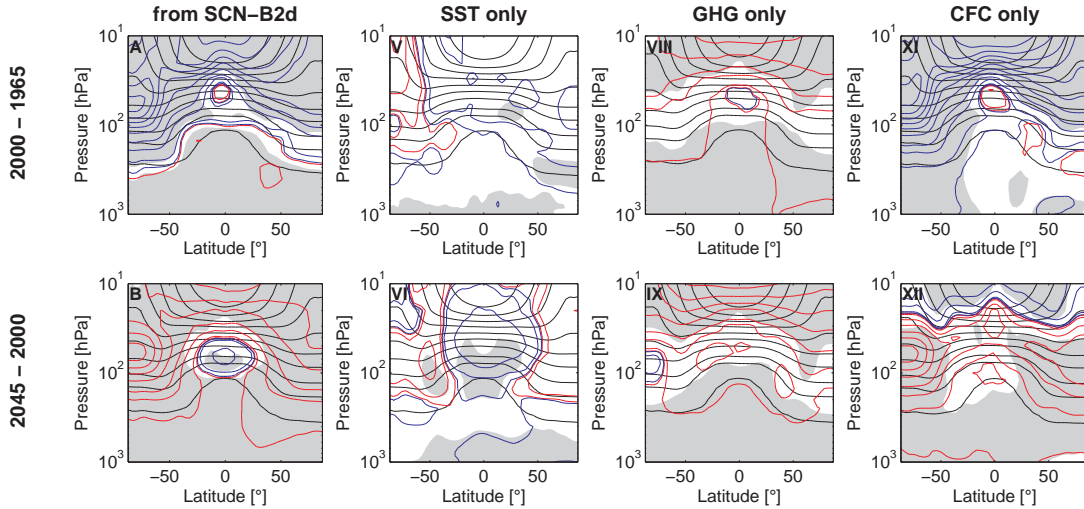


**Figure 6.3:** Response of ozone mixing ratios to changes in all boundary conditions (left), to SSTs only (middle left), to GHGs only (middle right) and to CFCs only (right). The upper panels show differences from periods 2000 - 1960s, the lower panels 2040s - 1960s. The number in the upper left corner of each panel refers to the differences as defined in Fig. 4.1. Black contours show the climatologies (contours at 10,100,500,1000:1000:8000 ppb), red and blue contours denote positive and negative responses, respectively (contours at 1, 10, 50, 100:100:800 ppb), and grey shading denotes significance on the 95% level.

atmosphere. Here, the response in ozone is shown in Fig. 6.3, following the definitions given in Chapter 4.

As seen in the trend pattern shown in Fig. 6.2, ozone is strongly decreasing in the stratosphere over the past 40 years. The response to the individual boundary conditions clearly reveals that this is the effect of changes in CFCs, as expected. Increases in GHGs counteract the decrease of ozone in the middle stratosphere as they lead to an enhancement in ozone mixing ratios. The annual mean change in ozone due to changes in SSTs is small and barely significant in the past.

In the future, the decrease in CFC loading does, as expected, lead to a regeneration of ozone in the polar regions<sup>1</sup>. As in the past, enhanced GHG concentrations lead to higher ozone concentrations in the middle stratosphere. In the future, a significant impact of SST changes on ozone is found. Ozone mixing ratios are decreased in the tropical lower stratosphere as response to changes in SSTs. In the extratropics only weak and barely significant increases in ozone in the lower stratosphere are induced by SSTs changes.

<sup>1</sup>Note that at the upper boundary there is an inconsistency in the boundary conditions in the 2040GHG+SST run, as  $NO_y$  concentrations were fixed at the 2000 level while  $N_2O$  was changed. Therefore in the comparison of the decades of the transient simulation with the time slice, the  $NO_y$  concentrations differ (2040 in the transient simulation, 2000 in the time-slice simulation). Thus the negative difference at the upper model levels in the 'CFC difference' plot are probably due to changes in  $NO_y$ .

The SST and GHG induced changes in ozone can be understood when considering the results of Chapter 4. There, it was shown that changes in SSTs lead to tropospheric warming and enhanced tropical upwelling but leave the temperatures in the stratosphere largely unchanged. In response to the direct radiative forcing by GHGs, on the other hand, stratospheric temperatures are decreased but the meridional circulation and tropical upwelling is barely affected. Therefore, the response in stratospheric ozone in the SST simulations can be regarded as the response to changes in the meridional circulation. As shown extensively in the last chapters, the change in the meridional circulation is characterised by stronger upwelling in the tropical lower stratosphere. Enhanced upwelling across the tropopause is expected to transport ozone-poor air from the troposphere into the lower stratosphere, therewith decreasing the ozone concentration here (as found in Fig. 6.3).

As most ozone destructing chemical cycles are temperature depended, and ozone is destroyed more slowly for lower temperatures, the cooling of the stratosphere is expected to lead to enhanced ozone concentrations. This explains the response of ozone to GHG changes.

Using the sensitivity simulations it was possible to disentangle two different effects on ozone caused by climate change: changes in chemistry due to stratospheric cooling on one hand and changes in transport of ozone due to changes in the meridional circulation on the other hand. The simulations suggest that the strong positive trend in ozone in the future in the stratosphere is in parts due to stratospheric cooling, while the negative trend in the tropical lower stratosphere is induced by enhanced tropical upwelling. While the drivers of ozone changes could be identified, the processes are not necessarily clearly assessable. In the next section, a method will be introduced that allows to attribute changes in ozone to changes in chemistry and transport.

## 6.2 Attribution of ozone changes to chemistry and transport

In this section, a new method will be presented that allows to attribute changes in ozone to changes in chemistry and transport. As it is known which processes act as sources and sinks for ozone in the model (and in reality), the ozone balance equation can be used to reconstruct changes in ozone from one timestep to the next, and to attribute these changes to the different source and sink terms. Therewith tendencies are decomposed into parts caused by chemistry and parts caused by transport. The chemistry term can be split up further into production and destruction of ozone, and it could even be split up further to study the relative importance of different chemical reaction cycles. However, as the focus of this work is on transport, the chemical tendencies are used here mainly to evaluate the relative importance of chemistry versus transport. The novel piece of diagnostic here is the break down of the transport tendencies into export

of ozone and import of ozone from different regions of the atmosphere. The ingredient needed for that is the ozone origin diagnostic which was developed by Grewe (2006) and used there to study a steady state ozone distribution. This diagnostic, modifications therein and some results are discussed in Sec. 6.2.1. With the decomposition of ozone tendencies in combination with the ozone origin diagnostic, it is possible to study the ozone budget in different regions of the atmosphere including ozone fluxes between these regions (shown in Sec. 6.2.2). This can be used to study and understand the annual cycle in ozone, interannual variability and also long-term changes in ozone. While some examples are given for how the annual cycle in ozone can be understood using the method presented here, the main focus in this work is on long-term changes in ozone. The last section (Sec. 6.2.3) shows how long-term changes in ozone can be attributed to changes in the sink and source terms within this concept.

### 6.2.1 Ozone origin diagnostic

#### Method

The ozone origin diagnostic was introduced by Grewe (2006) and adopted for the model simulations used in this study. This diagnostic allows to partition ozone at any point in the atmosphere into the amount of ozone that originates from 9 predefined regions dividing the atmosphere. Technically, 9 additional ozone fields are introduced. Each ozone field consists of ozone that is produced in one of the regions only. The destruction on the other hand is applied to all ozone fields according to their relative contribution. The tendency of the ozone field  $i$  at a location in region  $j$  can be expressed as:

$$\frac{\partial O_3^i}{\partial t} = P\delta_{ij} - D\frac{O_3^i}{O_3}O_3 + T_i \quad (6.1)$$

Here  $O_3^i$  denotes the ozone field  $i$ , which consists of ozone produced in region  $i$ .  $O_3$  is the full ozone field, consisting of ozone produced in the whole atmosphere.  $P$  is the total amount of ozone produced,  $D$  is the destruction rate and  $T_i$  is the amount of ozone of origin  $i$  transported to the respective point in the atmosphere. The delta operator  $\delta_{ij}$  is one only if  $i = j$ , as the produced ozone is only added to ozone field  $O_3^i$ . It can be easily shown that the sum of all nine ozone fields equals mathematically exact the full ozone field at all times if it does so for the initial condition. Also for all other initial conditions, the sum of the ozone fields converges exponentially to the full ozone field, i.e. the method is convergent. In practice, the sum might, however, differ from the full ozone field due to numerical diffusion that acts differently on the tracer fields as they have different gradients. Therefore, the mass of the sum of the 9 partitioned ozone fields is scaled to the mass of the full ozone field after each time step. Hence it is always given that

$$O_3(lat, long, level, t) = \sum_{i=1}^9 O_3^i(lat, long, level, t) \quad (6.2)$$

In Grewe (2006) it was shown that the numerical error is less than 2% almost everywhere in the atmosphere, only small regions in the tropical tropopause region and at high latitudes showed errors of more than 5%. Since in the model version used in the current study the semi-lagrangian advection scheme of the model in Grewe (2006) was replaced by the fully lagrangian scheme ATTILA, the errors due to numerical diffusion are expected to be even smaller.

The partitioning of the atmosphere into the 9 regions of ozone origin is shown in Fig. 6.4. The regions are chosen so that 3 boxes represent the troposphere (northern and southern mid-latitudes and tropics) and the 6 remaining represent different regions of the stratosphere. In contrast to Grewe (2006), the extratropical stratosphere is not subdivided into lower and middle stratosphere but into mid-latitudes and high latitudes. Grewe (2006) showed that ozone produced in the extratropical lower stratosphere is not a major contributor to the total amount of ozone anywhere in the atmosphere. The objective of the subdivision done here is to be able to examine the role of ozone production at high latitudes in summer and to study transport of ozone between high, middle and low latitudes.

The latitudinal boundaries are chosen to resemble barriers to transport, i.e. the tropical and polar barrier, and to subdivide the atmosphere according to regions of ozone production and destruction. Fig. 6.5 shows the net ozone production in the solstice seasons in the 2000s. The boundary between tropics and mid-latitudes is chosen so that in the winter hemisphere the boundary divides the tropical region of net production from the region of net destruction in the winter extratropics. The boundary between middle and high latitudes resembles approximately the separation of air masses within and outside the polar vortex, which acts as transport barrier (see grey dashed lines in Fig. 6.5). Obviously the location of the jet (and the transport barrier) is variable and, especially in the northern hemisphere, the vortex is not zonally symmetric. The location of the wind maxima in the seasonal mean, as shown in Fig. 6.5, is, however, relatively stable from year to year (as indicated by the horizontal bars that represent one standard deviation) and close to the defined boundaries between middle and high latitudes. The model levels that separate the three tropospheric regions from the stratospheric regions are chosen to roughly represent the tropopause. The structure of the dynamical tropopause (specified at 3.5 PVU, see Grewe and Dameris, 1996) varies for different seasons (see Fig. 6.5), but the interannual variability in the location of the tropopause is relatively small (as indicated by the  $1\sigma$  vertical bars). The location of the tropopause, the wind jets and the zero-line of ozone net production is almost unchanged in the future (2040-49) compared to the 2000s that are shown in Fig. 6.5. Therefore, it can be assumed that air masses with similar properties are described by the fixed boxes in both present and future.

For simplicity, fixed boundaries following model levels and latitudinal grids are used here. This allows to analyse the properties of ozone from a certain region, but air masses are not separated according to their dynamical origin (i.e. air masses within the polar

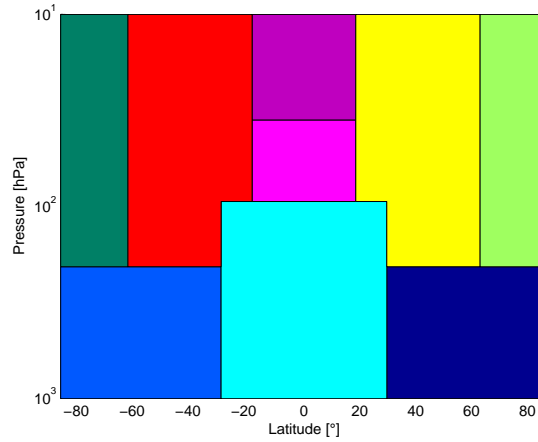


**Figure 6.4:** Defined regions of the ozone origin diagnostic with each region being marked in one colour.

vortex). Therefore, it is, for example, not possible to conclude on transport across the polar barrier if ozone molecules originating from a polar box are detected in mid-latitudes - they might have been outside the polar barrier already in the polar box. The same is true for cross-tropopause transport: as the boundary between the 'tropospheric' and 'stratospheric' boxes does not equal the tropopause, air masses that are transported across this boundary are not necessarily crossing the tropopause. Therefore, by using fixed boundaries, the question can be addressed how much ozone originating from different geographical regions contributes to the ozone amount at a certain point. It can, however, not be concluded explicitly whether ozone crossed dynamical boundaries. To separate air masses unambiguously it would be desirable to use flexible boundaries like the tropopause or mixing barriers defined by e.g. PV gradients. However, this would require online calculation of these quantities, and would therewith be much more expensive.

The origin diagnostic is illustrated schematically in Fig. 6.6. Here ozone from two different source regions is shown. The ozone molecules that are produced in the tropics ('purple ozone') is either destroyed again locally in the tropics, or transported out of the source region. At some point in the atmosphere, these tropical ozone molecules are destroyed and thus the information of the origin is lost. The same is true for ozone from southern mid-latitudes (here marked as 'red' ozone molecules). At any point in the atmosphere, the ozone molecules that originate from different origins can be 'counted' and therewith it is possible to partition ozone into parts originating from the defined regions. When averaging over one source region, a statement can be made about the amount of ozone produced locally (in the example in the Figure 60% is produced locally in the SH mid-latitudes) and the amount of ozone being transported from another region (e.g. 40% of the ozone in SH mid-latitudes was transported there from the tropics).

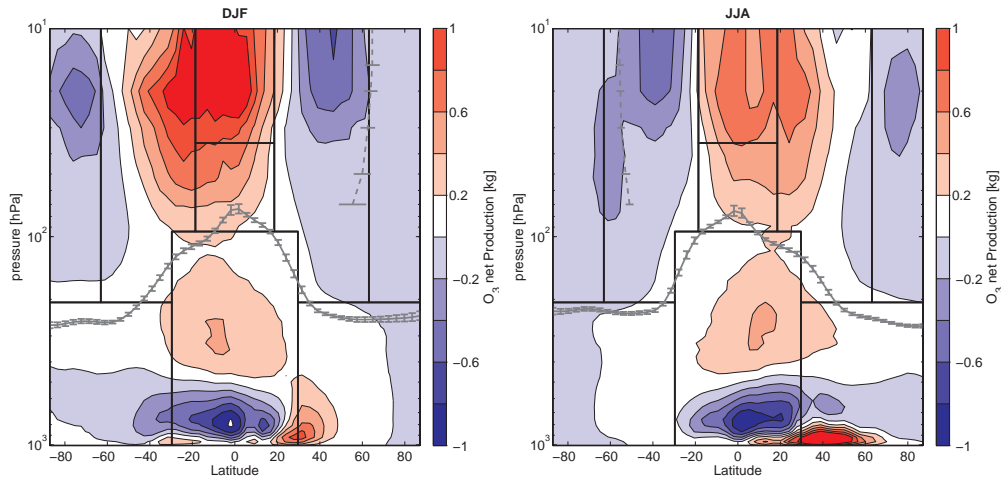


**Figure 6.5:** Climatology (2000-2009) from SCN-B2d of the net ozone production in ozone mass for DJF (left) and JJA (right). The grey solid line is the mean position of the dynamical tropopause, the grey dashed line the location of the winter hemisphere jet (latitude of maximal zonal wind speed). The vertical and horizontal bars denote the inter-annual variability as  $1\sigma$ .

The ozone origin diagnostic was incorporated in the model for the SCN-B2d simulation, but due to technical reasons the diagnostic is available only for model years 2000 to 2049. Therefore, the following analysis will focus on the development of the ozone layer in the future.

## Results

In the following, some results obtained with the ozone origin diagnostic are shown. At first, the informations obtained with this diagnostic is discussed on the example of ozone in the NH mid-latitudes. Climatologies over a decade (2000 to 2009) from the transient simulation SCN-B2d are shown. Fig. 6.7 (left) shows the annual cycle in ozone averaged over the NH mid-latitudinal source region (the yellow region in Fig. 6.4). The mean ozone mixing ratio (black line) has an annual cycle with highest values in northern spring and lowest values in northern autumn. The partitioning of ozone into its region of origin shows that the individual ozone fields do have a much larger annual cycle, but partly cancel each other. Ozone that was produced locally (yellow line) has highest mixing ratios in summer and lowest in winter. Tropical ozone on the other hand clearly shows the wintertime maximum, explaining the maximum in full ozone. Even though on the whole local ozone makes the largest contribution (67% in the annual mean), the annual cycle is determined by tropical ozone (which only contributes 22% in the annual mean). Ozone from other regions has negligible small mixing ratios in the NH mid-latitudes. The fact that the annual cycle in mid-latitude ozone is induced by transport of tropical ozone into mid-latitudes is commonly known. It is, however, somewhat surprising that tropical ozone still only makes a relatively small contribution to the total amount of ozone compared to what is produced locally. This result is in

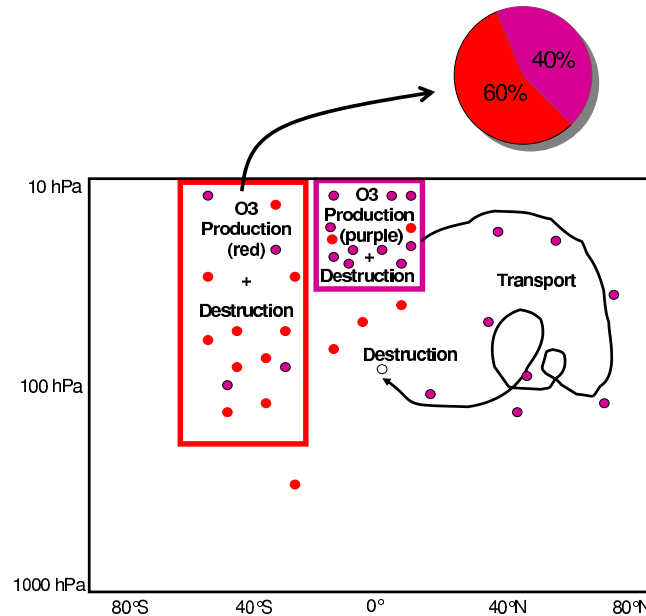


**Figure 6.6:** Schematic illustrating the  $O_3$  Origin diagnostic. Two source regions are defined (red and purple boxes), in which ozone molecules of the respective colour are produced. The molecules can be transported out of their region of production, contributing to the total amount of ozone in other than their source regions and are destroyed eventually.

agreement with the findings by Grewe (2006).

As discussed above, in this study the extratropical stratosphere was subdivided into middle and high latitudes rather than into low and middle stratosphere as in Grewe (2006). In Fig. 6.8 the contributions of ozone of different origin in the newly defined polar regions is shown. It is found that both in the southern and northern hemisphere the largest part of ozone in the polar regions was produced in mid-latitudes throughout the year. Locally produced ozone maximises in summer during the polar day, while in winter during polar night ozone production in the high latitudes vanishes as there is no sunlight available. Ozone originating in the mid-latitudes peaks in winter, as expected since transport is stronger in wintertime. In the southern hemisphere, ozone from mid-latitudes is reduced again in September and October after the build-up in winter, which can be understood as a result of strong local ozone destruction due to heterogeneous chemistry (the climatology is shown for 2000 to 2009 where the CFC loading is still close to its peak values). The maximal values of mid-latitude ozone mixing ratio in southern high latitudes is found in November. This is most likely due to the breakup of the vortex, which rapidly mixes mid-latitude air to high latitudes and which takes place around November in the model (about a month delayed compared to reality). Also tropical ozone has a contribution to ozone at high latitudes, maximising in spring in both hemispheres. The mixing ratio of tropical ozone at high latitudes is about twice as high in the northern hemisphere compared to the southern hemisphere. As the BDC is

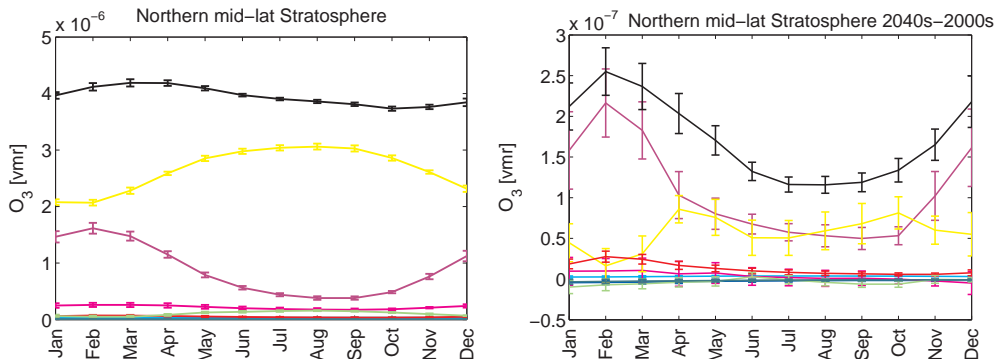


**Figure 6.7:** Left: Climatology (2000-2009) of the annual cycle in mean ozone in the NH mid-latitudes (black) and in the 9 ozone origin tracers (colours follow Fig. 6.4; yellow: local, purple: tropical middle stratosphere, pink: tropical lower stratosphere). The vertical bars denote the  $1\sigma$  variability over the analysed decade. Right: As left, but difference 2040s minus 2000s. Here, the vertical bars denote the  $1\sigma$  uncertainty in the differences.

stronger in the northern hemisphere and transport of air into high latitudes is strongly inhibited in the southern hemisphere while the vortex persists, this is to be expected. However, as discussed above the contribution of ozone from mid-latitudes or tropics to high latitude ozone can not necessarily be seen as cross-barrier transport. Especially in the northern hemisphere, where the vortex is often zonally asymmetric and variable, it is likely that parts of the air masses that are included in the polar region are outside the vortex. The variability in the mixing ratios of transported ozone, for example tropical ozone in the northern polar region, is much higher than the variability in the chemically determined peak of locally produced ozone. Again, this can be easily understood as transport especially in the northern hemisphere has a high interannual variability while chemical production is almost entirely determined by the solar irradiance only, and therewith almost identical every year.

All in all, by employing the high latitudes as separate regions it could be shown that most ozone in the polar regions is of non-local origin. This corrects the findings by Grewe (2006), who stated that most ozone at high latitudes originates from local ozone production, as in his study it could not be distinguished between ozone produced at high and middle latitudes.

The relative contribution of each ozone field to the absolute ozone mixing ratio at each point is shown as a latitude-height map in Fig. 6.9. Each panel illustrates the ozone field from one source region, so that the sum of the nine plots equals to one everywhere. It can be seen that in the middle stratosphere locally produced ozone dominates over transported ozone, which can be expected from strong ozone production and short life times. In the tropics the contribution of local ozone is highest, while in the polar regions only about 30% of the ozone at the upper levels is of local origin. In the lower stratosphere even less ozone is locally produced in the polar regions, but is mostly originating from the mid-latitudes. Ozone originating from the tropical stratosphere is

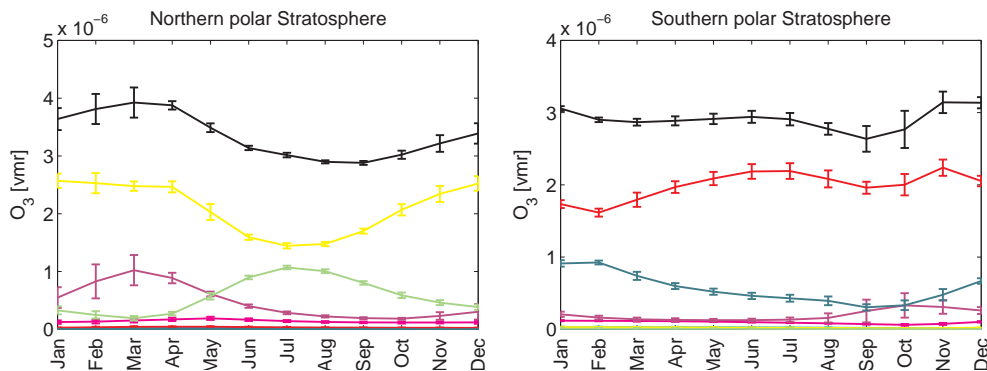


**Figure 6.8:** As in Fig. 6.7, but for the annual cycle in mean ozone mixing ratios in the NH polar region (left) and SH polar region (right). Again, colours follow Fig. 6.4 with NH (SH) mid-latitudes in yellow (red), NH (SH) high latitudes in light green (dark green) and the tropical MS in purple.

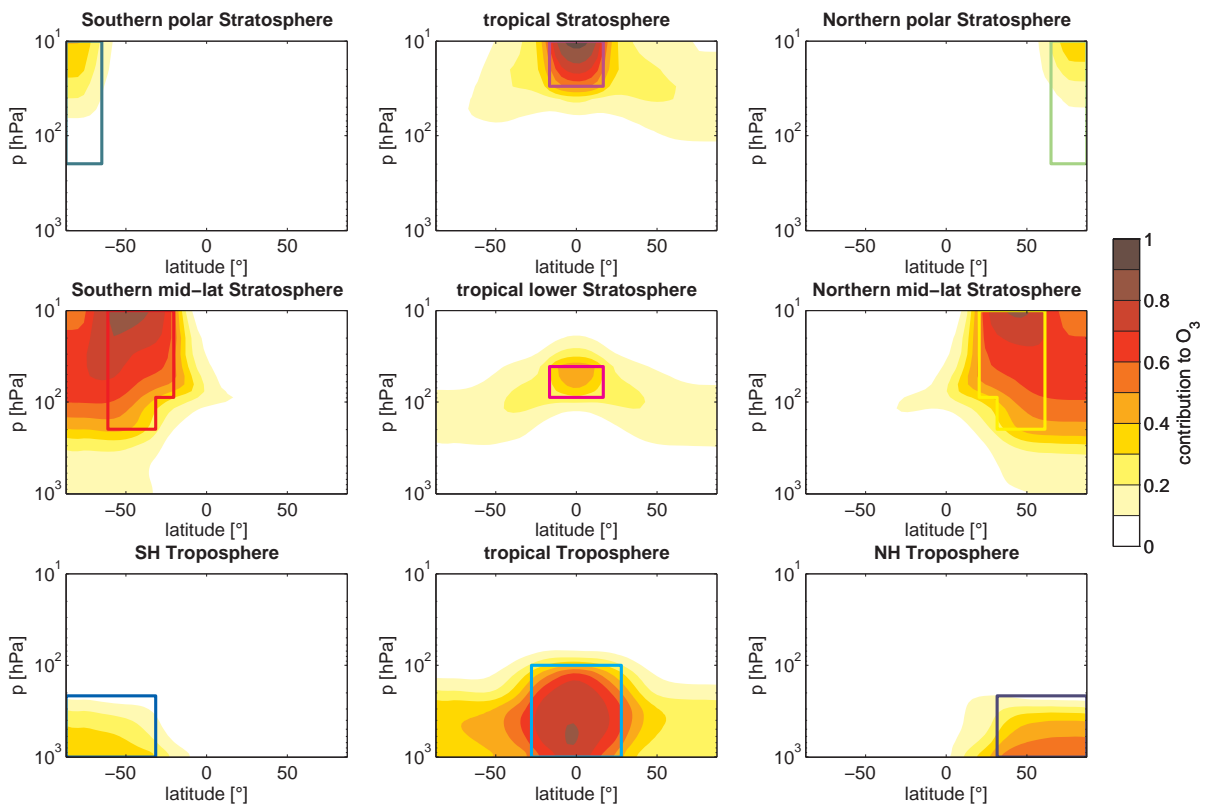


**Figure 6.9:** Climatology (2000-2009) of the contribution of ozone originating from the indicated regions to the full ozone field ( $O_3^i/O_3$ ) for each of the 9 source regions.

transported poleward and downward, apparent by the regions of enhanced contribution in the extratropics. As the BDC is stronger in the northern hemisphere, tropical ozone contributes more there. In the annual mean, the contribution of tropical ozone in the mid-latitudes is, however, only about 10-20%, but shows a distinct annual cycle (as it was shown for tropical ozone in the northern mid-latitudes above). Another interesting feature is the spread of ozone originating from the tropical lower stratosphere to higher latitudes in the lower stratosphere, which is roughly following the structure of isentropic levels in this region. Also mid-latitude ozone shows tongues of intermediate contribution (around 10%) reaching into low latitudes. These features are indicative of frequent wave breaking events that mix tropical and extratropical air (e.g. Randel et al., 1993), leading to transport of ozone between low latitudes and extratropics.

As the ozone origin diagnostic was incorporated in a transient simulation, differences in the contribution of ozone from different regions of the atmosphere can be analysed. The difference in mean ozone mixing ratios in the NH mid-latitudes between the present (2000s) and the future (2040s) is shown in Fig. 6.7 (right). Ozone mixing ratios increase throughout the year, and the annual cycle becomes more pronounced. The individual ozone fields suggest, that this increase is largely due to enhanced ozone amounts originating from the tropics. At first sight, this seems to suggest that enhanced transport of ozone from tropics to mid-latitudes is the cause of increasing ozone mixing ratios in the mid-latitudes. However, care has to be taken in the interpretation of these results: the enhancement of tropical ozone in the mid-latitudes could also result from a decrease in the destruction rates in mid-latitudes. The same problem arises for the enhancement of locally produced ozone: the increase could result from more ozone production, decreased destruction rates, or more export of mid-latitude ozone. This demonstrates the need to define a method which separates the effects of dynamics (transport) and chemistry (production and destruction) in order to assign long-term changes in ozone to these processes. In the next section, a method which allows the attribution of changes to transport and chemistry will be presented.

### 6.2.2 Transport of ozone and air masses

#### Method

The amount of ozone at a given point in the atmosphere is changing due to chemical production and destruction and due to transport of ozone to or from this point. The ozone balance equation (Eq. 6.1) can be used to estimate the transport tendency of ozone:

$$T_i = \frac{\partial O_3^i}{\partial t} - (P\delta_{ij} - D\frac{O_3^i}{O_3}) \quad (6.3)$$

$T_i$  is the amount of ozone of origin  $i$  transported to (or from) a given point in the atmosphere. To obtain  $T_i$  it is necessary that the production and destruction rates

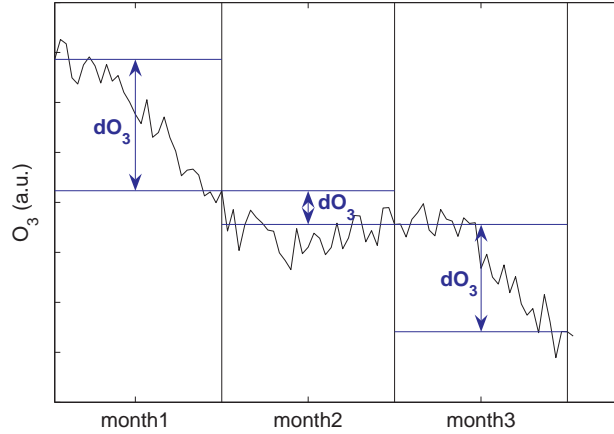


**Figure 6.10:** Schematic illustrating monthly ozone tendencies. Shown is an arbitrary ozone time series (with arbitrary units) over three months. The difference between the ozone value at the beginning and the end of the months (blue horizontal lines) equals the accumulated change in ozone over the course of each month (blue arrows).

of ozone are known, i.e. these fields need to be available as model output. Here the production and destruction is available as accumulated (i.e. mean over one time interval) variable. The ozone tendency  $\frac{\partial O_3^i}{\partial t}$  is the accumulated change in  $O_3$  over the course of a month, which is equal to the difference of  $O_3$  at the first and last timestep of the month. This is illustrated in Fig. 6.10, where the ozone tendency is marked by the blue vertical arrows. The sum over the production and destruction at each time step over the month is the total ozone production and destruction tendency. The monthly tendencies are used to obtain a monthly transport tendency using Eq. 6.3.

Note that the production and destruction terms are dominant in the equation, and the transport tendency  $T$  is a small residual and therefore subject to numerical uncertainties. A numerical discrepancy arises from the fact that the rate of change of a tracer is calculated using a semi-implicit numerical integration scheme. In the case of the model used here, an Eulerian backward formulation was used in the chemistry scheme which leads to a discrepancy between the saved production and destruction term and the ozone tendencies. To account for this, the production and destruction was adjusted subsequently so that the global ozone budget is closed, with the constraint that the adjusted production and destruction terms should be as close as possible to the initial values. For the full global ozone field, the adjustments are as small as in the order of 1%. The estimated mass fluxes  $T_i$  are affected by the adjustment mostly by less than 10%.

With the production and destruction tendencies being available, it is possible to estimate the total transport tendency  $T$  for each point of the atmosphere. This is the net transport, i.e. the sum of ozone transported away from this region and ozone imported from other regions. Incorporating the ozone origin diagnostic allows to distinguish between export of ozone and import subdivided into the eight remaining pre-defined

regions. Therefore it is possible to determine the ozone fluxes to and from each region to each other.

In order to compare the transport of ozone to transport of air masses, the trajectories from the Lagrangian advection scheme ATTILA are used to calculate air mass fluxes. The trajectories, that are calculated online and are used for the transport of all passive and active trace gases, are saved with a 12-hourly interval so that a data basis of about 500.000 trajectories is available at each time step (see also Chapter 2). To calculate the mass fluxes, the atmosphere is then divided into the regions as in the ozone origin diagnostic. The trajectories that are located in one region at the end of the month are followed backward over the course of the month. As each trajectory represents an equal mass of air, simple counting of trajectories originating from the nine regions gives the total mass flux of air within one month. Due to mass conservation, the imported and exported mass in each region equals to zero, contrarily to ozone fluxes since ozone has chemical sinks and sources.

## Results

The results for the northern mid-latitudes are shown here as example for the decomposition of ozone tendencies in production, destruction and transport. Fig. 6.11 shows a climatology of the monthly tendencies of the nine ozone fields averaged over the NH mid-latitude region. As the ozone tendencies are the changes within one month they are basically the time derivative of the annual cycle of ozone shown in Fig. 6.7. While local ozone is accumulating from February to August, it decreases in the other half of the year. Tropical ozone, that is the second important player here, basically shows a reversed annual cycle with negative tendencies in the first half and positive tendencies in the second half of the year. The lower panel in Fig. 6.11 decomposes the tendencies into the contributions by production (obviously only for the local region), destruction and transport. First of all note that the scale of these tendencies is one magnitude larger than the net tendencies, i.e. the net change in ozone is a small residual.

Local ozone in the mid-latitudes is produced largely in summer, when the solar radiance is strongest. The destruction of local ozone shows a similar annual cycle as the production term, but lagging slightly behind. The net production is only roughly 1/5 of the total production, i.e. production is compensated mostly by destruction. The transport tendency of local ozone is negative throughout the year, as expected as local ozone can only be exported. The transport tendencies show a relatively small annual cycle.

Ozone from the tropical middle stratosphere makes an important contribution to northern mid-latitude ozone. The transport tendency is close to zero in summer, increases in autumn until winter, and decreases again in spring. This behaviour is expected as the transport by the BDC is strongest in northern winter. The destruction of tropical ozone in the mid-latitudes follows the transport tendencies, but lags behind by

about 1-2 months. Therefore, the net tendency (= sum of transport and destruction) is positive until February, when the amount of ozone transported into the mid-latitudes exceeds the destruction. After February, more tropical ozone is destroyed in the mid-latitudes than resupplied, and the concentration of tropical ozone decreases.

The incorporation of this diagnostic allows to explain the annual cycle in ozone in the mid-latitudes. Ozone of tropical origin peaks in February (see Fig. 6.7), but the reason is not that transport is strongest in this month but that the balance between transport and destruction is positive until February. The annual cycle in local mid-latitude ozone is dominated by the seasonal dependence of ozone production. The sum of these two ozone fields determines the annual cycle of ozone in the mid-latitudes: The maximum in mid-latitude ozone in about March to April is due to a combination of still high amounts of tropical ozone (that is destroyed and thus decreases strongly afterwards) and increasing production of local ozone (which was low earlier in the year). Thus, the classical understanding of a spring-time maximum in ozone due to transport accumulation over the winter has to be readjusted as follows: transport itself peaks in January, and the accumulation of tropical ozone peaks in February. The maximum in ozone is, however, found in March to April due to the additional effect of local ozone production. That is if only the transport effect would determine the spring-time maximum it would take place about 1-2 months earlier as it is the case. This detailed analysis of the causes of the annual cycle in ozone is possible with the method as described here also for the other regions, and this can help to deepen the understanding of processes relevant for ozone. As the focus of this work are long-term changes in ozone, this is left for future studies. Also, it will be important to use different model systems to test the robustness of the results.

The transport tendencies for all regions are illustrated in Fig. 6.12 as annual mean mass fluxes between the different regions of the atmosphere. Fluxes are shown only between neighbouring regions and where a considerable amount of ozone is transported. Also shown are the total air mass fluxes between the regions (lower panel). The air mass fluxes are about 6 orders of magnitude larger, which is reasonable considering that ozone concentrations lies in the order of magnitude of  $10^{-6}kg/kg$ . Many previous studies dealt with mass or tracer exchange across the tropopause, but there are almost no estimates of mass fluxes between different regions of the stratosphere. To validate the results obtained with the method described here, they can be compared to the estimates of troposphere-stratosphere mass exchange of previous studies. For example, Grewe and Dameris (1996) analyse cross-tropopause mass exchange using reanalysis data. They found strongest downward mass fluxes into the troposphere in confined regions around  $30^{\circ}N$  and  $30^{\circ}S$ , with peak values of about  $25$  to  $35 \times 10^{16}kg/year$  (with exact values depending on the definition of the tropopause and the method used to calculate the mass flux). Also in the estimates of mass transport between the crudely defined tropospheric and stratospheric boxes presented here (shown in Fig. 6.12 bottom) the downward mass flux is strongest in the mid-latitude regions. The values of net

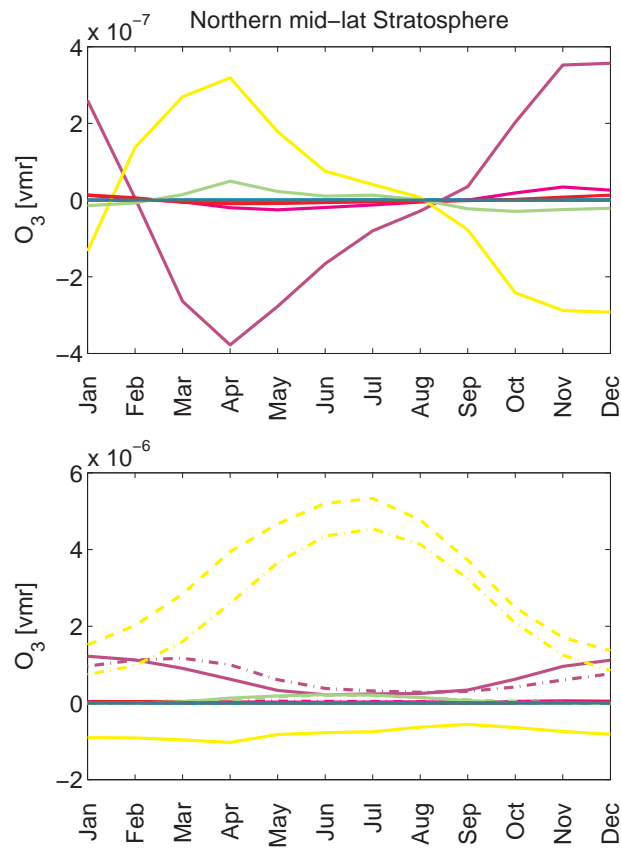


**Figure 6.11:** Climatology (2000-2009) of the annual cycle in the net monthly tendencies in ozone (top) and in the lower panel the tendencies due to transport (solid line), production (dashed line) and destruction (dash-dotted line) in the northern mid-latitudes. Yellow lines are local mid-latitude ozone, purple lines tropical ozone.

downward mass flux of around  $25 \times 10^{16}$  kg/year in the mid-latitudes agrees well with the estimates by Grewe and Dameris (1996). Gettelman et al. (1997) estimated cross-tropopause mass fluxes of trace gases, including ozone. They find a total net ozone mass flux across the tropopause of 515 Tg/year with a range from 450 to 590 Tg/year. This agrees very well with the value of total net ozone mass flux from the stratospheric to the tropospheric regions of 570 Tg/year obtained here (calculated as the sum of all arrows between tropospheric and stratospheric boxes). The good agreement of the values obtained here to observational estimates show that 1) the method of estimating (ozone) mass fluxes is adequate, 2) the model is simulating transport reasonably well and 3) the crude separation of troposphere and stratosphere by the fixed boundaries still provides good estimates of cross-tropopause fluxes. Of course it could also be possible that the agreement of the values is due to the cancellation of errors in these three points.

As mass is conserved, the mass fluxes to and from each box equal to zero (as rounded numbers are shown the sum of the numbers that are shown might differ slightly from zero). Ozone, on the other hand, has chemical sources and sinks and the net ozone mass flux for a region can therefore be different from zero. The mean chemical production and destruction (and in the case of the troposphere deposition) of ozone, whose sum equals the net transport, is indicated in each region.

The air mass fluxes clearly reflect the well-known circulation in the stratosphere, with net upwelling in the tropics, net poleward transport of air from low to higher latitudes and downwelling into the troposphere in the extratropics. The largest downward mass flux into the troposphere occurs in the mid-latitudes. In the tropical middle stratosphere the positive net air mass fluxes into the mid-latitudes are balanced by upward fluxes. The ozone mass fluxes show that in the tropical stratosphere more ozone is transported away (into the extratropics) than into this region. As it is known that the tropical stratosphere is a source region for ozone this is what is to be expected. What is less well known and can be studied with the diagnostic used here, is the finding that transport is not acting one-way only but a considerable exchange of air masses takes place. The (ozone) mass fluxes into mid-latitudes of about  $40 \times 10^{16}$  kg/year (350 Tg/year) are partly balanced by fluxes into the tropics of roughly  $20 \times 10^{16}$  kg/year (250 Tg/year). The same is true for the tropical lower stratosphere.

Obviously the net flux of air mass and of ozone mass between two regions can be of different sign, depending on the ozone gradient in this region. For example the mass flux from the troposphere into the lower stratosphere in the tropics is positive (as expected from upwelling in this region), but the net ozone flux is downward. This can be easily understood as the ozone concentration is much smaller in the troposphere compared to the lower stratosphere. In the extratropics, the net fluxes from the stratosphere into the troposphere are downward both for mass and ozone mass, but while the upward ozone flux is close to zero the upward mass fluxes are not negligible.

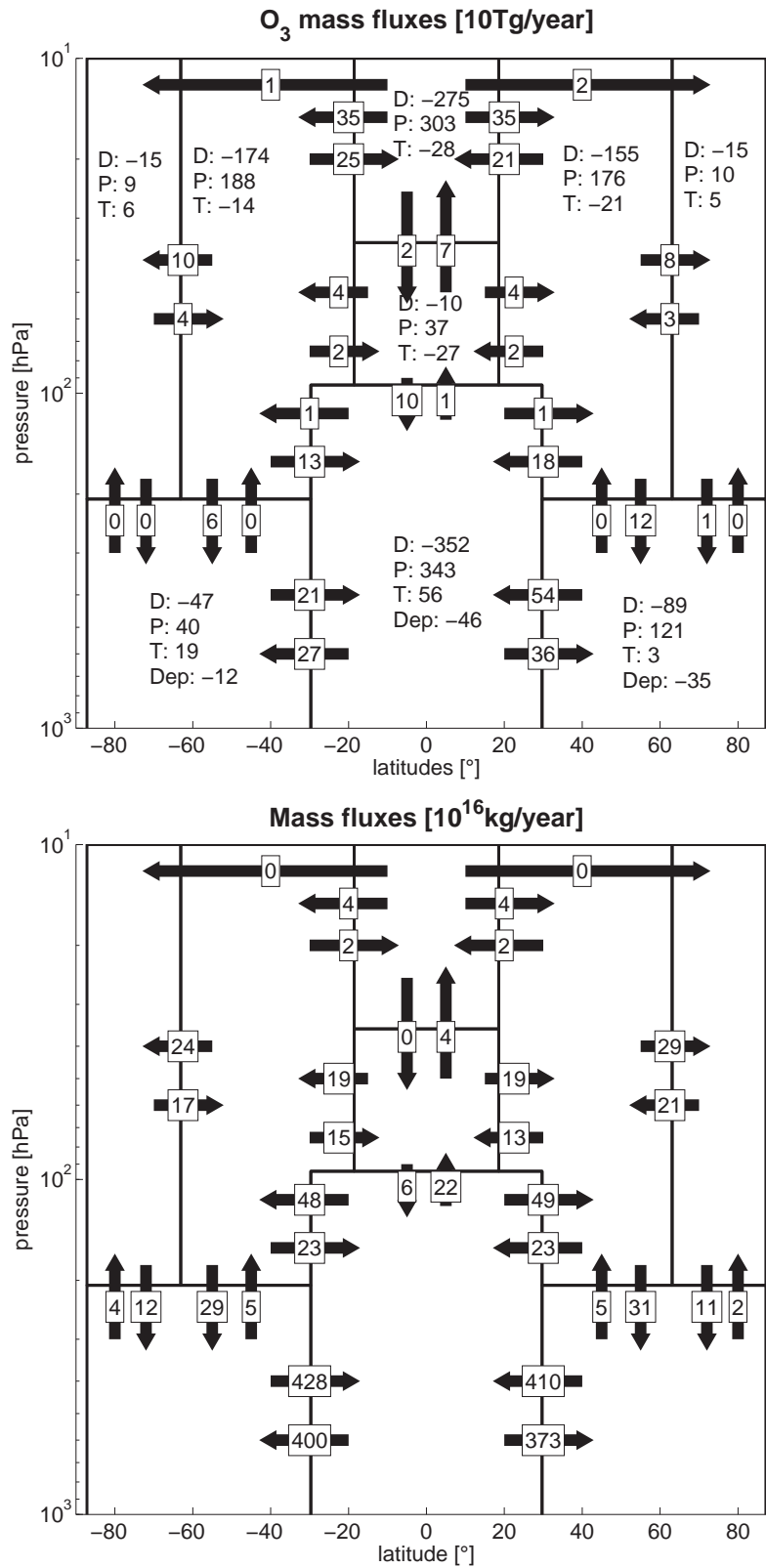


**Figure 6.12:** Annual mean ozone mass fluxes [ $10^{10}$ kg/year] (top) and air mass fluxes [ $10^{16}$ kg/year] (bottom). In the upper figure, the annual mean ozone budget of each region is shown, i.e. the total destruction (D), production (P) and net transport (T). In the troposphere, also the deposition (Dep) is listed separately.

### Long-term changes in transport

As the diagnostics used here were employed in a transient simulation, they can be used to study long-term changes of (ozone) mass fluxes in a changing climate. Annual mean differences in ozone and air mass fluxes between the present (years 2000-09) and the future (2040-49) are shown in Fig. 6.13. The differences in air mass fluxes show enhanced upwelling in the tropics across the tropopause and associated with it enhanced outflow of mass into the mid-latitudes. This reflects the results found earlier that the meridional circulation is enhanced in the tropical lower stratosphere. In Chapter 3, the increase in mass flux measured by tropical upwelling at 100 hPa was estimated to  $31 \times 10^{15}$  kg/yr over the period of 2000 to 2049 (deduced from Fig. 3.3). This value compares very well with the change in net air mass flux between the tropical troposphere and stratosphere of  $30 \times 10^{15}$  kg/yr as deduced from the trajectories (Fig. 6.13). This shows that the estimations of changes in mass fluxes with a Lagrangian and Eulerian method, respectively, yield the same results and verify the methods.

Furthermore, enhanced exchange of mass between middle and high latitudes in the northern hemisphere are found here as well as enhanced mass fluxes from the stratosphere into the troposphere in northern mid-latitudes. So how are these changes in mass fluxes translated to changes in ozone mass fluxes? The upper panel of Fig. 6.13 shows that changes in ozone mass fluxes do not necessarily occur where changes in mass fluxes are taking place. Also changes in the ozone concentration and ozone gradients lead to changes in ozone mass fluxes even if air mass fluxes remain the same (or the other way round).

The strengthening in tropical upwelling and the circulation in the tropical lower stratosphere also affects ozone transport. In particular, the exchange of ozone between troposphere and stratosphere is enhanced. Likewise to the climatology the net direction of the mass flux change in the tropics is downward for the ozone mass flux but upward for the mass flux, as ozone concentrations increases strongly with height. The largest change in ozone mass flux is the enhanced downward flux of ozone from the tropical lower stratosphere to the troposphere, which seems to contradict enhanced upwelling in this region. However, as the changes in air mass fluxes show, not only the upward but also downward mass flux is enhanced. This can be understood as the enhanced circulation cells in the model are narrow within the (sub-)tropics, i.e. the air mass partly recirculates in the inner tropics.

The ozone flux from the stratosphere into the troposphere is enhanced both in the tropics and extratropics. The flux of air mass from stratosphere to troposphere is, however, changing only in some regions, so that part of the enhanced ozone mass flux is most likely due to enhanced ozone concentrations in the stratosphere. The same is true for the inter-hemispheric mass exchange in the troposphere, which is enhanced for ozone mass but not for air mass (which is even reduced between southern extratropics and tropics). As tropospheric ozone concentrations increase in the future (see Fig. 6.2)

this explains the enhanced ozone fluxes despite invariable mass fluxes.

A reduction in the ozone mass flux from middle to high latitudes of about 20% occurs in the southern hemisphere in the stratosphere. This inhibited ozone mass flux does not coincide with an inhibited annual mean decrease in mass flux. As ozone concentrations in mid-latitudes increase, this discrepancy can in this case not easily be explained by changes in ozone concentrations. However, note that the fluxes are the integrated flux over a large range in altitude. As the distribution of mass and of ozone mass differs (more mass is situated at lower levels, while ozone mass maximises at the model top), changes in mass fluxes of different signs at different levels might result in a net decrease in ozone mass flux but not in air mass flux. Also, only the annual mean is shown, and as ozone concentrations do have a pronounced annual cycle this might also obscure the results. The changes in (ozone) mass fluxes from middle to high southern latitudes will be discussed in more detail below.

### 6.2.3 Attribution of long-term changes in ozone

#### Method

The ozone balance equation (Eq. 6.1) partitions the ozone tendency into parts caused by transport and by chemistry. The chemistry and transport tendencies for different climate states can be compared, but do not necessarily explain the causes of the ozone changes as the ozone concentration at one point is the result of the balance between the different sources and sinks. The attribution of ozone changes with time to the changes in sources and sinks can be obtained as follows:

Two different states of the atmosphere, for example two time periods ( $p_1$  and  $p_2$ ) are compared, and it is assumed that ozone is approximately in balance within each period. As ozone changes rapidly during some episodes that might be critical, but as will be shown later the assumption is valid for the decades compared here. For each period, the ozone balance equation for the annual mean change in ozone is:

$$\begin{aligned}\frac{\partial O_3^{p_1}}{\partial t} &= P_{p_1} - D_{p_1} O_3^{p_1} + T_{p_1} \approx 0 \\ \frac{\partial O_3^{p_2}}{\partial t} &= P_{p_2} - D_{p_2} O_3^{p_2} + T_{p_2} \approx 0\end{aligned}\tag{6.4}$$

As we assumed ozone to be in balance, the mean over the annual tendency of ozone over each time period equals to zero. The equations above can be transformed to describe the relative change in ozone as:

$$R_{O_3} := \frac{O_3^{p_2} - O_3^{p_1}}{O_3^{p_1}} = \frac{D_{p_1}}{D_{p_2}} \left[ \frac{P_{p_2} - P_{p_1}}{P_{p_1} + T_{p_1}} + \frac{T_{p_2} - T_{p_1}}{P_{p_1} + T_{p_1}} + 1 \right] - 1\tag{6.5}$$

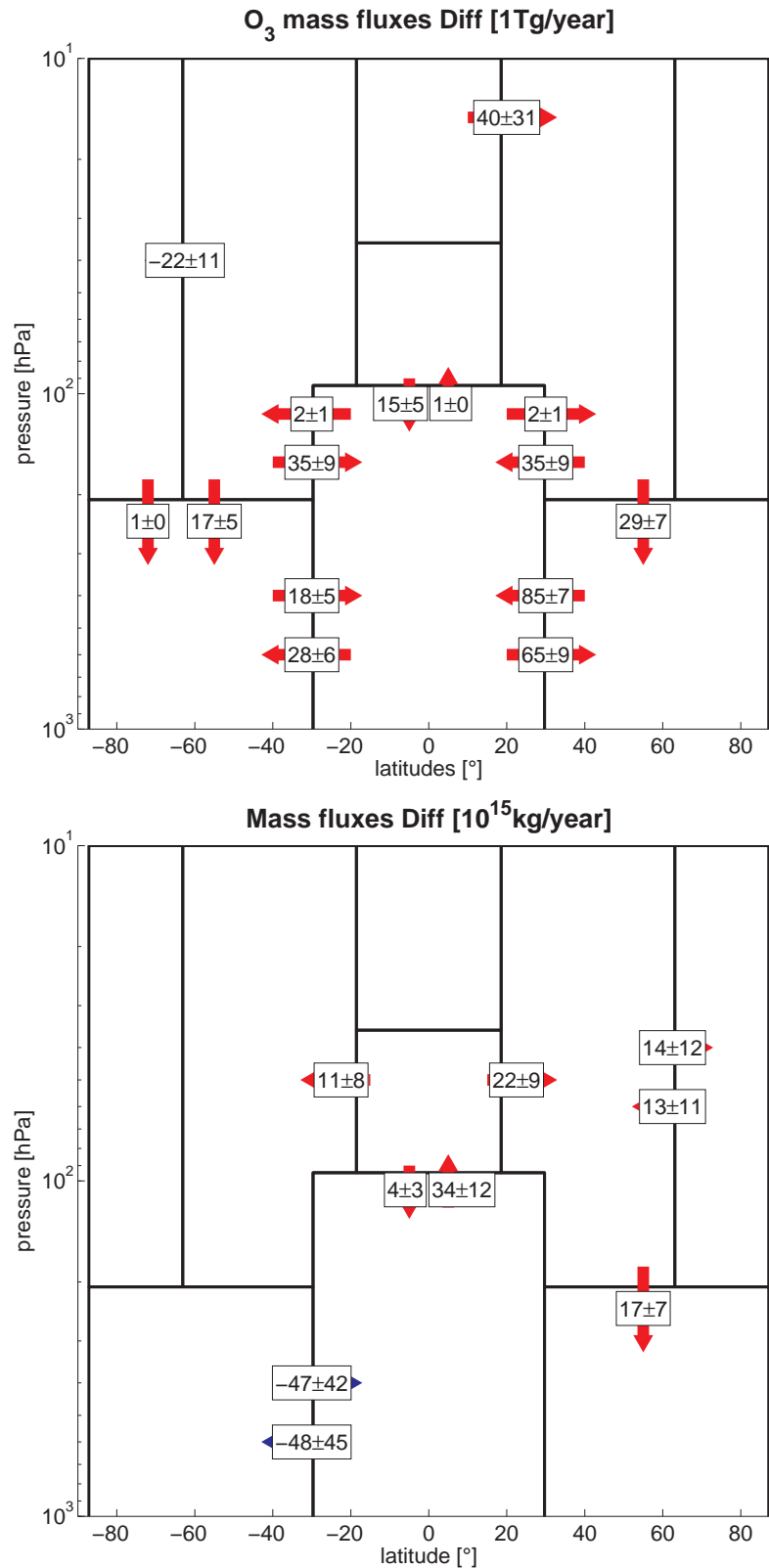


**Figure 6.13:** Difference in annual mean ozone mass fluxes [ $10^9$ kg/year] (top) and air mass fluxes [ $10^{15}$ kg/year] (bottom) between decades 2040-49 and 2000-09. Shown are changes only if the difference is larger than one joint standard deviation (which is given together with the flux changes).

It can be seen from this equation that if there were only changes in the destruction rate, the resulting changes in ozone are  $R_{O_3}^D = D_{p_1}/D_{p_2} - 1 = (D_{p_1} - D_{p_2})/D_{p_2}$ . Accordingly, changes in production cause changes in ozone of  $R_{O_3}^P = (P_{p_2} - P_{p_1})/(P_{p_1} + T_{p_1})$  and changes in transport cause ozone changes of  $R_{O_3}^T = (T_{p_2} - T_{p_1})/(P_{p_1} + T_{p_1})$ . Changes in the destruction rate are directly transferable to changes in ozone (i.e. a 10% reduction in the local destruction rate translates to 10% more ozone). Changes in production or transport, on the other hand, have to be seen relative to the total amount of a potential ozone 'source', i.e. the sum of production and transport.

The relative change in ozone can then be written as:

$$\begin{aligned} R_{O_3} &= (R_{O_3}^D + 1)(R_{O_3}^P + R_{O_3}^T + 1) - 1 \\ &= R_{O_3}^D + R_{O_3}^P + R_{O_3}^T + R_{O_3}^D(R_{O_3}^P + R_{O_3}^T) \end{aligned} \quad (6.6)$$

When relative changes are small ( $\approx \leq 0.1$ ) the last term is by one magnitude smaller than the first terms and can be neglected, so that the total relative change in ozone is approximately equal to the sum of the relative changes due to destruction, production and transport changes:

$$R_{O_3} \approx R_{O_3}^D + R_{O_3}^P + R_{O_3}^T \quad (6.7)$$

The change in ozone due to transport can further be split up into transport of ozone from different regions by using the ozone origin diagnostic. As  $T = \sum_{i=1}^9 T_i$ , the change in ozone due to transport equals  $R_{O_3}^T = \sum_{i=1}^9 (T_{p_2}^i - T_{p_1}^i)/(P_{p_1} + T_{p_1})$ . This allows to specify whether changes in ozone are due to changes in export or due to changes in import, and for the latter the region ozone is imported from.

## Results

The relative difference of the mean ozone mixing ratios in each region was calculated between the decades 2040-49 and 2000-09 from the SCN-B2d simulation. The relative changes in ozone due to changes in production, destruction and transport were calculated using Eq. 6.5. Fig. 6.14 shows the results for each region with the transport term split up into changes due to import and export of ozone. The first two bars in each plot show the relative difference in ozone calculated from the right and left hand side of Eq. 6.5. If the assumption in Eq. 6.4 of ozone being in balance was correct, the two bars should be equal. It can be seen that within the uncertainty bounds of the directly calculated difference the two bars can not be distinguished in the stratosphere.

In the tropospheric regions, especially in the northern extratropics, the relative change in ozone calculated from the right hand side is slightly lower than the directly calculated difference (from the left hand side). However, overall it can be concluded that the assumption of ozone being in equilibrium is fulfilled good enough as for the following results to be valid.

The ozone mixing ratios increase from 2000 to the mid 21st century in most parts of the atmosphere, only in the tropical lower stratosphere the difference is close to zero. The attribution method allows to contribute the changes in ozone to chemical and dynamical processes. In the stratospheric regions the changes in ozone are generally largely driven by changes in chemistry. A decrease in the destruction rates leads to higher ozone mixing ratios in the mid-latitudes, the tropical middle stratosphere and the polar regions. In the southern polar region, the largest relative difference in ozone in the stratosphere occurs (about 10%) and it can be seen that reductions in destruction rates would lead to an increase in ozone mixing ratios of approximately 20%. The increase is, however, counteracted by a negative effect on ozone due to less import of ozone into the southern polar stratosphere. The changes in the southern polar stratosphere are examined in more detail below. Another region in the stratosphere in which changes in transport play an important role is the tropical lower stratosphere. Even though the overall changes in ozone are close to zero here, it turns out that this is due to the cancellation of changes in transport and chemistry. While production is increasing, the overall change due to transport results in a reduction of ozone due to enhanced export of ozone. The finding that transport has a larger impact in the lower stratosphere compared to regions that include the middle stratosphere can be expected, as short life times of ozone in the middle stratosphere compared to timescales of transport cause ozone concentrations to be chemically controlled there. In the lower stratosphere, where ozone life times are longer, ozone concentrations are controlled by dynamics to a larger degree.

In the troposphere, ozone increases by about 10 to 20%. This is largely due to an increase in production, counteracted by more export. The increase in export can simply be understood as increased ozone mixing ratios will lead to an increase in export even if the air mass flux remains the same (see Sec. 6.2.2). In the southern hemisphere, enhanced import of ozone is the largest contributor to the positive trend.

Employing the ozone origin diagnostic allows to separate not only import and export, but also the region ozone is imported from. In Fig. 6.15 the changes in ozone mixing ratios in the southern polar stratosphere are shown with the changes due to transport partitioned into the 9 ozone origin regions. As noted above, the strong increase in ozone due to decreased destruction rates is partly counteracted by decreased import of ozone. The partitioning reveals that the decrease in import is a decrease of ozone imported from the southern mid-latitudes (denoted as region 7 in Fig. 6.15), while import of ozone from all other regions does not cause changes in ozone in the southern polar region.

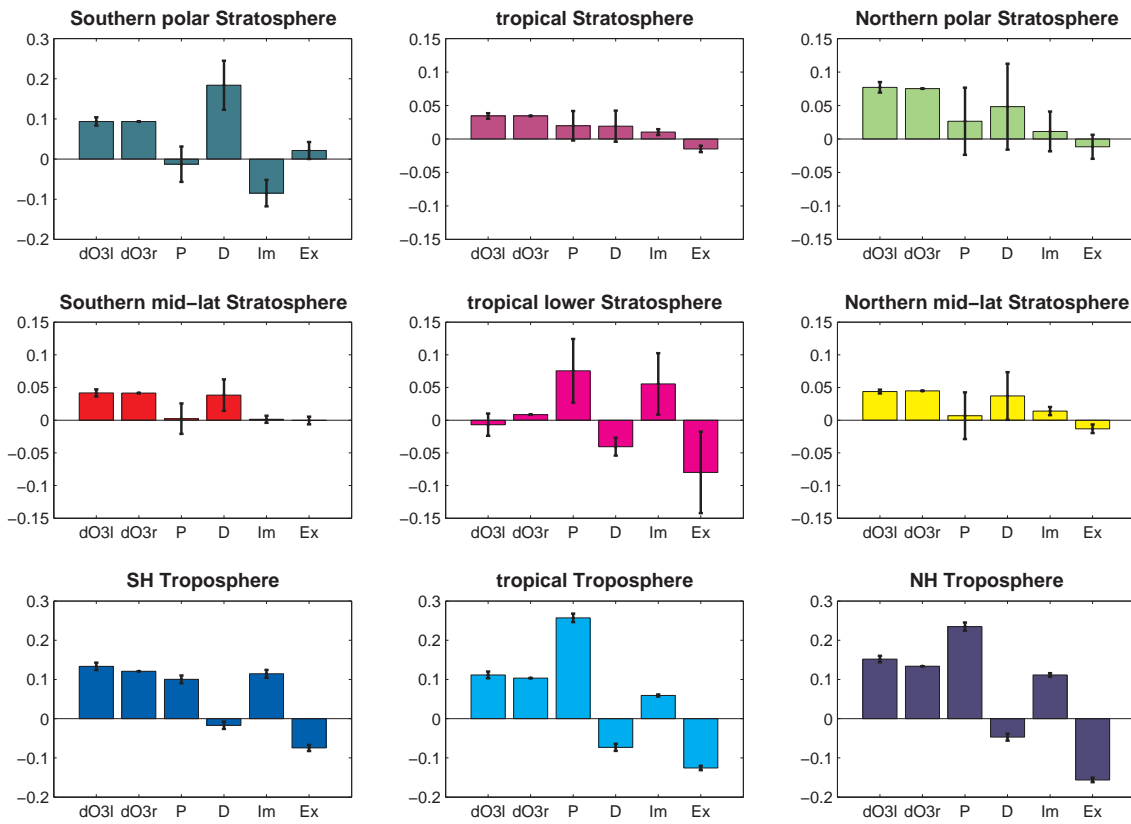


**Figure 6.14:** Relative differences 2040s - 2000s in mean ozone mixing ratios of each region and changes in ozone due to chemistry (production and destruction) and dynamics (import and export). The errorbars denote the 1 sigma uncertainty in the differences. For more details see text.

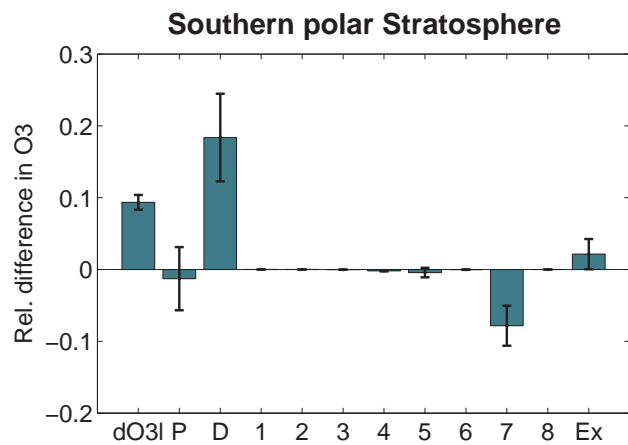


**Figure 6.15:** As in Fig. 6.14 but for the southern polar stratosphere only and with the changes due to import split up into import from each region.

### 6.3 Discussion and summary

Two different methods were used here to identify drivers and processes that lead to changes in atmospheric ozone. With these methods it is possible to separate and quantify the impact of circulation changes on ozone.

The usage of sensitivity simulations allowed different drivers of ozone changes to be distinguished. As the simulations with SST or GHG changes only imply changes in the meridional circulation and changes in temperature in the middle stratosphere, respectively, these simulations could be used to separate the effects of these two consequences of climate change in the stratosphere on ozone. As expected, stratospheric cooling leads to enhanced ozone concentrations in the middle stratosphere<sup>2</sup>. Strengthening of the meridional circulation in the lower stratosphere, on the other hand, was shown to imply a negative trend in ozone in the tropical lower stratosphere but has little impact on ozone in other regions. The circulation-induced changes in ozone were found to be stronger and significant only in the future.

In addition, a new method was presented which allows to attribute ozone changes to changes in chemistry and dynamics in a quantitative manner. The attribution of ozone changes between the present and future (mid 21st century) revealed that in the stratosphere, the increase in ozone mixing ratios in most regions is driven largely by local chemistry rather than by changes in transport of ozone. Furthermore, it could be confirmed that the negative trend in ozone in the tropical lower stratosphere is due to transport. This was indicative in the results from the sensitivity simulations and also suggested by many previous studies. It is found that enhanced export of ozone leads to a reduction of ozone mixing ratios in the tropical lower stratosphere. However, due to the choice of the boundaries for this region, the change in ozone averaged over the whole region is close to zero. As can be seen in Fig. 6.16, within the boundaries of the box representing the tropical lower stratosphere, negative ozone trends maximising at 80 hPa occur at the same time as positive trends above about 50 hPa, leading to a trend close to zero in the mean. The decrease in ozone due to transport is cancelled by an increase due to chemistry when averaging over the region.

In Fig. 6.16, the relative difference in ozone between the 2040s and the 2000s is shown. Superimposed is the relative change in ozone that would have occurred if it was only for changes in chemistry. Also, the changes in ozone mass flux are shown in this Figure, which aims to summarise the results presented in the previous sections. It can be seen that changes in chemistry lead to enhanced ozone concentrations almost everywhere in the atmosphere.

It was found that the enhanced meridional circulation in the lower stratosphere leads to enhanced mass fluxes from the tropical troposphere into the lower stratosphere, and consequently enhanced poleward mass fluxes that partly recirculate into the upper

---

<sup>2</sup>The same effect is expected in the upper stratosphere, but can not be shown here as the model E39CA extends only to 10 hPa

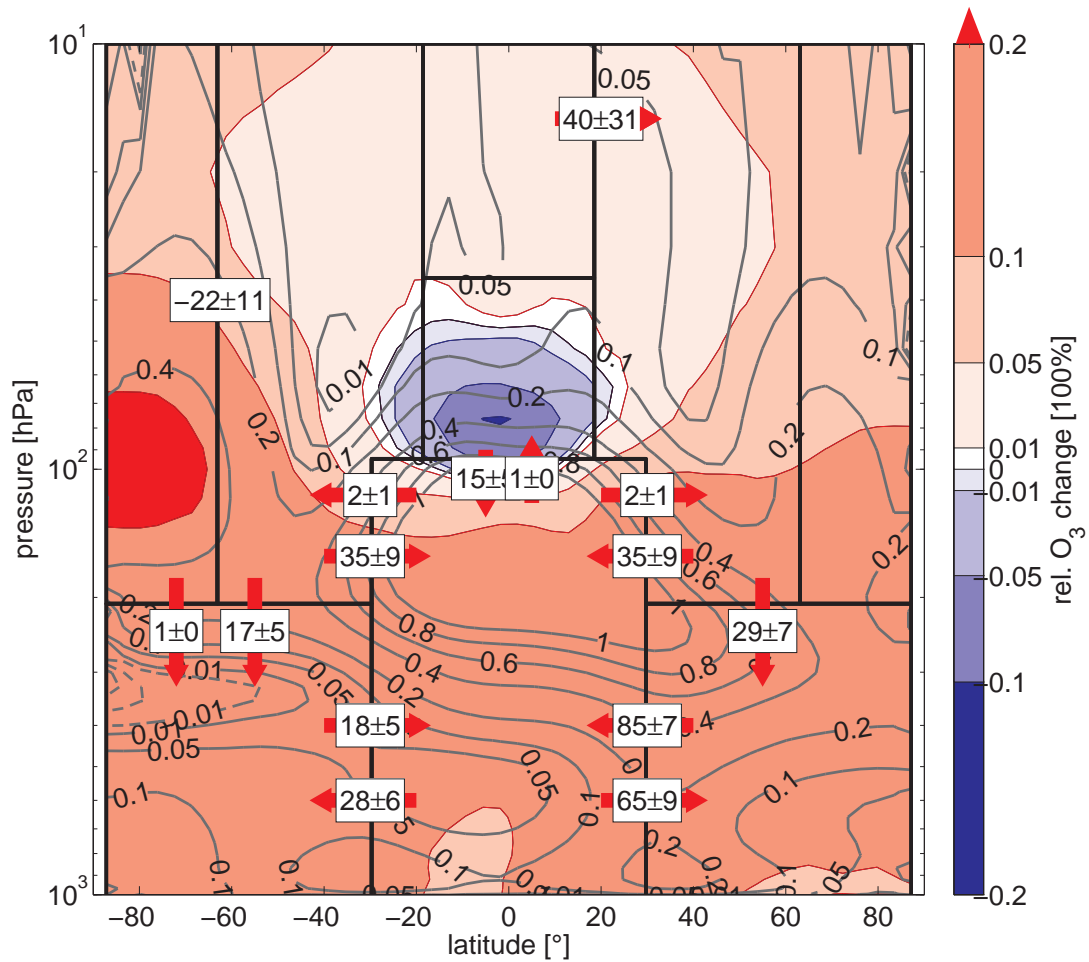


**Figure 6.16:** Relative changes in ozone mixing ratio between the 2040s and 2000s (in colour). Superimposed in grey contours are the relative changes in ozone due to changes in chemistry in 100% (i.e.  $R_{O_3}^D + R_{O_3}^P$  as defined in Eq. 6.6). Also plotted are changes in ozone mass flux in  $10^9$  kg/year adapted from Fig. 6.13.

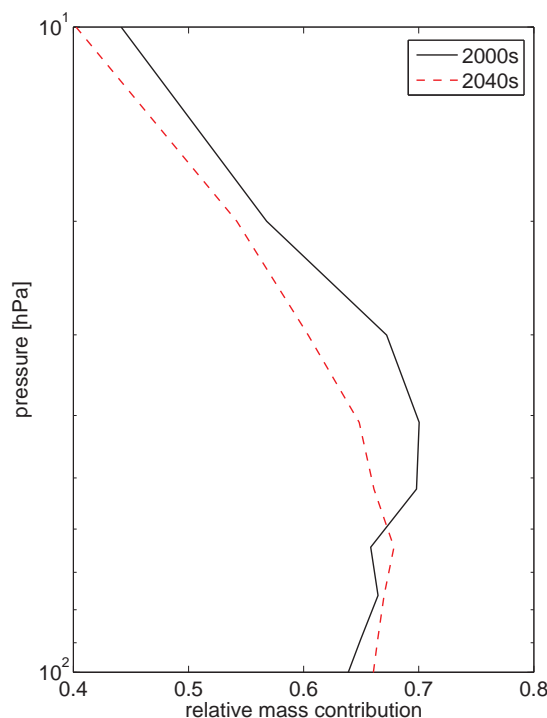


**Figure 6.17:** Relative contribution of mass [100%] in the southern high latitudes ( $65^{\circ}$ - $90^{\circ}$ S) originating from southern mid-latitudes as a function of height in DJF for the 2000s (black) and the 2040s (red).

troposphere (see Fig. 6.13). In terms of ozone, this is reflected in enhanced export of ozone in the tropical lower stratosphere which leads to a reduction in the ozone concentration in this region, in contrast to what would be expected from changes in chemistry (see Fig. 6.16). That is, effects of transport changes counteract the chemically induced trend, so that the overall trend is negative.

Otherwise, significant changes of ozone mass transport in the stratosphere are also found from the tropics into northern mid-latitudes and from southern mid-latitudes to southern high latitudes. As shown in Fig. 6.14 the enhanced ozone mass flux into northern mid-latitudes contributes only slightly to the positive trend in ozone concentrations here. In southern high latitudes, on the other hand, the reduction in the ozone flux from mid-latitudes almost halves the increase in ozone implied by chemistry changes. So how can the decrease in ozone flux from the middle to high latitudes, despite higher ozone concentrations in the mid-latitudes, be understood?

It was shown in Chapter 3 that the hemisphere-wide BDC in the southern hemisphere is strengthening from 1960 to the present in southern summer, and decreasing in strength again in the future. This was linked to dynamical changes implied by the radiational feedback of ozone changes themselves. These circulation changes are not reflected in the annual mean air mass flux changes as shown in Fig. 6.13. However, when considering DJF only, the contribution of mass in southern high latitudes that

originated from mid-latitudes is decreasing above 60 hPa in the 2040s compared to the 2000s (see Fig. 6.17). As density decreases with height, changes in the mass flux at higher levels are reflected less in the total mass fluxes as shown in Fig. 6.13 than changes at lower levels. This explains why we do see the change in ozone mass flux between the defined high and middle latitude region, but not the change in air mass flux. Hence the reduced contribution of mid-latitude air at high latitudes indicates that the reduced ozone mass flux does indeed result from reduced air mass transport. As discussed above, this change in mass flux corresponds to a weakening in the BDC in southern summer, which is in turn induced by the recovery of polar ozone. Consequently, the effect found here is a negative feedback between dynamics and ozone: with ozone recovering (i.e. chemical enhancement of ozone concentrations), dynamics are influenced in a way that the BDC is weakened and less ozone is transported into higher latitudes. This delays ozone recovery, which in turn slows down the weakening of the BDC. How important this negative feedback is for future ozone, and how important it was in the past (where we would expect a less deep ozone hole due to the strengthening of the BDC) will need further investigation, which will be possible using the methods developed in this work. It will be particularly important to apply this method also to other model systems to investigate whether the results obtained here are robust or only the artefact of the particular model used in this study.

To summarise, the effects of changes in the stratospheric meridional circulation on ozone were quantified in this chapter. It was found that enhanced tropical upwelling induces a negative trend in ozone in the tropical lower stratosphere. Otherwise, future stratospheric ozone changes are largely determined by changes in local chemistry.

# Chapter 7

## Conclusions and Outlook

### 7.1 Conclusions

The aim of this study was to investigate changes in the meridional circulation, to reveal the responsible drivers and mechanisms for these changes, and to study their impact on ozone transport.

**Changes in the meridional circulation in models and observations.** The analysis of the transient simulations performed with the model E39CA showed that long-term changes in the residual circulation occur mainly in the tropical lower stratosphere. In particular, tropical upwelling is strengthened in the tropical lower stratosphere, and the upward mass flux is balanced by downward flow in the subtropics at latitudes of around 20°-40°N/S. This shallow branch of the meridional circulation can be seen as a 'secondary circulation' superimposed on the BDC. The finding of strengthened upwelling in the lowermost stratosphere agrees with other recent studies with different model systems (see Introduction), but in many models the increase in the meridional circulation extends to higher latitudes and altitudes (e.g. Butchart et al., 2010). Also, not all models consistently show that resolved<sup>1</sup> waves are responsible for the increased forcing. As mentioned in the Introduction, resolved wave forcing was, however, found as primary contributor to enhanced forcing in the lower stratosphere (McLandress and Shepherd, 2009). This is in agreement with the results presented here. In the middle stratosphere gravity waves become more important (McLandress and Shepherd, 2009). Gravity waves are parametrised in the models, and are yet a large factor of uncertainty. The model used in the study presented here uses a parametrisation for orographic gravity wave drag (OGWD) but neglects non-orographic gravity waves. Also, the model is confined to the lower and middle stratosphere as it extends only up to 10 hPa. Therefore, it might well be that these limitations lead to the absence

---

<sup>1</sup>The term resolved waves refers to waves that are explicitly resolved in atmospheric models, i.e. the term is somewhat artificial. Transferred to reality one should think of waves with wavenumbers typically smaller 10, as most wave energy lies in large-scaled waves (e.g. Randel and Held, 1991)

of simulated changes in the BDC in the middle stratosphere. As the strengthening of upwelling in the lower stratosphere appears to be a robust result across models while the changes in the hemisphere-wide BDC are not as consistent, it seems possible that this uncertainty results from different treatment of gravity waves in the models. A recent study by Sigmond and Scinocca (2010) investigated the sensitivity of the climate response to different settings of the OGWD parametrisation. They showed that even though the direct climate response of the zonal wind does not depend on the OGWD settings, the difference in the basic state due to differing OGWD settings feeds back to the response of the circulation on climate change. They conclude that the changes in OGWD forcing that contribute to strengthening of the BDC might be altered by different settings of the OGWD. This supports the hypotheses that the differences in the BDC changes across different models is due to the treatment of gravity waves.

In addition to the steady long-term changes in the secondary circulation, modifications in the southern summer BDC were found in the study presented here. These changes could be attributed to dynamical changes induced by ozone depletion and recovery. This feedback of ozone on the circulation is in agreement with various other studies, and it is well understood that this change in the BDC is driven by changes in the zonal wind field due to altered temperature gradients in the stratosphere (e.g. Li et al., 2008).

As discussed in the Introduction, observational evidence for a strengthening of the meridional circulation is poor to the present day. It is so far not known whether this lack of evidence results from the possibility that the strengthening of the meridional circulation is purely an artefact of the models, or whether the data basis is not appropriate to detect changes in the regions where they are occurring. The most-cited work that is used to state the apparent contradiction between models and measurements is the study by Engel et al. (2009) (hereafter E09). In this study, trends in age of air measurements are analysed. In mid-latitudes at levels around 24-35 km a positive but not significant trend of 0.24 yrs/decade is found (i.e. indicative of a slower circulation). However, within the error bounds of 90% confidence the trend can lie between +0.6 and -0.12 yrs/decade. In the 90-year trend of age of air in the simulation (SCN-B2d) used in this study, a decrease of about 0.05 yrs/decade is found at levels corresponding to the region in E09, i.e. above 30 hPa (see Chapter 3). Therefore, the modelled change in age of air does actually not contradict the measurements by E09. The lack of a significant trend in age of air above 30 hPa does, however, not exclude the possibility of changes in the meridional circulation below this level. E09 noted that it might be possible that tropical upwelling increases at lower levels and the air parcels recirculate within the lower stratosphere, not affecting age of air at the levels of their measurements. This is exactly what is found in the study presented here: a strengthening of the meridional circulation in the tropical lower stratosphere. In the 90-year trend of age of air, the weak decrease of 0.05 yrs/decade does suggest that the change in upwelling in the lower stratosphere does affect age of air also at higher levels, but the trend is too weak as to

be detectable in the 30 years worth of data that are analysed in E09. Also the lack of trends in estimated upwelling found by Sinnhuber and Wohltmann (2010) on a level of 70 hPa are consistent with the results found here as trends in upwelling are significant only at lower levels.

Overall, the results of this study are not found to contradict published observational evidence of trends in the meridional circulation. The increase in the 'secondary circulation' is thus not inconsistent with observations, but could not be 'proven' from observations so far either. Probably the strongest indicator of an increase of tropical upwelling in the lower stratosphere in observations is the finding of negative ozone trends in the tropics in radiosonde and satellite data [W. Randel, personal communication]. The discrepancy across models in simulated trends in the meridional circulation in the extratropics and in the middle stratosphere coincides with an inconsistency of these changes to observations (e.g. Engel et al., 2009, see discussion above). As stated above, changes in the extratropical BDC are assigned to changes in gravity wave drag in some studies (McLandress and Shepherd, 2009), which bear large uncertainties (Simmond and Scinocca, 2010). Therefore it might well be that these changes are after all a model artefact due to the lack of understanding of gravity wave forcing, while the changes in the tropical lower stratosphere are robust across models and not inconsistent with observations.

Another result found here is the decrease of the width of the region of upwelling in the lower stratosphere. Recently, evidence was presented that indicates a widening of the tropics as defined by tropopause heights and by the width of the Hadley circulation (e.g. Seidel and Randel, 2007; Schneider et al., 2010). The dynamical causes for this widening are, however, not yet understood (Schneider et al., 2010). The widening reported on in Seidel and Randel (2007), based on the region with high tropopause heights, is of the order of  $3^\circ$  latitude per decade. With a model resolution of approximately  $3.75^\circ$  in latitude as for the model used here, this widening is only detectable on long timescales and if the variability is small enough. Whether the decrease in the width of the upwelling region is in any way connected to, or even contradicting to the widening of the tropics in terms of tropopause heights and the Hadley circulation is to be clarified.

**Drivers and mechanism of circulation changes.** While the mechanisms that drive the BDC are well understood, there is still a lack of understanding of the reasons for strong upwelling in the tropical lower stratosphere especially in the summer hemisphere (see Introduction). In this study it was shown that changes in the meridional circulation mainly occur in the tropical lower stratosphere. To be able to explain these changes, it is necessary to better understand the mechanisms that control upwelling in the lower stratosphere. Therefore, the forcing of tropical upwelling in the lower stratosphere by resolved waves was investigated, and it was shown that large parts of upwelling are accounted for by resolved wave forcing that occurs locally in the (sub-)

tropics.

The annual cycle in tropical upwelling could be explained by the seasonality of resolved wave activity. While in the solstice seasons the major wave source are planetary waves originating in the tropics, also transient synoptic scale waves that originate from the extratropics contribute to tropical wave forcing, especially in northern spring. Tropical upwelling and its wave forcing in the model was compared to a corresponding analysis with ERAInterim reanalysis data. The findings on wave driving of tropical upwelling could be confirmed with the reanalysis data. However, a discrepancy was found in the absolute values of the residual vertical velocities. The reanalysis are supported by poor observational data in the tropics, especially for the vertical velocities so that they are essentially a result of the model integration ERAInterim is based on. It is known that in the predecessor version of ECMWF reanalysis (ERA40) the estimated vertical velocities have large deficits, but considerably improved in the ERAInterim data set (Simmons et al., 2006). E39CA has an exceptional high vertical resolution in the upper troposphere and lower stratosphere (16 model levels in altitudes between 400 and 100 hPa, compared to 12 levels in ERAInterim). Therefore, the question which of the data sets lies closer to reality can not be easily verified. However, the overall good agreement between E39CA and ERAInterim in the forcing of tropical upwelling by resolved waves raises the confidence in E39CA. It can be assumed that the model adequately simulates processes in the tropical lower stratosphere, and thus estimated long-term trends can be regarded as reliable.

A number of recent studies analysed forcing mechanisms of tropical upwelling in the lower stratosphere (e.g. Boehm and Lee, 2003; Kerr-Munslow and Norton, 2006; Randel et al., 2008). The common picture arises from these studies that the strength and annual cycle in tropical upwelling is driven by local resolved wave forcing, a conclusion also reached in this study. This implies that in addition to the hemisphere-wide BDC, a more confined meridional circulation is superimposed in the tropics. While the BDC is driven by the well-known "extratropical wave pump" (e.g. Holton et al., 1995; Haynes et al., 1991), the tropical circulation is driven by local resolved wave forcing in the (sub-)tropics. This is illustrated in Fig. 7.1: the BDC provides an upward suction of air in the tropics (arrow marked with a), but the mass flux is weak in the lower stratosphere as the density strongly decreases with height. A secondary circulation is induced in the tropics (arrows marked with b). High SSTs in the summer (sub-)tropics lead to enhanced deep convection, which transports latent heat and warms the upper troposphere. The zonally asymmetric latent heat release triggers waves, that propagate upward but are strongly damped by the prevailing easterly shear. In addition extratropical waves (mostly of transient nature), that are refracted towards the equator dissipate in the (sub-)tropical lower stratosphere. This results in EP convergence (marked light blue), that in turn drives the secondary meridional circulation in the tropics.

The finding of a superimposed secondary circulation in the tropical lower stratosphere is in agreement with other recent studies. For example Birner and Boenisch

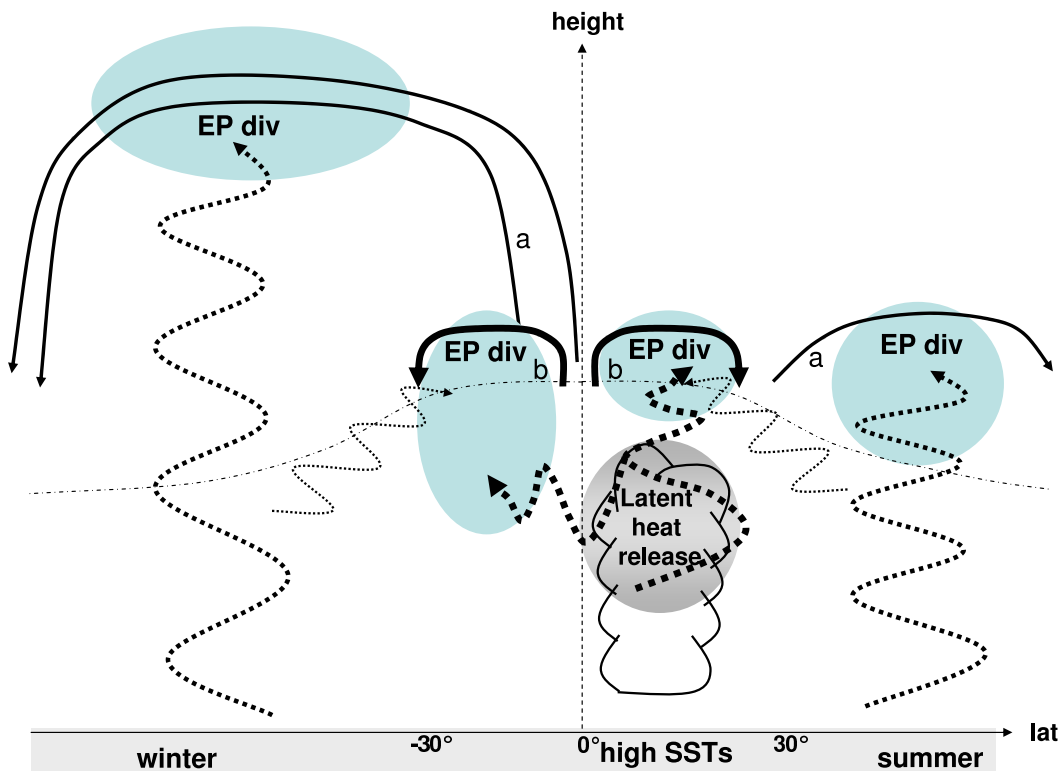


**Figure 7.1:** Schematic of the two branches of the meridional circulation in the stratosphere and its wave driving. Wave flux convergence is indicated in light blue patches (negative EP divergence). The global classical BDC (a) is driven by extratropical waves and a deep hemisphere wide cell exists in the winter hemisphere. The secondary circulation (b) is confined to the (sub-) tropical lower stratosphere and driven locally by wave dissipation. Both tropical waves (that are mostly generated by strong deep convection in the summer tropics) and extratropical waves (that are refracted to low latitudes) contribute to the wave convergence in the UTLS.

(2010) show that the meridional circulation can be separated into a deep branch and a shallow branch (which corresponds to the 'secondary circulation') with much faster transit times. The mass flux along this secondary, or shallow, circulation is far larger than the mass flux transported by the deep branch of the BDC.

The causes of changes in tropical upwelling were investigated using additional sensitivity simulations. It was shown that the changes in the residual circulation and wave fluxes in the lower stratosphere found in the transient simulation in E39CA are driven by changes in the troposphere due to the indirect effect of changes in SSTs. In particular, enhanced tropical SSTs lead to a response in tropical upwelling that resembles the trends in the transient simulation. Therefore, it can be concluded that processes associated with tropospheric warming are responsible for the increase in tropical upwelling, confirming earlier studies by Fomichev et al. (2007), Sigmond et al. (2004) and Oman et al. (2009). Furthermore the new and additional sensitivity simulations showed that the region that triggers changes in upwelling can be confined to the tropics. On the

other hand, SST changes in northern mid-latitudes were shown to have almost no impact on the stratospheric meridional circulation. Therefore, mechanisms connected to changes in planetary wave generation due to extratropical SST changes can be excluded as driver of tropical upwelling changes.

The warming of the tropical sea surface has two effects that might be relevant for wave forcing in the (sub-)tropics. Firstly, the tropical upper troposphere is warmed, and therefore the meridional temperature gradient increases. This leads to an increase in the subtropical jets due to the thermal wind balance. Secondly, higher SSTs lead to changes in deep convection and changes in the water content of the atmosphere and therefore latent heat release is altered (both in strength and location) in the upper tropical troposphere. While the former alters the background conditions for wave propagation and dissipation, the latter modifies the tropical wave response to the heating (i.e. wave generation). The redistribution of heat from the sea surface into the troposphere is driven by convective processes and latent heat fluxes. Therefore, the same processes cause 1) the strengthening of the jets and 2) the modification of tropical wave generation. Thus, it is not possible to design a simulation with a free running model in which only the wave propagation (controlled by 1), or only the wave generation (controlled by 2) is subject to changes. The question which process is dominant for the changes in wave forcing in the lower stratosphere can therefore not easily be answered by running specific sensitivity simulations with the model system used in this study.

It is found in this study that the increase in local wave forcing in the tropics is due to both stationary and transient waves. In the solstice seasons, the contribution of planetary stationary waves prevails, while in the transition seasons also transient synoptic waves contribute to the increased forcing. The analyses indicate that the generation of planetary stationary waves in the solstice seasons is modified, namely the region of wave generation is slightly shifted. This is in agreement with the hypothesis by Deckert and Dameris (2008), suggesting that the increased wave forcing in the lower stratosphere is due to enhanced generation of tropical waves. However, the additional sensitivity simulation with modified tropical SSTs performed in this study could not confirm the important role of wave generation changes. Rather, it became apparent that increased wave propagation into the lower stratosphere can occur in the absence of changes in the tropical wave source region. Also, the relative importance of stationary versus transient waves is found to differ in the sensitivity simulation from the long-term trends. That does not imply that modifications to wave generation do not act to change wave activity in the lower stratosphere. This mechanism probably contributes to the changes in wave forcing in the lower stratosphere as suggested in Deckert and Dameris (2008). However, the additional informations obtained by the tropical SST simulation suggest that this is not the dominating mechanism in driving long-term changes in tropical upwelling.

The findings presented in this study indicate that the increase and shift of the subtropical jets due to the enhanced meridional temperature gradient favours vertical

propagation of tropical waves. The changes in the zonal wind lead to an upward shift of the zero wind line and of the zone of easterly shear. Therefore, wave damping is inhibited in the upper troposphere and waves are permitted to penetrate to higher levels. The changes in wave damping due to the background conditions do act on waves of all scales and frequencies. That is for all westward-propagating waves, the Doppler-shifting of the frequency results in enhanced (inhibited) damping in easterly (westerly) winds. This would explain the fact that the annual cycle in wave forcing by stationary and transient waves is not altered, but wave forcing is generally increasing both for stationary and transient waves. Therefore, tropical upwelling is found to increase throughout the year. If it was only changes in the generation of large-scale waves, it would be expected that tropical upwelling increases mainly in the solstice seasons. Furthermore, this explained the finding that the relative contribution of stationary versus transient waves is not robust across simulations and sub-periods of simulations. Again, if the dominating mechanism for stronger upwelling was increased planetary wave generation in the tropics, it would be expected that the enhanced wave forcing was in all cases due to enhanced forcing by stationary tropical waves.

As it is found that tropical SSTs are driving changes in tropical upwelling by modifying tropical wave activity, the question arises whether natural variability in tropical SSTs, namely ENSO, causes a response in tropical wave fluxes and upwelling in a similar manner as the trend and whether the same processes act there. While it is well understood that ENSO influences the stratosphere by modifying extratropical waves (e.g. Calvo et al., 2008), also the local tropical wave response might play a role in influencing tropical upwelling in the stratosphere. Indeed, as was shown here, the response of EP fluxes to ENSO does as well show enhanced wave propagation into the lower stratosphere, causing an increase in the secondary circulation. Interestingly, the generation of tropical planetary waves is inhibited during ENSO warm phases compared to cold phases, so that the enhanced wave forcing can not be due to stronger wave generation. For ENSO, as for the trend, the subtropical jets are enhanced and shifted, so that it appears likely that the same mechanism of changes in wave damping and propagation through modified background winds acts here to modify tropical upwelling.

However, care has to be taken in assigning cause and effect of the dynamical changes in the tropics. The zonal wind in the deep tropics is the product of the balance of momentum fluxes by eddies and momentum transport by the mean meridional circulation (Lee, 1999). Due to this complex interaction between waves and the zonal mean flow it is very hard, if not impossible, to entangle the cause-effect relationship of zonal wind changes and wave propagation and dissipation. Probably only studies with simpler mechanistic models, in which the strength of the jets can be adjusted and fixed, might be able to reveal the exact chain of processes.

Overall, the results presented here show that the secondary circulation is driven by local resolved wave forcing. The strength of this forcing is controlled by tropical SSTs. Both enhanced propagation and tropical wave generation by deep convection lead to

changes in the resolved wave forcing and therewith tropical upwelling. The evidence presented in this study suggest that the most robust and dominant mechanism for the long-term increase in tropical upwelling is inhibited damping of tropical waves by an upward shift of the easterly shear zone.

**Impact on ozone transport** In addition to the investigation of dynamical processes of the meridional circulation, its impact on transport of ozone was investigated. It was found that the strengthening in the secondary circulation is reflected as expected in Lagrangian air mass transport and leads to negative trends in ozone in the tropical lower stratosphere. Also the changes in the BDC in the southern hemisphere were found to impact ozone transport, leading to a strong reduction (about half) of the positive ozone trend in southern high latitudes, i.e. a delay of ozone recovery.

It is widely understood that future changes in ozone will be determined by an interplay of reductions in CFC abundances, cooling by GHG increases and changes in the meridional circulation. In the upper stratosphere, where ozone is largely chemically controlled, the effect of CFCs and GHGs is expected to dominate ozone changes while in the lower stratosphere also transport changes are expected to play a role. The major challenge in determining the importance of these processes is to untangle their influence on ozone. Up to date, most studies only diagnose the impact of circulation changes on ozone in a speculative manner (e.g. Oman et al., 2010; Eyring et al., 2010). In this study, a method is introduced that quantifies ozone transport and estimates the impact of changes in transport on ozone trends. This allows for the first time to quantify the role of transport changes on ozone changes. It was confirmed that the ozone decrease in the tropical lower stratosphere is due to changes in transport. However, the decrease due to more export of ozone is in part balanced by an enhancement in ozone due to chemistry. In particular, more local ozone production enhances ozone concentrations. The enhancement of production probably results from changes in the available amount of radiation necessary for photodissociation, which can be explained by changes in the amount of radiation absorbed at upper levels (the so-called 'self-healing' effect).

The results presented in this study show that mid-latitudinal ozone is barely affected by changes in ozone transport. The positive trend in the mid-latitudes is almost entirely caused by decreases in destruction rates. This is due to 1. slower destruction rates caused by the lower temperatures induced by GHGs and 2. less destruction by the halogen catalytic cycles due to declining CFC abundances. This finding corrects the speculations by the recent studies on the basis of the most up-to-date CCM simulations of Oman et al. (2010), Eyring et al. (2010) and Austin et al. (2010b), that also mid-latitudinal ozone is subject to modifications by changes in the BDC. As stated by Oman et al. (2010), the reason for the difference in hemispheric return dates (with northern hemispheric ozone returning earlier to 1960 values compared to the southern hemisphere) might be either the stronger ozone loss in the SH, which is reflected also in mid-latitudes, or changes in the circulation (i.e. stronger tropics-to-pole transport).

The findings presented in this study show that changes in transport do have little impact on ozone in mid-latitudes. The only extratropical region that is strongly affected by changes in transport are the southern high latitudes, where ozone recovery through decreased destruction is counteracted by decreased transport of mid-latitude air into the polar region. However, this was shown only for the model system used here. As discussed above, the changes in the meridional circulation in this model are mostly limited to the tropical lower stratosphere (intensification of the secondary circulation). In models that simulate enhancements also in the hemisphere-wide BDC it is likely that ozone transport is becoming important also in the mid-latitudes.

## 7.2 Outlook

In this study, the changes in the residual circulation and the dynamical causes of changes therein were analysed extensively. As discussed above, the strengthening of tropical upwelling and the secondary circulation in the lower stratosphere is a robust result across models. Yet, the question remains whether changes in the hemisphere-wide BDC as simulated by some models are robust as well, or for example an artefact of gravity wave parametrisations. Specifically for the model used in this study it would be interesting to know how strong the results are influenced by the lack of a parametrisation of non-orographic gravity waves, and by the low upper boundary of 10 hPa. The lid at 10 hPa does cause waves (both resolved and parametrised) to break below this level, so that the momentum transfer occurs collectively at this level and is not spread over the middle and upper stratosphere as in reality. Since the momentum transfer by waves interacts with the zonal mean flow this might have implications for the dynamical balances in the model.

The dynamical reasons of the intensification of the secondary circulation were analysed using data from the CCM E39CA. The problem with a fully coupled free running climate model is that it is not easy to verify cause-effect relationships of modelled changes. The wave-mean flow interaction is a classical chicken-egg problem: The background mean flow influences the ability of waves to propagate in certain regions, and determines the regions of wave breaking and damping. Dissipation of waves does, in turn, act as a force on the mean flow by depositing momentum, changing the background conditions. Hence, the cause-effect relationship of the mechanism that is found to intensify wave forcing and thus tropical upwelling can not be completely unravelled using a free running model. In order to verify whether the mechanisms do act as suggested in this study it would be desirable to use more simplified models, in which, for example, the zonal wind can be fixed or adjusted externally.

Another open issue for future research on the stratospheric meridional circulation is the attempt to diagnose changes in the meridional circulation in observational data. As discussed above, the findings of the current work are not contradicting studies that analyse observations, but the enhancement of tropical upwelling is still to be shown

in observations. It seems most promising to perform joint studies with model and observational data, mostly to secure that the same quantities are analysed in both data sets. Much of today's confusion on the apparent contradiction between models and the real world stems from the fact that different quantities are analysed, and even different definitions of the term 'Brewer-Dobson Circulation' are used. The new concept of differentiating between the deep BDC and the shallow secondary circulation, as introduced in this study and in other recent studies (e.g. Birner and Boenisch, 2010), might help to reach clearer definitions of terms used to describe the meridional circulation. From observations it is often easier to assess transport-related quantities like age of air or tracer distributions. These are, however, also influenced by other factors than transport by the residual circulation. Even if a tracer does not have any sources or sinks but is purely advected passively in the stratospheric flow, the transport by the residual circulation acts together with two-way mixing to redistribute the tracer. The term 'mixing' is somewhat vague and used in different contexts, for example to describe the amount of dynamical stirring (e.g. Garny et al., 2007) or the complexity of tracer distributions (e.g. Haynes and Shuckburgh, 2000). A major problem is how to transfer these diagnostics to the actual amount of tracer that is redistributed by mixing. This would be required to be able to quantify how strong tracer distributions are influenced by mixing versus the influence by advection with the mean meridional circulation. Also the inferences on changes in the residual circulation from age of air might strongly be influenced by mixing, as age of air will obviously be determined by both ways of transport. Indeed, using a very simple 'tropical pipe' one dimensional model, it can be shown that changes in age of air of the magnitude measured in Engel et al. (2009) can be reproduced both by adjusting the residual circulation or adjusting mixing across the tropical barrier [E. Ray, personal communication]. A better understanding of the interplay of transport processes and pathways will be an important task to better understand changes in the stratospheric circulation and its impact on tracer redistribution. The model used in this study has the Lagrangian advection scheme ATTILA incorporated, which provides a large set of online calculated trajectories during the whole course of the simulations. These trajectory data provide an excellent data base to study Lagrangian transport, its connection to Eulerian transport (i.e. the residual circulation) and to identify transport pathways. Also, the mean age of stratospheric air can be derived from the trajectory data in a unambiguous manner. In addition to mean age of air, also spectra of age of air can be derived (Reithmeier et al., 2008). As in many observational studies a constant spectra of age of air is assumed in the derivation (Engel et al., 2009), it would be interesting to study with the model system whether this assumption is validated.

The impact of changes in the meridional circulation on tracers is studied here on the example of ozone. A new method was developed that allows to quantify the impact of changes in transport on ozone changes, and this method was applied to a simulation with E39CA that models the future ozone development. In order to assess whether the

findings presented here are valid generally, it will be crucial to apply the method to other model systems. To capture also the upper part of the ozone layer, models that fully include the middle and upper stratosphere would be desirable. The attribution of ozone tendencies and changes on monthly, interannual and long-term timescales to chemistry and transport can help to analyse various processes of ozone variations. For example, it is known that the QBO or the solar cycle impact ozone (e.g. Randel and Cobb, 1994; Bodeker et al., 2007; Dameris et al., 2006), and the processes are widely understood (e.g. Kinnersley and Tung, 1999; Gray and Pyle, 1989). However, using the new methodology introduced here it will be possible to explicitly quantify how much of the anomalies are induced by transport changes and how far local chemistry is responsible.

So far, in this study the influence of chemistry on ozone was split up into production and destruction. It is possible to further split up these terms into production and destruction by different reaction cycles. Especially in the light of recent studies on the role of future emissions of nitrous oxide (Ravishankara et al., 2009) it would be interesting to assess the role of this substance in depleting ozone in a quantitative way.

The attribution method does also have a wide field of applications in model assessments. By applying the method to various CCMs, it will be possible to have a tool of process oriented comparison of these models. So far, mostly only statements about the total difference in ozone between different models or between models and observations can be made. Only derived quantities are used to estimate the contribution of chemical or dynamical processes to these differences (e.g. Austin et al., 2010a). When applying the ozone attribution method to different models it will be possible to track down the differences in simulated ozone to differences in the amount of ozone produced, destroyed or transported. Unfortunately, it will obviously not be possible to apply the method directly to observational data. Yet there is the possibility to use chemistry-transport models that are based on observed wind fields, or even assimilated data sets like the one by Kiesewetter et al. (2010). A comparison of these data sets to CCMs using the ozone attribution method will allow to evaluate the processes modelled by CCMs in a quantitative manner.

The ozone attribution method as presented in this study is in its first stage, and there is room for improvement and modifications. So far, only fixed geographical regions are used to divide the ozone field. It would be desirable to divide the atmosphere according to its dynamical regions, e.g. use the actual tropopause to divide the troposphere from the stratosphere instead of the fixed pressure levels. Also, it would be an improvement to separate air masses within and outside the polar vortex by using, for example, PV gradients to determine the polar barrier. This would require larger modification of the implementation, as PV and tropopause heights would have to be calculated online and passed to the chemistry routine where the ozone fields are calculated. An easier way could be to use climatological values of the tropopause as boundary between the pre-defined regions, which is probably a good approximation as

the interannual variability of the tropopause height is small compared to the vertical model resolution. As mentioned above, another improvement will be to further separate the chemical terms into different reaction cycles. This can easily be done as long as the production and destruction terms are saved as model output. It would also be desirable to be able to separate the effect of the available radiation for photodissociation. Even if the concentrations of all chemical species remain the same, changes in the amount of available photons by absorption at layers above the region of interest (i.e. non-local influence of ozone above this layer) can change ozone production and destruction. This is so far not incorporated in the method, and will be subject of future improvements.

# Appendix A

## Glossary and Abbreviations

### General

**Lower and Middle stratosphere** The term lower stratosphere is used here for the region between the tropopause (which lies around 300 to 100 hPa) and 50 hPa. Since the model used in this study extends only to 10 hPa, the term middle stratosphere refers to the layer between 50 hPa and 10 hPa.

**Upper troposphere/ Lower stratosphere (UTLS)** The UTLS is commonly defined as the region around the tropopause, i.e. the transition layer between the troposphere and stratosphere.

**Climate change** In this study, the term climate change refers to the long-term changes of the atmosphere induced by the emission of long-lived GHGs. In the model system, climate change is forced by the combined effect of changes in GHG concentrations and in SSTs.

**El-niño Southern Oscillation (ENSO)** ENSO is an atmospheric-oceanic oscillation in the region of the pacific ocean. It has two phases in addition to the normal phase, the El niño and the La niña phase, where sea surface temperatures in the eastern pacific are higher or lower as in the normal phase, respectively. Here the ENSO is quantified by the Nino3.4 index, the average of sea surface temperatures over a specific region in the eastern pacific.

**Quasi-biennial oscillation (QBO)** The QBO is an oscillation of tropical winds in the stratosphere. Zonal winds oscillate from easterlies to westerlies with an average period of 27 months. The wind anomalies propagate downward in the tropics, and amplitudes are highest between 10 and 40 hPa. In the model used here, the QBO is prescribed externally.

## Meridional circulation

**Brewer-Dobson circulation (BDC)** The BDC is defined in this study as the meridional circulation that is driven by the 'extratropical wave-pump', i.e. the hemisphere-wide high reaching circulation that is responsible for transport from low to high latitudes.

**Residual meridional circulation** The term residual meridional circulation, or only meridional circulation, is used here to describe the entire mass flow in the meridional plane.

**Secondary circulation** The secondary circulation is the shallow circulation in the (sub-)tropical lower stratosphere that is induced locally by (sub-)tropical wave forcing. The secondary circulation is superimposed on the BDC.

## Waves

**Resolved and parametrised waves** Resolved waves are waves that are explicitly modelled on the grid, i.e. that have a horizontal and vertical scale that exceeds the model resolution (that is about  $3.75^\circ \times 3.75^\circ$  on the latitude-longitude grid of the model used in this study). Waves with smaller scale can not be captured by the model and need to be parametrised, such as gravity waves.

**Stationary and transient waves** In this study, stationary waves are defined to be waves that are stationary over the course of one month, i.e. they have a period  $\geq 30$  days. Transient waves are all resolved waves with shorter periods.

**Planetary and synoptic waves** Planetary waves are defined as waves with zonal wavenumber 1, 2 and 3, while all smaller-scaled (but still resolved) waves are defined as synoptic scaled waves.

## Model related

**Chemistry-climate model (CCM)** CCMs are atmospheric general circulation models that are interactively coupled with a chemistry scheme, so that radiatively active tracers do feed back on the climate. Commonly, CCMs do not have an interactive ocean so far due to limited computing power. Therefore, SSTs are prescribed externally.

**Transient simulation** In a transient simulation, a period of time is simulated with varying prescribed boundary conditions. The boundary conditions are chosen to resemble the development of the real atmosphere in the past, or to simulate possible future projections of the atmosphere. In this study, one transient simulation is designed to closely resemble the past from 1960 to 1999 (**REF-B1**), and one simulation is designed to model consistently past and future developments of the atmosphere from 1960 to 2049 (**SCN-B2d**).

**Time-slice simulation** A time-slice simulation runs under constant boundary conditions and thus represents the climate under certain fixed conditions (i.e. a certain point in time). The model years of a simulation of this kind only vary due to the internal variability of the system.

**Sea surface temperatures (SSTs)** The term SSTs is used here to describe the prescribed temperatures of the sea surface and the sea ice cover at the lower boundary of the model.

**Greenhouse Gases (GHGs)** Greenhouse gases (GHGs) refers to the long-lived GHGs  $CO_2$ ,  $N_2O$  and  $CH_4$ . The concentrations of these gases are prescribed as external forcing in the model.

**Chlorofluorocarbons (CFCs)** The CFCs are prescribed as external boundary condition in the model, and this class includes: F11( $CCl_3F$ ), F12( $CCl_2F_2$ ), F10( $CCl_4$ ),  $CH_3Cl$  and  $CH_3CCl_3$ .

#### Other Abbreviations

**Seasons** December-January-February (**DJF**),  
March-April-May (**MAM**),  
June-July-August (**JJA**),  
September-October-November (**SON**)

**Hemispheres** Southern Hemisphere (**SH**), Northern Hemisphere (**NH**)

**Dynamics** Downward control (**DC**), Eliassen-Palm (**EP**) flux



## Appendix B

# The TEM equations and downward control

The concept of the transformed eulerian mean (TEM) equations is used for studying the global zonal mean circulation in the stratosphere. The TEM equations are derived from the conventional eulerian mean equations to address the following problem: the induced conventional eulerian mean meridional circulation  $(\bar{v}, \bar{w})$  cancels the meridional and vertical motion produced by non-dissipative waves (Andrews et al., 1987). Non-dissipative waves lead to a Lagrangian movement of air parcels that form a circle in the meridional plane, and hence induce no real transport ( $\rightarrow$  non-transport theorem, see Andrews et al., 1987). Therefore, it is convenient to transform the eulerian meridional circulation in a way that this cancellation is eliminated, which is accomplished with the TEM framework.

The TEM equations are obtained from the conventional ones by introducing a transformed, or residual meridional circulation:

$$\bar{v}^* = \bar{v} - \frac{\partial}{\partial p} (\overline{v'\Theta'} / \frac{\partial\Theta_0}{\partial p}) \quad (\text{B.1})$$

$$\bar{w}^* = \bar{w} + \frac{1}{r \cos \phi} \frac{\partial}{\partial \phi} (\overline{v'\Theta'} / \frac{\partial\Theta_0}{\partial p}) \quad (\text{B.2})$$

Here  $u$ ,  $v$  and  $w$  are the velocity in x, y and p-direction, respectively,  $\Theta$  the potential temperature and  $r$  the radius of Earth. The meridional circulation defined in this manner represents a ‘diabatic’ circulation, as the adiabatic part is subtracted. The vertical motion now represents the motion following diabatic forcing, and air parcel movements can be associated with the residual meridional circulation. The TEM equations can then be written as:

$$\frac{\partial \bar{u}}{\partial t} + \hat{f} \bar{v}^* + \bar{w}^* \frac{\partial \bar{u}}{\partial p} = \bar{X} + \frac{1}{r \cos \phi} \nabla \cdot F \quad (\text{B.3})$$

$$\frac{\partial \bar{\Theta}}{\partial t} + \frac{\partial \Theta_0}{\partial p} \bar{w}^* = \bar{Q} \quad (\text{B.4})$$

$$\frac{1}{r \cos \phi} \frac{\partial \bar{v}^* \cos \phi}{\partial \phi} + \frac{\partial \bar{w}^*}{\partial p} = 0 \quad (\text{B.5})$$

where  $\hat{f} = f - 1/(r \cos \phi) \frac{\partial}{\partial \phi}(\bar{u} \cos \phi)$ ,  $\bar{Q}$  is the diabatic heating term,  $\bar{X}$  is the zonal forcing due to small scale eddies (e.g. gravity wave forcing) and  $\nabla \cdot F$  is the divergence of the Eliassen-Palm (EP) Flux  $F$ , that is defined as:

$$\begin{aligned} F_\phi &= r \cos \phi \left( -\overline{u'v'} + \overline{v'\Theta'}/\Theta_p \frac{du}{dp} \right) \\ F_p &= r \cos \phi \left( \overline{\hat{f}v'\Theta'}/\Theta_p - \overline{u'w'} \right) \\ \nabla \cdot F &= \frac{1}{r \cos \phi} \frac{d}{d\phi}(F_\phi \cos \phi) + \frac{d}{dp} F_p \end{aligned} \quad (\text{B.6})$$

The EP flux is the flux of wave activity, and its divergence is the force on the zonal mean flow by dissipation of waves.

For illustrating EP fluxes and their divergence correctly, the fluxes are scaled by the mass of an annular ring of a certain latitude band and pressure interval, following the conventions of Edmon et al. (1980) (see their Eq. 3.12). The EP flux  $F$  as given above is therefore converted to:

$$\begin{aligned} \hat{F}_\phi &= 2\pi r \cos(\phi)/g F_\phi \\ \hat{F}_p &= 2\pi r^2 \cos(\phi)/g F_p \\ \nabla \cdot \hat{F} &= \frac{d}{d\phi} \hat{F}_\phi + \frac{d}{dp} \hat{F}_p \end{aligned} \quad (\text{B.7})$$

Due to the mass scaling, the EP flux is in units [ $m^3 \text{rad}, m^3 Pa$ ] and the divergence in  $m^3$ , which equals  $Nm/Pa$ , i.e. energy/pressure (Edmon et al., 1980).

The meridional residual circulation  $(\bar{v}^*, \bar{\omega}^*)$  is used here for quantifying the large-scale circulation in the stratosphere. As a measure of the strength of the upwelling branch of the circulation, mean tropical upwelling is calculated by integrating over all latitudes within  $60^\circ \text{N/S}$  where the residual vertical velocity points upward (i.e. negative  $\bar{\omega}^*$  since  $\omega = \frac{\partial p}{\partial t}$ ):

$$U_{\text{tropics}} = \int_{\phi_{\bar{\omega}^* < 0}} \frac{2\pi \cos(\phi) r^2}{g} \bar{\omega}^* d\phi \quad (\text{B.8})$$

Alternatively, the integration can be performed over a fixed latitude band, for example over  $20^\circ \text{S}$  to  $20^\circ \text{N}$  (as in Chapter 5).

From the continuity equation for  $(\bar{v}^*, \bar{\omega}^*)$ , the mass-weighted residual streamfunction  $\bar{\chi}^*$  can be introduced:

$$(\bar{v}^*, \bar{\omega}^*) = \frac{g}{2\pi r \cos(\phi)} \left( -\frac{\partial \bar{\chi}^*}{\partial p}, \frac{1}{r} \frac{\partial \bar{\chi}^*}{\partial \phi} \right) \quad (\text{B.9})$$

This mass-weighted streamfunction is used in Chapters 3, 4 and 5 to quantify the meridional circulation. It is calculated from the residual vertical velocity as:

$$\overline{\chi^*}(\phi, p) = \int_{\phi'=90^\circ}^{\phi} \frac{2\pi r^2 \cos(\phi')}{g} \overline{\omega^*}(\phi', p) d\phi' \quad (\text{B.10})$$

In addition to this direct calculation from the residual vertical velocity, tropical upwelling and the residual streamfunction can be calculated using the downward control (DC) principle (Haynes et al., 1991). The DC principle states that the residual circulation at a certain level is driven by the forcing on the mean flow above this level. By using the EP divergence as forcing, the contribution of resolved wave activity in driving the residual meridional circulation can be quantified.

The DC calculations were performed as follows. Using the TEM momentum equation and assuming a non-zero meridional gradient of the zonal mean angular momentum  $\overline{m}=r \cos(\phi)(\overline{u}+r\Omega \cos(\phi))$  and stationary conditions, the mass-weighted residual streamfunction  $\overline{\chi^*}$  can be expressed as (for details see Haynes et al., 1991):

$$\overline{\chi^*}_{\overline{m}_0}(p) = \int_p^0 \left[ \frac{2\pi r^3 / g \cos(\phi)^2 G}{\partial \overline{m} / \partial \phi} \right]_{\phi=\phi(\overline{m}_0)} dp' \quad (\text{B.11})$$

Here  $G$  is assumed to be the EP divergence, and the subscript  $\phi=\phi(\overline{m}_0)$  denotes integration along lines of constant angular momentum. The condition  $d\overline{m}/d\phi \neq 0$  limits the latitude region of the calculation to outside the inner tropics. In practice, the integration along constant angular momentum can only be performed when  $\overline{m}_0$  is a real function of pressure, i.e. the  $\overline{m}_0$  contour is not closed in the domain of calculation.

For estimating tropical upwelling as given in Eq. B.8, it is used that

$$\overline{\omega^*} = g / (2\pi r^2 \cos \phi) \partial \overline{\chi^*} / \partial \phi$$

so that upwelling between latitudes  $\phi_1$  and  $\phi_2$  is given by  $[\overline{\chi^*}(\phi_2) - \overline{\chi^*}(\phi_1)]$  (Randel et al., 2002).



## Appendix C

# Linear least square regression modelling

Regression models are used for investigating the underlying drivers of variability in geophysical diagnostics. In this work, regression models are used for example to estimate trends while taking account of other known forcings on variables. The theory and methods of applying least square regression models are described here.

The time series of a quantity  $y(t)$  shall be expressed as a function of basis functions which represent processes that are believed to play a role in the variability of quantity  $y(t)$ . The relation between  $y(t)$  and the basis functions is assumed to be linear and  $y(t)$  is expressed as linear combination of basis functions  $x_k(t)$  (von Storch and Zwiers, 2002):

$$y(t_i) = \sum_{k=1}^M a_k x_k(t_i) + r(t_i) \quad (i = 1 \dots N) \quad (\text{C.1})$$

where  $a_k$  are the  $M$  regression coefficients for basis functions  $x_k$ , and  $N$  the length of the time series. The residual term  $r(t)$  denotes the difference between the modeled quantity and the observed value. Note that the term 'linear regression model' refers to linearity in the parameters  $a_k$  and not to linearity of the basis functions in time.

Given a time series of length  $N$ , the  $N$  equations given by C.1 can be written in matrix-form as (Puls and Stinzing, 2005):

$$\mathbf{y} = \mathbf{X}\mathbf{a} + \mathbf{r} \quad (\text{C.2})$$

$\mathbf{X}$ , the 'design-matrix', is a  $N \times M$  matrix, containing the basis function  $x_k$  at times  $t_1$  to  $t_N$  as  $k$ th column. The time series  $y(t)$  and  $r(t)$  are expressed as vectors of length  $N$  ( $\mathbf{y}$  and  $\mathbf{r}$ , respectively) and the  $M$  parameters  $a_k$  form vector  $\mathbf{a}$ .

In order to determine the parameters  $a_k$ , the sum of squared residuals  $\chi^2 = \sum_{i=1}^N r(t_i)^2$  is minimised.  $\chi^2$  can be expressed as:

$$\begin{aligned}
\chi^2 &= \mathbf{r}^T \mathbf{r} = \\
&= (\mathbf{y} - X\mathbf{a})^T (\mathbf{y} - X\mathbf{a}) = \\
&= \mathbf{y}^T \mathbf{y} - 2(X^T \mathbf{y})^T \mathbf{a} - \mathbf{a}^T X^T X \mathbf{a}
\end{aligned} \tag{C.3}$$

The deviation of  $\chi^2$  in respect to  $a_k$  (for  $k = 1..M$ ) is to be set zero, yielding the equation:

$$2(X^T \mathbf{y} + X^T X \mathbf{a}) = 0 \tag{C.4}$$

This set of linear equations can be easily solved, obtaining an estimate for  $\mathbf{a}$ . The modeled quantity is then given by  $\mathbf{y}_m = X\mathbf{a}$ .

**Uncertainties in the parameters** The uncertainty in the  $k$ -th regression parameter can be estimated to:

$$\sigma_{a_k}^2 = \frac{\chi^2}{N - M} [(X^T X)^{-1}]_{kk} \tag{C.5}$$

where it is assumed that the residuals are white noise i.e. normally distributed with zero mean and statistically independent in time. The full derivation for this expression is not given here (see e.g. von Storch and Zwiers, 2002).

This method of estimating uncertainties is applied for data with an unknown standard deviation. If taking e.g. measurements with a known measurement error  $\sigma_{ym}$ , the uncertainty in the parameters  $a$  can be directly obtained by  $\sigma_{a_k}^2 = \sigma_{ym}^2 [(X^T X)^{-1}]_{kk}$ .

If the assumption of a white-noise residual is violated, the uncertainties in the regression parameters will be significantly underestimated (Tiao et al., 1990). A more accurate estimate of the uncertainties in the parameters must be calculated by correcting the residual term for its autocorrelation. This method is described in the next paragraph.

**Autocorrelation in the residual** A better estimation of the parameter uncertainty can be obtained when preprocessing the data in a way which accounts for the autocorrelation in the residual.

An autoregressive model of first order (or higher order) is applied to the residual:

$$r_t = \varrho r_{t-1} + z_t \tag{C.6}$$

where  $\varrho$  is the autocorrelation coefficient. In this model,  $z_t$  is the residual and is assumed to be white noise (with mean 0 and standard deviation  $\sigma_z^2$ ). Basically, the residual  $r$  is split into a ‘white noise’ part and a ‘dependent’ part (depending on the residual one time step earlier, so having a ‘memory’ in contrary to white noise).

Assuming this autoregressive relationship, the regression model equations can be

transformed from

$$\begin{aligned} y_{i-1} &= \sum_{k=1}^M a_k x_{ki-1} + r_{i-1} \\ y_i &= \sum_{k=1}^M a_k x_{ki} + r_i \end{aligned} \quad (\text{C.7})$$

using  $r_i = \rho r_{i-1} + z_i$  into

$$y_i - \rho y_{i-1} = \sum_{k=1}^M a_k (x_{ki} - \rho x_{ki-1}) + z_i \quad (\text{C.8})$$

Now a regression equation with the transformed variables  $y_i - \rho y_{i-1}$  and  $x_{ki} - \rho x_{ki-1}$  and the white-noise residual  $z$  is obtained.

Practically, the procedure is done in the following steps: At first, an estimate of the residual is obtained by running the regression model in the original set-up (equation C.2). The autocorrelation coefficient is calculated for the obtained residual. Then the variables are transformed as stated above and the model is rerun with the transformed variables. Now, estimating the uncertainties in the parameters with equation C.5 will lead to corrected values.

**Significance of parameters** The significance of the model parameters  $a_k$  can be tested by a statistical test of the null hypothesis  $a_k = 0$ . The test variable is

$$T = \frac{a_k}{\sigma_{a_k}} = \frac{a_k}{\sqrt{\frac{R^2}{N-M} [(X^T X)^{-1}]_{kk}}} \quad (\text{C.9})$$

using the estimate for the parameter uncertainties as derived above.  $T$  is student-t distributed since it is of the form  $\frac{A}{\sqrt{B/m}}$  (where  $A$  is normally distributed and  $B$   $\chi^2$ -distributed with degree of freedom  $m$ ). Therefore the  $T$ -value can be compared with values for the student-t-statistic in tables for certain confidence levels. Note that for degrees of freedom larger than 30, the student-t distribution converges against the normal distribution, so that for long time series a good rule is to reject the null hypothesis (and consider the corresponding basis function to be of significant importance) when  $T > 2$  (corresponding to a significance level of 95%).

**The regression model** In this work, regression models are applied to e.g. temperature time series or zonal wind time series in order to estimate the trends or detect the response to the QBO. Hence, time series of forcings that are known to affect the dynamical state in the stratosphere are used as basis functions, and the regression model

is of the form:

$$\begin{aligned}
y_m(\phi, t) = & a_1(\phi, t) + \\
& a_2(\phi, t) \cdot \text{Linear}(t) + \\
& a_3(\phi, t) \cdot \text{QBO}(t + \Delta t) + \\
& a_4(\phi, t) \cdot \text{Solar}(t) + \\
& a_5(\phi, t) \cdot \text{ENSO}(t)
\end{aligned} \tag{C.10}$$

where  $\phi$  is the latitude,  $t$  is the time in months and  $y_m(\phi, t)$  is the modelled variable. In addition to an offset and mean annual cycle, a linear term, the QBO, the solar cycle, and ENSO have been included as basis functions. The QBO basis function is described with equatorial zonal mean winds at one pressure level (40 hPa), and a time lag  $\Delta t$  was allowed. The optimal value for  $\Delta t$  was identified by taking the best fit (minimal sum of squared residuals) of runs with  $\Delta t$  varying from -12 to +12 months. This method is used if the aim of the regression is to analyse the response to the QBO. Otherwise, if the QBO is included only to remove variability that can be assigned to it, instead of shifting the QBO timeseries by  $\Delta t$ , a second QBO basis function that is chosen to be orthogonal to the QBO timeseries is included.

The coefficients  $a_i$  of all basis functions are expanded to account for seasonal variability as follows:

$$\begin{aligned}
a_i(\phi, t) = & a_{i0}(\phi) + \sum_{k=1}^N [a_{iks}(\phi) \sin(2\pi k(t - 0.5)/12) + \\
& + a_{ikc}(\phi) \cos(2\pi k(t - 0.5)/12)]
\end{aligned} \tag{C.11}$$

$N$  is commonly set to 4 for the constant term  $a_1$ , and for all other basis functions it is set to 2. Setting  $N$  to 4 for the constant term allows for accurate representation of the annual cycle which is simply the Fourier expansion of the constant term, while restricting  $N$  to 2 for the other terms allows for annual and semi-annual structure in the coefficients without over-fitting the regression model. The regression model fit is obtained by the linear least squares fit as described above, and the autocorrelation in the residual is accounted for.

The total variance for coefficient  $a_i$  is obtained by

$$\begin{aligned}
\sigma^2(a_i) = & \sigma^2(a_{i0}) + \sum_{k=1}^N [\sigma^2(a_{iks}) \sin^2(2\pi k(t - 0.5)/12) + \\
& + \sigma^2(a_{ikc}) \cos^2(2\pi k(t - 0.5)/12)]
\end{aligned}$$

In the following, coefficients are considered as significant when  $a_i \geq 2\sigma(a_i)$ , which corresponds to a significance level of about 95% (the ratio  $a_i/\sigma(a_i)$  is student-t distributed and converges to the normal distribution for  $N-M \geq 30$ ). This means that with a certainty of 95% the null hypothesis  $a_i=0$  can be rejected if  $a_i/\sigma(a_i) > 2$ .

# Bibliography

- Andrews, D., Holton, J., and Leovy, C.: Middle Atmosphere Dynamics, Academic Press, San Diego, California, 1987.
- Austin, J., Scinocca, J., Plummer, D., Oman, L., Waugh, D., Akiyoshi, H., Bekki, S., Braesicke, P., Butchart, N., Chipperfield, M., Cugnet, D., Dameris, M., Dhomse, S., Eyring, V., Frith, S., Garcia, R., Garny, H., Gettelman, A., Hardiman, S. C., Kinnison, D., Lamarque, J., Mancini, E., Marchand, M., Michou, M., Morgenstern, O., Nakamura, T., Pawson, S., Pitari, G., Pyle, J., Rozanov, E., Shepherd, T., Shibata, K., Stolarski, R., Teysedre, H., Wilson, R., and Yamashita, Y.: The decline and recovery of total column ozone using a multi-model time series analysis, *J. Geophys. Res.*, accepted, 2010a.
- Austin, J., Struthers, H., Scinocca, J., Plummer, D., Akiyoshi, H., Baumgaertner, A., Bekki, S., Bodeker, G., Braesicke, P., Brühl, C., N. Butchart, Chipperfield, M., Cugnet, D., Dameris, M., Dhomse, S., Frith, S., Garny, H., Gettelman, A., Hardiman, S. C., Jöckel, P., Kinnison, D., Lamarque, J., E. Mancini, Marchand, M., Michou, M., Morgenstern, O., Nakamura, T., Nielsen, J., Pitari, G., Pyle, J., Rozanov, E., Shepherd, T., Shibata, K., Smale, D., Teysedre, H., and Y. Yamashita: Chemistry-climate model simulations of the Antarctic ozone hole, *J. Geophys. Res.*, accepted, 2010b.
- Baldwin, M. and Dunkerton, T.: Downward propagation of the Arctic Oscillation from the stratosphere to the troposphere, *J. Geophys. Res.*, 104, 937–946, 1999.
- Birner, T. and Boenisch, H.: Residual circulation trajectories and transit times into the extratropical lowermost stratosphere, *Atmos. Chem. Phys. Discuss.*, 10, 16 837–16 860, 2010.
- Bodeker, G. E., Garny, H., Smale, D., Dameris, M., and Deckert, R.: The 1985 Southern Hemisphere mid-latitude total column ozone anomaly, *Atmos. Chem. Phys.*, 7, 5625–5637, 2007.
- Boehm, M. T. and Lee, S.: The Implications of Tropical Rossby Waves for Tropical Tropopause Cirrus Formation and for the Equatorial Upwelling of the Brewer-Dobson Circulation., *J. Atmos. Sci.*, 60, 247–261, 2003.

- Brasseur, G. and Solomon, S.: *Aeronomy of the middle atmosphere: chemistry and physics of the stratosphere and mesosphere*, Springer, 2005.
- Brewer, A. W.: Evidence for a world circulation provided by the measurements of helium and water vapor distribution in the stratosphere, *QJR Meteorol. Soc.*, **75**, 351–363, 1949.
- Butchart, N., Scaife, A., Bourqui, M., de Grandpre, J., Hare, S., Kettleborough, J., Langematz, U., Manzini, E., Sassi, F., Shibata, K., Shindell, D., and Sigmond, M.: Simulations of anthropogenic change in the strength of the Brewer-Dobson circulation, *Clim. Dyn.*, **27**, 727–741, 2006.
- Butchart, N., Cionni, I., Eyring, V., Waugh, D. W., Akiyoshi, H., Austin, J., Bruehl, C., Chipperfield, M. P., Cordero, E., Dameris, M., Deckert, R., Frith, S. M., Garcia, R. R., Gettelman, A., Giorgetta, M. A., Kinnison, D. E., Li, F., Manzini, E., McLandress, C., Pawson, S., Pitari, G., Rozanov, E., Sassi, F., Shepherd, T. G., Shibata, K., and Tian, W.: Chemistry-climate model simulations of 21st century stratospheric climate and circulations changes, *J. Clim.*, accepted, 2010.
- Calvo, N. and Garcia, R. R.: Wave Forcing of the Tropical Upwelling in the Lower Stratosphere under Increasing Concentrations of Greenhouse Gases, *J. Atmos. Sci.*, **66**, 3184–3196, 2009.
- Calvo, N., García-Herrera, R., and Garcia, R. R.: The ENSO Signal in the Stratosphere, *New York Academy Sciences Annals*, **1146**, 16–31, 2008.
- Charney, J. G. and Drazin, P. G.: Propagation of planetary-scale disturbances from the lower into the upper atmosphere, *J. Geophys. Res.*, **66**, 83–109, 1961.
- Dameris, M., Grewe, V., Ponater, M., Deckert, R., Eyring, V., Mager, F., Matthes, S., Schnadt, C., Stenke, A., Steil, B., Brühl, C., and Giorgetta, M.: Long-term changes and variability in a transient simulation with a chemistry-climate model employing realistic forcing, *Atmos. Chem. Phys.*, **5**, 2121–2145, 2005.
- Dameris, M., Matthes, S., Deckert, R., Grewe, V., and Ponater, M.: Solar cycle effect delays onset of ozone recovery, *Geophys. Res. Lett.*, **33**, L03 806, doi:10.1029/2005GL024 741, 2006.
- Deckert, R. and Dameris, M.: Higher tropical SSTs strengthen the tropical upwelling via deep convection, *Geophys. Res. Lett.*, **35**, L10 813, 2008.
- Dobson, G. M. B.: Origin and Distribution of the Polyatomic Molecules in the Atmosphere, *Royal Society of London Proceedings Series A*, **236**, 187–193, 1956.
- Edmon, H. J., Hoskins, B. J., and McIntyre, M. E.: Eliassen-Palm cross sections for the troposphere, *J. Atmos. Sci.*, **37**, 2600–2616, 1980.

- Engel, A., Mobius, T., Bonisch, H., Schmidt, U., Heinz, R., Levin, I., Atlas, E., Aoki, S., Nakazawa, T., Sugawara, S., Moore, F., Hurst, D., Elkins, J., Schauffler, S., Andrews, A., and Boering, K.: Age of stratospheric air unchanged within uncertainties over the past 30 years, *Nature Geoscience*, 2, 28 – 31, 2009.
- Eyring, V., Chipperfield, M., Giorgetta, M., Kinnison, D. E., Manzini, E., Matthes, K., Newman, P., Pawson, S., Shepherd, T., and Waugh, D.: Overview of the New CCMVal Reference and Sensitivity Simulations in Support of Upcoming Ozone and Climate Assessments and Planned SPARC CCMVal, *SPARC Newsletter*, 30, 20–26, 2008.
- Eyring, V., Cionni, I., Bodeker, G. E., Charlton-Perez, A. J., Kinnison, D. E., Scinocca, J. F., Waugh, D. W., Akiyoshi, H., Bekki, S., Chipperfield, M. P., Dameris, M., Dhomse, S., Frith, S. M., Garny, H., Gettelman, A., Kubin, A., Langematz, U., Mancini, E., Marchand, M., Nakamura, T., Oman, L. D., Pawson, S., Pitari, G., Plummer, D. A., Rozanov, E., Shepherd, T. G., Shibata, K., Tian, W., Braesicke, P., Hardiman, S. C., Lamarque, J. F., Morgenstern, O., Smale, D., Pyle, J. A., and Yamashita, Y.: Multi-model assessment of stratospheric ozone return dates and ozone recovery in CCMVal-2 models, *Atmos. Chem. Phys. Discuss.*, 10, 11 659–11 710, 2010.
- Farman, J. C., Murgatroyd, R. J., Silnickas, A. M., and Thrush, B. A.: Ozone photochemistry in the Antarctic stratosphere in summer, *Q. J. R. Meteorol. Soc.*, 111, 1013–1028, 1985.
- Fomichev, V. I., Jonsson, A. I., de Grandpré, J., Beagley, S. R., McLandress, C., Semeniuk, K., and Shepherd, T. G.: Response of the Middle Atmosphere to CO<sub>2</sub> Doubling: Results from the Canadian Middle Atmosphere Model, *J. Clim.*, 20, 1121–1144, 2007.
- Fu, Q., Solomon, S., and Lin, P.: On the seasonal dependence of tropical lower-stratospheric temperature trends, *Atmos. Chem. Phys.*, 10, 2643–2653, 2010.
- Garcia, R. and Randel, W.: Acceleration of the Brewer–Dobson Circulation due to Increases in Greenhouse Gases, *J. Atmos. Sci.*, 65, 2731–2739, 2008.
- Garcia, R. R. and Salby, M. L.: Transient Response to Localized Episodic Heating in the Tropics. Part II: Far-Field Behavior., *J. Atmos. Sci.*, 44, 499–532, 1987.
- García-Herrera, R., Calvo, N., Garcia, R. R., and Giorgetta, M. A.: Propagation of ENSO temperature signals into the middle atmosphere: A comparison of two general circulation models and ERA-40 reanalysis data, *J. Geophys. Res.*, 111, D06 101, 2006.
- Garny, H., Bodeker, G. E., and Dameris, M.: Trends and variability in stratospheric mixing: 1979–2005, *Atmos. Chem. Phys.*, 7, 5611–5624, 2007.

- Garny, H., Dameris, M., and Stenke, A.: Impact of prescribed SSTs on climatologies and long-term trends in CCM simulations, *Atmos. Chem. Phys.*, 9, 6017–6031, 2009.
- Gottelman, A., Holton, J. R., and Rosenlof, K. H.: Mass fluxes of O<sub>3</sub>, CH<sub>4</sub>, N<sub>2</sub>O and CF<sub>2</sub>Cl<sub>2</sub> in the lower stratosphere calculated from observational data, *J. Geophys. Res.*, 102, 19 149–19 160, 1997.
- Gottelman, A., Lauritzen, P. H., Park, M., and Kay, J.: Processes regulating short-lived species in the tropical tropopause layer, *Geophys. Res. Lett.*, 114, D13 303, 2009.
- Gottelman, A., M., Hegglin, I., Son, S.-W., Kim, J., Fujiwara, M., Birner, T., Kremser, S., Rex, M., Anel, J. A., Akiyoshi, H., Austin, J., Bekki, S., Braesike, P., Brühl, C., Butchart, N., Chipperfield, M., Dameris, M., Dhomse, S., Garny, H., Hardiman, S. C., Jöckel, P., Kinnison, D. E., Lamarque, J. F., Mancini, E., Marchand, M., Michou, M., Morgenstern, O., Pawson, S., Pitari, G., Plummer, D., Pyle, J. A., Rozanov, E., Scinocca, J., Shepherd, T. G., Shibata, K., Smale, D., Teysse, H., and Tian, W.: Multi-model Assessment of the Upper Troposphere and Lower Stratosphere: Tropics and Global Trends, *J. Geophys. Res.*, submitted, 2010.
- Gill, A. E.: Some simple solutions for heat-induced tropical circulation, *Q. J. R. Meteorol. Soc.*, 106, 447–462, 1980.
- Giorgetta, M. A. and Bengtsson, L.: Potential role of the quasibiennial oscillation in the stratosphere-troposphere exchange as found in water vapor in general circulation model experiments, *J. Geophys. Res.*, 104, 6003–6019, 1999.
- Gray, L. and Pyle, J.: A two-dimensional model of the quasi-biennial oscillation of ozone, *J. Atmos. Sci.*, 46, 203–220, 1989.
- Grewe, V.: The origin of ozone, *Atmos. Chem. Phys.*, 6, 1495–1511, 2006.
- Grewe, V. and Dameris, M.: Calculating the global mass exchange between stratosphere and troposphere, *Annales Geophysicae*, 14, 431–442, 1996.
- Hall, T. M. and Plumb, R.: Age as a diagnostic of stratospheric transport, *J. Geophys. Res.*, 99, 1059–1070, 1994.
- Hardiman, S. C., Butchart, N., Haynes, P. H., and Hare, S. H. E.: A note on forced versus internal variability of the stratosphere, *Geophys. Res. Lett.*, 34, L12 803, 2007.
- Haynes, P.: Stratospheric Dynamics, *Annual Review of Fluid Mechanics*, 37, 263–293, 2005.
- Haynes, P. and Shuckburgh, E.: Effective diffusivity as a diagnostic of atmospheric transport 1. Stratosphere, *J. Geophys. Res.*, 105, 22 777–22 794, 2000.

- Haynes, P., Marks, C., McIntyre, M., Shepherd, T., and Shine, K.: On the 'downward control' of extratropical diabatic circulations by eddy-induced mean zonal forces, *J. Atmos. Sci.*, 48, 651–678, 1991.
- Hegglin, M. I., Gettelman, A., Hoor, P., Krichevsky, R., Manney, G. L., Pan, L. L., Son, S.-W., Stiller, G., Tilmes, S., Walker, K. A., Eyring, V., Shepherd, T. G., Waugh, D., Akiyoshi, H., Austin, J., Baumgaertner, A., Bekki, S., Braesicke, P., Brühl, C., Butchart, N., Chipperfield, M., Dameris, M., Dhomse, S., Frith, S., Garny, H., Hardiman, S. C., Jöckel, P., Kinnison, D. E., Lamarque, J. F., Mancini, E., Michou, M., Morgenstern, O., Nakamura, T., Olivie, D., Pawson, S., Pitari, G., Plummer, D. A., Rozanov, E., Scinocca, J. F., Shibata, K., Smale, D., Teyssedre, H., Tian, W., and Yamashita, Y.: Multi-Model Assessment of the Upper Troposphere and Lower Stratosphere: Extra-tropics, *J. Geophys. Res.*, accepted, 2010.
- Hein, R., Dameris, M., Schnadt, C., Land, C., Grewe, V., Köhler, I., Ponater, M., Sausen, R., Steil, B., Landgraf, J., and Brühl, C.: Results of an interactively coupled atmospheric chemistry- general circulation model: Comparison with observations, *Ann. Geophysicae*, 19, 435–457, 2001.
- Holton, J., Haynes, P., McIntyre, M., Douglass, A., Rood, R., and Pfister, L.: Stratosphere-troposphere exchange, *Reviews of Geophysics*, 33, 403–439, 1995.
- Holton, J. R.: An introduction to dynamic meteorology, International geophysics series, San Diego, New York: Academic Press, 4th ed., 2004.
- Ineson, S. and Scaife, A. A.: The role of the stratosphere in the European climate response to El Niño, *Nature Geoscience*, 2, 32–36, 2009.
- IPCC: Climate Change 2001 – The scientific basis, Tech. rep., Intergovernmental Panel on Climate Change, Cambridge University Press, New York, USA, 2001.
- IPCC: Climate Change 2007 – The physical science basis, Tech. rep., Intergovernmental Panel on Climate Change, Cambridge University Press, New York, USA, 2007.
- Johns, T. C., Durman, C. F., Banks, H. T., Roberts, M. J., McLaren, A. J., Ridley, J. K., Senior, C. A., Williams, K. D., Jones, A., Rickard, G. J., Cusack, S., Ingram, W. J., Crucifix, M., Sexton, D. M. H., Joshi, M. M., Dong, B.-W., Spencer, H., Hill, R. S. R., Gregory, J. M., Keen, A. B., Pardaens, A. K., Lowe, J. A., Bodas-Salcedo, A., Stark, S., and Searl, Y.: The New Hadley Centre Climate Model (HadGEM1): Evaluation of Coupled Simulations, *J. Clim.*, 19, 1327–1353, 2006.
- Kerr-Munslow, A. M. and Norton, W. A.: Tropical Wave Driving of the Annual Cycle in Tropical Tropopause Temperatures. Part I: ECMWF Analyses., *J. Atmos. Sci.*, 63, 1410–1419, 2006.

- Kiesewetter, G., Sinnhuber, B.-M., Vountas, M., Weber, M., and Burrows, J. P.: A long-term stratospheric ozone data set from assimilation of satellite observations: High-latitude ozone anomalies, *J. Geophys. Res.*, 115, D10 307, 2010.
- Kinnersley, J. and Tung, K.: Mechanisms for the extratropical QBO in circulation and ozone, *J. Atmos. Sci.*, 56, 1942–1962, 1999.
- Kushnir, Y., Robinson, W. A., Bladé, I., Hall, N. M. J., Peng, S., and Sutton, R.: Atmospheric GCM Response to Extratropical SST Anomalies: Synthesis and Evaluation, *J. Clim.*, 15, 2233–2256, 2002.
- Lamarque, J.-F. and Solomon, S.: Impact of changes in climate and halocarbons on recent lower stratosphere ozone and temperature trends, *J. Clim.*, 23, 2599–2611, 2010.
- Land, C., Feichter, J., and Sausen, R.: Impact of vertical resolution on the transport of passive tracers in the ECHAM4 model, *Tellus B*, 54, 344–360, 2002.
- Lean, J., Rottmann, G., Kyle, H., Woods, T., Hickey, J., and Puga, L.: Detection and parameterisation of variations in solar mid- and near-ultraviolet radiation (22–400 nm), *J. Geophys. Res.*, 102, 29 939–29 956, 1997.
- Lee, S.: Why Are the Climatological Zonal Winds Easterly in the Equatorial Upper Troposphere?., *J. Atmos. Sci.*, 56, 1353–1363, 1999.
- Leuthold, E.: Ueber den Einfluss der Variabilitaet tropischer Meeresoberflaechentemperaturuenn auf die Dynamik der unteren Stratosphaere, Master's thesis, Ludwig-Maximillians Universitaet Muenchen, 2010.
- Li, F., Austin, J., and Wilson, J.: The Strength of the Brewer Dobson Circulation in a Changing Climate: Coupled Chemistry Climate Model Simulations, *J. Clim.*, 21, 40–47, 2008.
- Lin, P. and Fu, Q., Solomon, S., and Wallace, J. M.: Temperature trend patterns in Southern Hemisphere high latitudes: novel indicators of stratospheric change, *J. Clim.*, 22, 6325–6341, 2009.
- Loyola, D. G., Coldewey-Egbers, R. M., Dameris, M., Garny, H., Stenke, A., Van Roozendaal, M., Lerot, C., Balis, D., and Koukouli, M.: Global long-term monitoring of the ozone layer - a prerequisite for predictions, *International Journal of Remote Sensing*, 30, 4295–4318, 2009.
- Martin, G. M., Ringer, M. A., Pope, V. D., Jones, A., Dearden, C., and Hinton, T. J.: The Physical Properties of the Atmosphere in the New Hadley Centre Global Environmental Model (HadGEM1). Part I: Model Description and Global Climatology, *J. Clim.*, 19, 1274–1301, 2006.

- Matsuno, T.: Lagrangian motion of air parcels in the stratosphere in the presence of planetary waves, *Pure and Applied Geophysics*, 118, 189–216, 1980.
- McLandress, C. and Shepherd, T. G.: Simulated Anthropogenic Changes in the Brewer-Dobson Circulation, Including Its Extension to High Latitudes, *J. Clim.*, 22, 1516–1540, 2009.
- Miller, M. J., Palmer, T. N., and Swinbank, R.: Parameterization and influence of sub-grid scale orography in general circulation and numerical weather prediction models, *Meteorol. Atmos. Phys.*, 40, 84–109, 1989.
- Molina, L. T. and Molina, M. J.: Production of Cl<sub>2</sub>O<sub>2</sub> from the self-reaction of the ClO radical, *J. Phys. Chem.*, 91(2), 433–436, 1987.
- Newman, M.: Interannual to Decadal Predictability of Tropical and North Pacific Sea Surface Temperatures, *J. Clim.*, 20, 2333–2356, 2007.
- Norton, W. A.: Tropical Wave Driving of the Annual Cycle in Tropical Tropopause Temperatures. Part II: Model Results., *J. Atmos. Sci.*, 63, 1420–1431, 2006.
- Oman, L., Waugh, D. W., Pawson, S., Stolarski, R. S., and Newman, P. A.: On the influence of anthropogenic forcings on changes in the stratospheric mean age, *J. Geophys. Res.*, 114, D3105, 2009.
- Oman, L. D., Plummer, D., Waugh, D., Austin, J., Scinocca, J., Douglass, A., Salawitch, R., Canty, T., Akiyoshi, H., Bekki, S., Braesicke, P., Butchart, N., Chipperfield, M., Cugnet, D., Dhomse, S., Eyring, V., Frith, S., Hardiman, S., Kinnison, D., Lamarque, J., Mancini, E., Marchand, M., Michou, M., Morgenstern, O., Nakamura, T., Nielsen, J., Olivie, D., Pitari, G., Pyle, J., Rozanov, E., Shepherd, T., Shibata, K., Stolarski, R., Teyssedre, H., Tian, W., , and Yamashita, Y.: Multi-model assessment of the factors driving stratospheric ozone evolution over the 21st Century, *J. Geophys. Res.*, submitted, 2010.
- Peng, S. and Whitaker, J. S.: Mechanisms Determining the Atmospheric Response to Midlatitude SST Anomalies., *J. Clim.*, 12, 1393–1408, 1999.
- Peng, S., Mysak, L. A., Ritchie, H., Derome, J., and Dugas, B.: The Differences between Early and Midwinter Atmospheric Responses to Sea Surface Temperature Anomalies in the Northwest Atlantic., *J. Clim.*, 8, 137–157, 1995.
- Plumb, R. A. and Eluszkiewicz, J.: The Brewer-Dobson Circulation: Dynamics of the Tropical Upwelling., *J. Atmos. Sci.*, 56, 868–890, 1999.
- Portmann, R. W. and Solomon, S.: Indirect radiative forcing of the ozone layer during the 21st century, *Geophys. Res. Lett.*, 34, L02813, 2007.

- Puls, J. and Stinzing, S.: Numerik für Physiker, lecture notes for lecture held at LMU Munich WS 2005/2006, 2005.
- Randel, W. and Cobb, J.: Coherent variations of monthly mean total ozone and lower stratospheric temperature, *J. Geophys. Res.*, 99, 5433–5447, 1994.
- Randel, W., Gille, J., Roche, A., Kumer, J., Mergenthaler, J., Waters, J., Fishbein, E., and Lahoz, W.: Stratospheric transport from the tropics to middle latitudes by planetary-wave mixing, *Nature*, 365, 533–535, 1993.
- Randel, W. J. and Held, I. M.: Phase Speed Spectra of Transient Eddy Fluxes and Critical Layer Absorption., *J. Atmos. Sci.*, 48, 688–697, 1991.
- Randel, W. J., Garcia, R. R., and Wu, F.: Time-Dependent Upwelling in the Tropical Lower Stratosphere Estimated from the Zonal-Mean Momentum Budget., *J. Atmos. Sci.*, 59, 2141–2152, 2002.
- Randel, W. J., Garcia, R., and Wu, F.: Dynamical Balances and Tropical Stratospheric Upwelling, *J. Atmos. Sci.*, 65, 3584–3595, 2008.
- Ravishankara, A. R., Daniel, J. S., and Portmann, R. W.: Nitrous Oxide (N<sub>2</sub>O): The Dominant Ozone-Depleting Substance Emitted in the 21st Century, *Science*, 326, 123–125, 2009.
- Rayner, N. A., Parker, D. E., Horton, E. B., Folland, C. K., Alexander, L. V., Rowell, D. P., Kent, E. C., and Kaplan, A.: Global Analyses of sea surface temperatures, sea ice, and night marine air temperature since the late nineteenth century, *J. Geophys. Res.*, 108, 4407, 2003.
- Reithmeier, C. and Sausen, R.: ATTILA: atmospheric tracer transport in a Lagrangian model, *Tellus B*, 54, 278–299, 2002.
- Reithmeier, C., Sausen, R., and Grewe, V.: Investigating lower stratospheric model transport: Lagrangian calculations of mean age and age spectra in the GCM ECHAM4, *Clim. Dyn.*, 30, 225–238, 2008.
- Rosenfield, J. E., Douglass, A. R., and Considine, D.: The impact of increasing carbon dioxide on ozone recovery, *J. Geophys. Res.*, 107(D6), 4049, 2002.
- Runde, T.: Impact of changing sea surface temperatures on convective activity in the tropics, Master's thesis, Ludwig-Maximilians-Universitaet Muenchen, 2009.
- Runde, T., Dameris, M., Brinkop, S., and Garny, H.: Impact of sea surface temperature on strength and frequency of convection in the Tropics, submitted to *J. Clim.*, 2010.
- Schneider, T., O’Gorman, P. A., and Levine, X. J.: Water vapor and the dynamics of climate changes, *Reviews of Geophysics*, 48, G3001, 2010.

- Seidel, D. J. and Randel, W. J.: Recent widening of the tropical belt: Evidence from tropopause observations, *J. Geophys. Res.*, 112, D20 113, 2007.
- Semeniuk, K. and Shepherd, T. G.: Mechanisms for Tropical Upwelling in the Stratosphere., *J. Atmos. Sci.*, 58, 3097–3115, 2001.
- Sigmond, M. and Scinocca, J. F.: The Influence of the Basic State on the Northern Hemisphere Circulation Response to Climate Change, *J. Clim.*, 23, 1434–1446, 2010.
- Sigmond, M., Siegmund, P. C., Manzini, E., and Kelder, H.: A Simulation of the Separate Climate Effects of Middle-Atmospheric and Tropospheric CO<sub>2</sub> Doubling., *J. Clim.*, 17, 2352–2367, 2004.
- Simmons, A., Uppala, S., Dee, D., and Kobayashi, S.: ERAInterim: New ECMWF reanalysis products from 1989 onwards, *ECMWF Newsl.*, 110, 25–35, 2006.
- Sinnhuber, B.-M. and Wohltmann, I.: Upwelling across the tropical tropopause diagnosed from meteorological re-analyses and ozone observations shows no increase over the past four decades, *Geophys. Res. Lett.*, x, submitted, 2010.
- SPARC-CCMVal: SPARC Report on the Evaluation of Chemistry-Climate Models, V. Eyring, T. G. Shepherd, D. W. Waugh (Eds.), SPARC Report No. 5, Tech. Rep. SPARC Report No. 5, WCRP-132, WMO/TD-No. 1526, <http://www.atmosp.physics.utoronto.ca/SPARC>, 2010.
- Steil, B., Dameris, M., Brühl, C., Crutzen, P. J., Grewe, V., Ponater, M., and Sausen, R.: Development of a chemistry module for GCMs: First results of a multiannual integration, *Ann. Geophysicae*, 16, 205–228, 1998.
- Steinbrecht, W., Haßler, B., Brühl, C., Dameris, M., Giorgetta, M., Grewe, V., Manzini, E., Matthes, S., Schnadt, C., Steil, B., and Winkler, P.: Interannual variation patterns of total ozone and lower stratospheric temperature in observations and model simulations, *Atmos. Chem. Phys.*, 6, 349–374, 2006.
- Stenke, A., Grewe, V., and Ponater, M.: Lagrangian transport of water vapour and cloud water in the ECHAM4 GCM and its impact on the cold bias, *Clim. Dyn.*, 31, 491–506, 2008.
- Stenke, A., Dameris, M., Grewe, V., and Garny, H.: Implications of Lagrangian transport for coupled chemistry-climate simulations, *Atmos. Chem. Phys.*, 9, 5489–5504, 2009.
- Stott, P., Jones, G., Lowe, J., Thorne, P., Durman, C., Johns, T., and Thelen, J.-C.: Transient Climate Simulations with the HadGEM1 Climate Model: Causes of Past Warming and Future Climate Change, *J. Clim.*, 19, 2763–2782, 2006.

- Thompson, D. W. J. and Solomon, S.: Recent Stratospheric Climate Trends as Evidenced in Radiosonde Data: Global Structure and Tropospheric Linkages, *J. Clim.*, 18, 4785–4795, 2005.
- Tiao, G., Reinsel, G., Xu, D., Pedrick, J., Zhu, X., Miller, A., DeLuisi, J., Mateer, C., and Wuebbles, D.: Effects of autocorrelation and temporal sampling schemes on estimates of trend and spatial correlation, *J. Geophys. Res.*, 95D12, 20 507–20 517, 1990.
- von Storch, H. and Zwiers, F. W.: *Statistical Analysis in Climate Research*, ISBN 0521012309. Cambridge, UK: Cambridge University Press, March 2002., 2002.
- WMO: *Scientific Assessment of Ozone Depletion: 2002 (under the Montreal Protocol)*, WMO Global Ozone Research and Monitoring Project-Report No. 47, Geneva, Tech. rep., ISBN 92-807-2261-1: 436 pages, 2003.
- WMO: *Scientific Assessment of Ozone Depletion: 2006*, Tech. rep., WMO Global Ozone Research and Monitoring Project Report No. 50, Geneva, Switzerland, 2007.
- WMO: *Scientific Assessment of Ozone Depletion: 2010*, Tech. rep., WMO Global Ozone Research and Monitoring Project Report, in press, 2010.

# Acknowledgements

First of all, I want to thank my supervisor Dr. Martin Dameris very much for his great commitment, motivation and support. Many thanks for always taking time to discuss my work, for your good advice and for your trust to give me freedom in my work. Also thanks for making it possible that I could spend time abroad, visit conferences and focus on my work without having to worry about 'organisational' issues at all.

I also want to thank Dr. George Craig very much for co-examining my PhD thesis on rather short notice.

Special thanks go to Dr. Greg Bodeker, who co-supervised my PhD thesis and made it possible for me to spend half a year at NIWA Lauder. Thanks for very valuable advice on many issues, which definitely helped me a lot.

Very valuable for this work were also the discussions with Dr. William Randel, whom I want to thank very much. Thanks for inviting me to NCAR and helping me with the interpretation of my work!

Dr. Volker Grewe contributed significantly to the development of my work on ozone transport, and I want to thank him for his very good advice and great help with this part of my work. Also special thanks to Dr. Andrea Stenke for introducing me to the E39CA model and supporting me especially during the first stage of my PhD. The thesis of Dr. Rudolf Deckert was the basis for my work, and I am very grateful for this. Thanks for providing me with this great starting point for my work, for collaboration and for helpful discussions. I also want to thank Theresa Runde and Eva Leuthold for great collaboration and help with my work. Special thanks also go to Stefanie Kremser and Dr. Birigt Hassler, who were always very helpful and with whom I had great discussions on our work. Dan Smale provided me with some software help and data, and I want to thank him for that. Furthermore, I want to thank all colleagues at the IPA for a good working atmosphere. Thanks to Dr. Robert Sausen and Dr. Ulrich Schumann for making it possible for me to work at the IPA and spend time at other institutes as well. Thanks to NIWA Lauder for supporting my visit, and all NIWA staff for always being extremely helpful. Also NCAR (Boulder) supported my visit generously, which was much appreciated.

Last but not least I want to thank all my friends and family for supporting me in various ways (including proof-reading parts of this thesis)!

# Lebenslauf

VON

Hella Garny

geboren am 25.2.1983 in Starnberg

## Ausbildung

1993-2002	Besuch des Gymnasiums mit Abschluß des Abiturs in Gauting
10/2002	Aufnahme des Diplom-Studiengangs Meteorologie an der Ludwig-Maximilians-Universität München
08/2004-07/2005	Auslandsstudium am University Center on Svalbard, Spitzbergen, Norwegen. Kurse in polarer Meteorologie, Ozeanographie und Glaziologie
06/2006	Diplom-Hauptprüfungen
07/2006-02/2007	Auslandsaufenthalt am National Institute for Water & Atmosphere in Lauder, Neuseeland, zur Arbeit an der Diplomarbeit zum Thema 'Stratospheric Mixing and Implications on Ozone Distributions'
03/2007	Abschluss des Studiums mit Auszeichnung

## Promotion

seit 08/2007	Wissenschaftliche Mitarbeiterin am Institut für Physik der Atmosphäre, DLR, Oberpfaffenhofen
01/2009-07/2009	Gastwissenschaftlerin am National Institute for Water & Atmosphere in Lauder, Neuseeland
01/2010-02/2010	Gastwissenschaftlerin am Natitonal Center for Atmospheric Research, in Boulder, USA

Oberpfaffenhofen, den 30. Juli 2010